

NEW MEXICO DEPARTMENT OF TRANSPORTATION

RESEARCH BUREAU

Innovation in Transportation

Improved Load Rating of Reinforced Concrete Slab Bridges

Prepared by:

New Mexico State University
Department of Civil Engineering
Box 30001, MSC 3CE
Las Cruces, NM 88003-8001

Prepared for:

New Mexico Department of Transportation
Research Bureau
7500B Pan American Freeway NE
Albuquerque, NM 87109

In Cooperation with:

The US Department of Transportation
Federal Highway Administration

Report NM05STR-02

SEPTEMBER, 2007

1. NMDOT Report No. NM05STR-02	2. Govt. Accession No.	3. Recipient Catalog No.:	
4. Title and Subtitle Improved Load Rating of Reinforced Concrete Slab Bridges		5. Report Date September 2007	
		6. Performing Organization Code	
7. Author(s) David V. Jáuregui, Alicia Licon-Lozano, and Kundan Kulkarni		8. Performing Organization Report No.	
9. Performing Organization Name and Address New Mexico State University Department of Civil Engineering Box 30001, MSC 3CE Las Cruces, NM 88003-8001		10. Work Unit No. (TRAIS)	
		11. Contract or Grant No. CO4759	
12. Sponsoring Agency Name and Address NMDOT Research Bureau 7500B Pan American Freeway NE PO Box 94690 Albuquerque, NM 87199-4690		13. Type of Report and Period Covered	
		14. Sponsoring Agency Code	
15. Supplementary Notes			
16. Abstract In New Mexico, many reinforced concrete slab (RCS) bridges provide service on interstates I-10, I-25, and I-40. An accurate strength evaluation of interstate bridges is essential to avoid unnecessary load restrictions. The AASHTO load rating factor for this type of bridge largely depends on the live-load moment per foot of slab width. As a result, the main objective of this study was to determine a more accurate value for the equivalent strip width (using higher level evaluation techniques including diagnostic load testing and finite element analysis) for use in the AASHTO rating. A continuous, RCS bridge located in Las Cruces, New Mexico was evaluated in this study. An AASHTO load rating analysis based on the Load and Resistance Factor Rating (LRFR) approach was first performed using code-prescribed equations for the equivalent strip width to determine the live-load effects. A diagnostic load test was then conducted to measure the strain response at selected points in the positive and negative moment regions of an exterior and interior span. The measured response showed that the slab stiffness fit within cracked and gross section behavior. Furthermore, bending moments from finite element analysis agreed reasonably well with those derived from the experimental strain data (using the average of the cracked and gross section modulus). Using refined analysis, it was shown that the equivalent strip widths for positive moment were 26.1% and 22.1% greater than those calculated by the AASHTO approximate method for the exterior and interior spans, respectively. Furthermore, the refined widths for negative moment were greater than AASHTO by 13.1% for the exterior span and 11.1% for the interior span. This increase in the equivalent strip width reduced the live-load effects, which proportionally increased the rating factors. Accordingly, the inventory and operating rating factors for the bridge increased from 0.84 to 0.93 and 1.08 to 1.20, respectively. The factors increased by just 11% (rather than over 20%) since the rating was controlled by negative moment.			
17. Key Words Load rating, slab bridge, reinforced concrete, diagnostic testing, finite element analysis, strain measurement		18. Distribution Statement Available from NMDOT Research Bureau	
19. Security Classification (of this report) Unclassified	20. Security Class. (of this page) Unclassified	21. No. of Pages 99	22. Price

IMPROVED LOAD RATING OF REINFORCED CONCRETE SLAB BRIDGES

by

David V. Jáuregui
Associate Professor
New Mexico State University

Alicia Licon-Lozano
Graduate Research Assistant
New Mexico State University

Kundan Kulkarni
Graduate Research Assistant
New Mexico State University

Report NM05STR-02

A report on research sponsored by

New Mexico Department of Transportation
Research Bureau

in cooperation with
The U.S. Department of Transportation,
Federal Highway Administration

September 2007

NMDOT Research Bureau
7500B Pan American Freeway
PO Box 94690
Albuquerque, NM 87199-4690

PREFACE

In New Mexico, there are many reinforced concrete slab bridges that service interstates I-10, I-25, and I-40. The AASHTO load rating for this bridge type mainly depends on the live-load moment per foot of slab width. Accordingly, the objective of this study was to determine a more realistic equivalent strip width (using diagnostic load testing and finite element analysis) for use in the rating. An increase in the equivalent strip width decreases the live-load effects, thereby increasing the rating factors.

NOTICE

The United State Government and the State of New Mexico do not endorse products or manufacturers. Trade or manufacturers' names appear herein solely because they are considered essential to the object of this report. This information is available in alternative accessible formats. To obtain an alternative format, contact the NMDOT Research Bureau, 7500B Pan American Freeway, Albuquerque, NM 87109 (P.O. Box 94690, Albuquerque, NM 87199-4690) or by telephone (505) 841-9145.

DISCLAIMER

This report presents the results of research conducted by the author(s) and does not necessarily reflect the views of the New Mexico Department of Transportation or the Department of Transportation Federal Highway Administration. This report does not constitute a standard or specification.

ABSTRACT

In New Mexico, many reinforced concrete slab (RCS) bridges provide service on interstates I-10, I-25, and I-40. An accurate strength evaluation of interstate bridges is essential to avoid unnecessary load restrictions. The AASHTO load rating factor for this type of bridge largely depends on the live-load moment per foot of slab width. As a result, the main objective of this study was to determine a more accurate value for the equivalent strip width (using higher level evaluation techniques including diagnostic load testing and finite element analysis) for use in the AASHTO rating.

A continuous, RCS bridge located in Las Cruces, New Mexico was evaluated in this study. An AASHTO load rating analysis based on the Load and Resistance Factor Rating (LRFR) approach was first performed using code-prescribed equations for the equivalent strip width to determine the live-load effects. A diagnostic load test was then conducted to measure the strain response at selected points in the positive and negative moment regions of an exterior and interior span. The measured response showed that the slab stiffness fit within cracked and gross section behavior. Furthermore, bending moments from finite element analysis agreed reasonably well with those derived from the experimental strain data (using the average of the cracked and gross section modulus).

Using refined analysis, it was shown that the equivalent strip widths for positive moment were 26.1% and 22.1% greater than those calculated by the AASHTO approximate method for the exterior and interior spans, respectively. Furthermore, the refined widths for negative moment were greater than AASHTO by 13.1% for the exterior span and 11.1% for the interior span. This increase in the equivalent strip width reduced the live-load effects, which proportionally increased the rating factors. Accordingly, the inventory and operating rating

factors for the bridge increased from 0.84 to 0.93 and 1.08 to 1.20, respectively. The factors increased by just 11% (rather than over 20%) since the rating was controlled by negative moment.

ACKNOWLEDGEMENTS

The authors thank the NMDOT Research Bureau for providing financial support to conduct this research project. The NMSU research team would also like to acknowledge the advice and review provided by Mr. Jimmy Camp (State Bridge Engineer, NMDOT), Dr. Steve Maberry (Bridge Rating Engineer, NMDOT), Mr. Jeff Vigil (Bridge Management Engineer, NMDOT), and Mr. Wil Dooley (Division Bridge Engineer, FHWA) for the implementation of higher level techniques for the strength evaluation of reinforced concrete slab bridges. The management provided by Mr. Rais Rizvi (Research Engineer, NMDOT) and Mr. Virgil Valdez (Research Analyst, NMDOT) is also greatly appreciated. Lastly, the authors thank Mr. Earl Franks (Bridge Engineer, NMDOT) and the bridge crew from NMDOT District I for their assistance in the field testing.

METRIC CONVERSION FACTORS PAGE

APPROXIMATE CONVERSIONS TO SI UNITS				
SYMBOL	WHEN YOU KNOW	MULTIPLY BY	TO FIND	SYMBOL
LENGTH				
in	inches	25.4	millimeters	mm
ft	feet	0.305	meters	m
yd	yards	0.914	meters	m
mi	miles	1.61	kilometers	km
AREA				
in²	square inches	645.2	square millimeters	mm ²
ft²	square feet	0.093	square meters	m ²
yd²	square yard	0.836	square meters	m ²
ac	acres	0.405	hectares	ha
mi²	square miles	2.59	square kilometers	km ²
VOLUME				
fl oz	fluid ounces	29.57	milliliters	mL
gal	gallons	3.785	liters	L
ft³	cubic feet	0.028	cubic meters	m ³
yd³	cubic yards	0.765	cubic meters	m ³
NOTE: volumes greater than 1000 L shall be shown in m ³				
MASS				
oz	ounces	28.35	grams	g
lb	pounds	0.454	kilograms	kg
T	short tons (2000 lb)	0.907	megagrams (or "metric ton")	Mg (or "t")
TEMPERATURE (exact degrees)				
°F	Fahrenheit	5 (F-32)/9 or (F-32)/1.8	Celsius	°C
ILLUMINATION				
fc	foot-candles	10.76	lux	lx
fl	foot-Lamberts	3.426	candela/m ²	cd/m ²
FORCE and PRESSURE or STRESS				
lbf	poundforce	4.45	newtons	N
lbf/in²	poundforce per square inch	6.89	kilopascals	kPa

TABLE OF CONTENTS

	Page
INTRODUCTION	1
Research Need	1
Research Objective	4
Research Approach	4
BACKGROUND	7
Design Methods	7
Load and Resistance Factor Rating	8
<i>Design Load Rating</i>	9
<i>Legal Load Rating</i>	10
Load Testing of Bridges	11
<i>Destructive vs. Non-destructive Load Testing</i>	13
<i>Proof vs. Diagnostic Load Testing</i>	13
Finite Element Modeling of Bridges	14
BRIDGE DESCRIPTION	17
Bridge Location	17
Bridge Detail	18
2005 Bridge Inspection	22
AASHTO LOAD RATING	24
RISA Bridge Model	24
Dead Load Analysis	25
Live Load Analysis	26
Bridge Rating using LRFR Method	30
<i>Equivalent Width</i>	30
<i>Nominal Resistance</i>	31
<i>Design Load Rating</i>	32
<i>Legal Load Rating</i>	34
<i>Rating Factors</i>	35
DIAGNOSTIC LOAD TEST	37
Test Equipment	37
<i>BDI Strain Transducers</i>	37
<i>BDI-STS II Modules and Power Unit</i>	38
<i>BDI Autoclicker</i>	39
Test Details	40
<i>Instrumentation Plan and Installation</i>	40
<i>Test Truck Configuration and Application</i>	43
<i>Load Test Execution</i>	45
Post-Processing of Strain Data	46
EVALUATION OF SLAB STIFFNESS	49
Theoretical Neutral Axis Positions	49
<i>Uncracked Section Analysis</i>	50
<i>Cracked Section Analysis</i>	51
Experimental Neutral Axis Positions	52

Theoretical vs. Experimental Neutral Axis Positions	54
Final Remarks	57
FINITE ELEMENT MODEL	61
Model Description	61
<i>Material Properties and Element Definition</i>	61
<i>Mesh Configuration and Boundary Conditions</i>	61
Application of Live Load	63
EVALUATION OF SLAB MOMENTS	65
Slab Moments from Field Data	65
Slab Moments from Finite Element Analysis	66
Experimental vs. Analytical Moments	67
Final Remarks	80
HIGHER LEVEL LOAD RATING	82
Slab Moments under One Loaded Lane	83
Slab Moments under Multiple Loaded Lanes	86
Rating Factors from Refined Analysis	89
SUMMARY AND CONCLUSIONS	92
Summary	92
Conclusions	93
REFERENCES	97

LIST OF TABLES

		Page
Tbl. 1.	Design rating information for positive bending	33
Tbl. 2.	Design rating information for negative bending	33
Tbl. 3.	Legal load moments for positive bending	35
Tbl. 4.	Legal load moments for negative bending	35
Tbl. 5.	Rating factors for positive moment	36
Tbl. 6.	Rating factors for negative moment	36
Tbl. 7.	Total analytical vs. experimental moments for 5YD truck	73
Tbl. 8.	Total analytical vs. experimental moments for 10YD truck	80
Tbl. 9.	Equivalent strip widths from refined analysis	89
Tbl. 10.	Rating factors from approximate and refined analysis for positive moment	91
Tbl. 11.	Rating factors from approximate and refined analysis for negative moment	91

LIST OF FIGURES

		Page
Fig. 1.	Flow chart of LRFR procedure (4)	5
Fig. 2.	AASHTO design loads: (a) design truck and (b) design tandem	9
Fig. 3.	AASHTO design truck couple at 90%	10
Fig. 4.	AASHTO legal loads: (a) Type 3, (b) Type 3S2, and (c) Type 3-3 ..	11
Fig. 5.	Photograph of the Tortugas Arroyo slab bridge	17
Fig. 6.	Location of the Tortugas Arroyo slab bridge	17
Fig. 7.	Cross-section of Bridge 7270 at pier location	18
Fig. 8.	Construction joint of Bridge 7270: (a) design details and (b) top view	19
Fig. 9.	Elevation view of Bridge 7270	20
Fig. 10.	Connection between slab and supports of Bridge 7270	20
Fig. 11.	Bottom reinforcing layout of Bridge 7270	21
Fig. 12.	Top reinforcing layout of Bridge 7270	22
Fig. 13.	Slab cross-section for RISA model	25
Fig. 14.	Longitudinal view of RISA model	25
Fig. 15.	RISA model under dead load	26
Fig. 16.	Moment envelope under dead load	26
Fig. 17.	Lane load pattern for maximum positive moment: (a) 1st & 3rd spans and (b) 2nd and 4th spans	27
Fig. 18.	Positive moment envelope due to lane load	27
Fig. 19.	Lane load pattern for maximum negative moment: (a) 1st pier, (b) 2nd pier, and (c) 3rd pier	28
Fig. 20.	Negative moment envelope due to lane load	28
Fig. 21.	Moment envelopes due to HS20 truck and design tandem	29

Fig. 22.	Moment envelopes due to legal trucks	34
Fig. 23.	BDI intelliducer assembly (19)	37
Fig. 24.	BDI intelliducer with extension (19)	38
Fig. 25.	BDI-STS II module (19)	39
Fig. 26.	BDI autoclicker assembly (19)	40
Fig. 27.	Instrumented sections of slab in (a) span 1 and (b) span 2	41
Fig. 28.	Gage layout at (a) midspan and (b) pier sections	42
Fig. 29.	View of installed gages on bottom side of span 1	42
Fig. 30.	Installation of BDI intelliducer (with extension)	43
Fig. 31.	Axle weights and spacings for (a) 5YD and (b) 10 YD test trucks ...	44
Fig. 32.	Transverse paths of test trucks	45
Fig. 33.	Load test in progress	46
Fig. 34.	Representative strain readings at midspan section M1: (a) gage pair and (b) single gage	48
Fig. 35.	Representative strain readings at pier section P1: (a) gage pair and (b) single gage	48
Fig. 36.	Effective reinforcement layout at midspan sections	50
Fig. 37.	Transformed uncracked section at midspan locations	50
Fig. 38.	Transformed cracked section at midspan locations	51
Fig. 39.	Theoretical neutral axis depths along bridge length	52
Fig. 40.	Assumed strain distribution between gage pair readings at midspan sections	53
Fig. 41.	Averaged range of strain measurements for neutral axis evaluation at midspan section M1	54
Fig. 42.	Neutral axis positions for 5YD truck at (a) midspan section M1 and (b) pier section P1	55
Fig. 43.	Neutral axis positions for 5YD truck at (a) midspan section M2 and (b) pier section P2	56
Fig. 44.	Neutral axis positions for 10YD truck at (a) midspan section M1 and (b) pier section P1	58
Fig. 45.	Neutral axis positions for 10YD truck at (a) midspan section M2 and (b) pier section P2	59
Fig. 46.	Finite element model of Bridge 7270	62
Fig. 47.	Nodal loads applied to finite element model representing (a) 5YD truck and (b) 10YD truck	64
Fig. 48.	Finite element model loaded with 5YD test truck	66
Fig. 49.	Slab moments for first path of 5YD truck: (a) first span and (b) second span	68
Fig. 50.	Slab moments for second path of 5YD truck: (a) first span and (b) second span	69
Fig. 51.	Slab moments for third path of 5YD truck: (a) first span and (b) second span	70
Fig. 52.	Slab moments for fourth path of 5YD truck: (a) first span and (b) second span	71
Fig. 53.	Slab moments for fifth path of 5YD truck: (a) first span and (b) second span	72

Fig. 54.	Slab moments for first path of 10YD truck: (a) first span and (b) second span	75
Fig. 55.	Slab moments for second path of 10YD truck: (a) first span and (b) second span	76
Fig. 56.	Slab moments for third path of 10YD truck: (a) first span and (b) second span	77
Fig. 57.	Slab moments for fourth path of 10YD truck: (a) first span and (b) second span	78
Fig. 58.	Slab moments for fifth path of 10YD truck: (a) first span and (b) second span	79
Fig. 59.	Critical longitudinal position of design tandem for positive moment at first midspan	83
Fig. 60.	Transverse positions of design tandem for positive moment	84
Fig. 61.	Slab moments due to design tandem at first midspan	84
Fig. 62.	Critical longitudinal position of design truck for negative moment at first pier	85
Fig. 63.	Slab moments due to HS20-14 design truck at first pier	86
Fig. 64.	Vehicle live load configurations for (a) one, (b) two, and (c) three loaded lanes	87
Fig. 65.	Slab moments from finite element analysis for (a) first span and (b) second span	88

INTRODUCTION

RESEARCH NEED

Highway bridges provide service around the United States on routes having varying traffic loads. To provide an efficient and safe highway system, it is important to maintain and update bridge condition records. This is accomplished by conducting field inspections and capacity evaluations on a regular basis. The Federal Highway Administration (FHWA) established the National Bridge Inspection Standards (NBIS) in 1971 to provide a guide for the inspection and rating of existing bridges. These standards came about as a result of the 1967 Silver Bridge collapse in West Virginia that killed 46 people. Prior to the collapse, new bridge construction was thriving and little attention was placed on the inspection and maintenance of in-service bridges (1).

According to the 2006 report of the National Bridge Inventory (NBI), there are approximately 600,000 bridges on public roads throughout the United States (2). To ensure bridges are safe for traffic, the NBIS require that every bridge be inspected no less frequently than every two years. Information about the bridge such as age, construction materials, deterioration, length of service, and damage are different factors collected during an inspection that all play an important role in determining the bridge's load capacity. Due to location and traffic demand, many bridges will experience an increase in the quantity and magnitude of heavy truck loads that may ultimately affect their service life.

The state of New Mexico has close to 3,850 bridges on file according to the 2006 NBI report (2). Approximately half provide service on heavy traffic routes including interstate and state highways. Furthermore, roughly a quarter were built between 1931 and 1956, a period when bridge construction was substantial. About 11% of New Mexico bridges (i.e., 406

bridges) are cataloged as structurally deficient (SD); the national average of SD bridges is about 12%. An SD bridge is defined as one where “1) significant load carrying elements are found to be in poor or worse condition due to deterioration and/or damage, or 2) the adequacy of the waterway opening provided by the bridge is determined to be extremely insufficient to the point of causing intolerable traffic interruptions” (1). Furthermore, an SD bridge has a deck, superstructure, or substructure in poor condition. About 8% of New Mexico bridges (i.e., 317 bridges) are cataloged as functionally obsolete (FO); the national average of FO bridges is about 16%. An FO bridge is defined as one with “deck geometry, load carrying capacity, clearance or approach roadway alignment that no longer meets the criteria for the system of which the bridge is a part” (1). More specifically, the FO classification arises when the lane widths, shoulder widths, or vertical clearances of a bridge are inadequate to serve the traffic demand. As a final point, approximately 19% of New Mexico bridges (i.e., 723 bridges) are classified as SD or FO, which is below the national total of 26%. An SD or FO bridge is not necessarily unsafe; however, techniques beyond those applied during the normal inspection and rating process are needed to assess the bridge’s true condition and load capacity.

New Mexico bridges are built of different materials including concrete, steel, and wood. Concrete is the most common material used in the state; over fifty percent of the state’s bridges are concrete. Of the total of 2062 concrete bridges, 356 are reinforced concrete slab (RCS) bridges, 29 of which are structurally deficient and 30 are functionally obsolete (2). An RCS bridge is designed primarily to span in the direction parallel to traffic and may consist of either simple or continuous spans. There are a total of 267 simple-span and 1,795 continuous-span concrete bridges in New Mexico. A simple-span RCS bridge is one having

joints at the abutments and pier locations. This type of bridge is statically determinate and easy to analyze but is not as efficient as a continuous-span RCS bridge which can sustain negative moments at the intermediate supports or piers. This continuity results in smaller positive moments compared to a simple-span configuration. Consequently, a continuous-span RCS bridge is a more economical and durable design but requires a more complicated, indeterminate analysis. A continuous-span RCS bridge has several advantages compared to a simple span. To start with, a smaller slab depth and less steel reinforcement is needed which reduces the structure weight and overall cost. This bridge type also experiences smaller deflections under loading due to the higher stiffness and less deterioration because of the elimination of deck joints over the piers. Furthermore, a continuous-span RCS bridge has more redundancy and greater load capacity than a simple span.

This research project is founded on the fact that the state of New Mexico may be overly restrictive to the trucking industry on interstate highways I-10, I-25, and I-40. On these routes, there are a significant number of RCS bridges that rate low when evaluated based on design assumptions and procedures set forth by the American Association of State Highway and Transportation Officials (AASHTO). Because of the state's need to provide an efficient and safe highway system, it is therefore necessary to determine a more realistic load rating for bridges that are susceptible to load restrictions. The load rating of a RCS bridge is heavily based on the distribution of live load. However, there is a lack of research focused on the application of higher level techniques to evaluate the live-load effects of RCS bridges, especially those with continuous spans.

RESEARCH OBJECTIVE

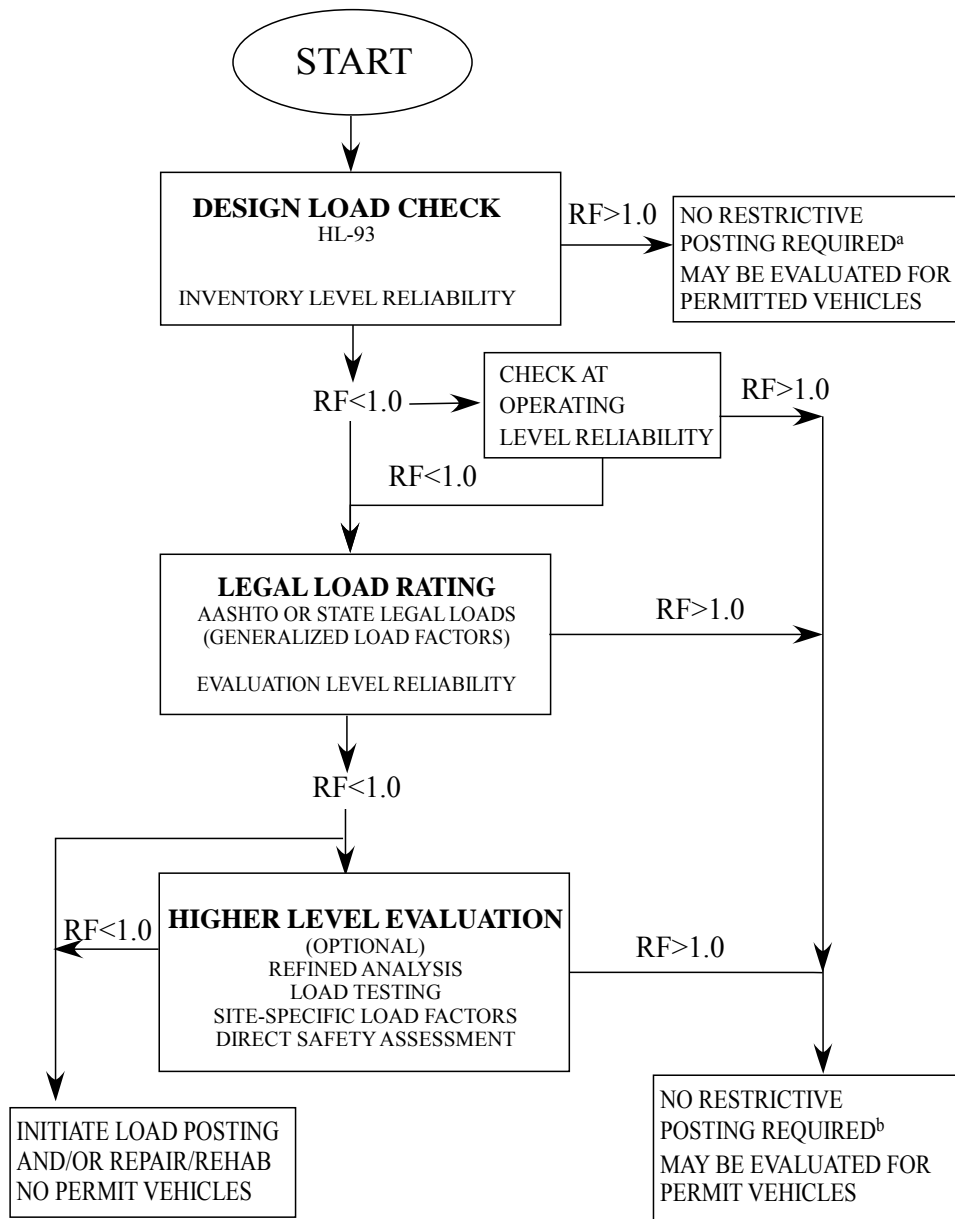
The primary objective of the research reported herein is to employ higher level evaluation techniques to determine a more realistic load rating for continuous-span RCS bridges. In particular, attention is given to more accurately evaluating the live-load effects (mainly the lateral load distribution factor) for use in the AASHTO rating analysis.

A proven approach for evaluating the response of a bridge under vehicular live loads is to perform a diagnostic load test. The measurements from the load test are subsequently used to develop and validate a finite element model from which the live-load effects may be determined. Previous studies have shown that the equivalent width for a RCS bridge, for example, determined based on field tests and advanced analysis are greater than those specified by AASHTO (3). An increase in the equivalent width signifies a decrease in the live-load effects per foot of slab in the transverse direction, which in turn increases the load rating factor.

RESEARCH APPROACH

To accomplish the objective of this project, the load rating procedure given in the *AASHTO Manual for Condition Evaluation and Load and Resistance Factor Rating (LRFR) of Highway Bridges* (4) was followed. This manual will be hereafter referred to as the LRFR Manual. Figure 1 provides the flow chart of the LRFR procedure and the discussion provided in the ensuing paragraphs references this flow chart.

The first step, which represents the START of the chart, was to select a representative continuous-span RCS bridge for evaluation. The New Mexico Department of Transportation (NMDOT) provided the location and year-built of several candidate bridges of this type throughout the state.



^a For AASHTO legal loads and state legal loads within the LRFD exclusion limits.

^b For AASHTO legal loads and state legal loads having only minor variations from the AASHTO legal loads.

FIGURE 1. Flow chart of LRFR procedure (4).

After the bridge specimen was selected, information including the original design plans and the most recent bridge inspection report were obtained.

The second step, which corresponds to the DESIGN LOAD CHECK and LEGAL LOAD RATING parts of the chart, was to perform a preliminary LRFR analysis of the selected bridge. The *Reinforced Concrete Slab Bridge* example given in the LRFR Manual was used as a guide for this analysis. This evaluation provided the design and legal load ratings of the bridge and was carried out using the original design characteristics including the main reinforcement layout, material strengths, and geometry of the bridge.

The third step, which corresponds to the first part of the HIGHER LEVEL EVALUATION, was to perform a diagnostic load test. The field test was planned based on the results from the preliminary LRFR analysis and the General Load-Testing Procedure given in the LRFR Manual (Appendix A.8.1). The fourth step, which also is part of the HIGHER LEVEL EVALUATION, was to develop a finite element model using the SAP2000 software program (5). The bridge specimen was modeled based on findings and recommendations from previous finite element studies of RCS bridges (6).

The last step was to complete the HIGHER LEVEL EVALUATION by re-evaluating the live-load effects via the field-verified finite element model and adjusting the original LRFR analysis results. Previous studies have found that the AASHTO equivalent width used for design overestimates the live-load moments in the slab (3). Thus, using the equivalent width from field testing and finite element analysis may increase the load rating considerably.

BACKGROUND

A highway bridge is an important element in a transportation system. It allows vehicular traffic to travel through a grade separation in a comfortable and safe manner. Through the years, the AASHTO specifications for bridge design have changed to adapt to current vehicular loading, engineering materials, construction techniques, and design philosophies. Load-rating procedures have also advanced to accommodate modern conditions.

This chapter provides general background related to the design and rating of highway bridges with emphasis on RCS bridges. A brief description of the AASHTO design methods and their relation to the load-rating process is first given. Then, the LRFR method is discussed, which is the most current method for load rating of bridges. Finally, the use of higher level techniques (including load testing and finite element modeling) in the field of bridge evaluation is covered.

DESIGN METHODS

The Allowable Stress Design (ASD) method was first developed in the early 1900's (1). In this method, the stresses in the bridge members under service loads must not exceed the strength of the material with an appropriate factor of safety (e.g., 0.55 times the yield strength of steel). Next, the Load Factor Design (LFD) method was adopted in the 1970's (1). In this method, the design strength (i.e., the product of the resistant factor and the nominal member capacity) must exceed the force effect caused by factored loads. The most recent method is Load and Resistance Factor Design (LRFD); the first edition of the LRFD Bridge Design Specifications came out in 1994 and the third edition was published in 2004 (7). The LRFD approach provides a more uniform level of safety for different limit states and bridge

types. As of October 2007, the FHWA requires that state Departments of Transportation use LRFD for all new bridge design using federal-aid funds.

Complementary to the three design methods just discussed, there is an associated load rating method: the ASR (Allowable Stress Rating), LFR (Load Factor Rating), and LRFR (Load and Resistance Factor Rating) method. The LRFR method that is discussed in the following section was employed in this research project.

LOAD AND RESISTANCE FACTOR RATING

The LRFR Manual was first published in 2003 (4) and is closely tied to the LRFD Bridge Design Specifications (7). The general LRFR equation is used to calculate a rating factor (RF) as follows:

$$RF = \frac{C - \gamma_{DC} \times DC - \gamma_{DW} \times DW}{\gamma_L \times LL \times (1 + IM)} \quad (1)$$

The capacity (C) of the bridge component is the product of the nominal resistance (R_n) and three factors: the resistance (ϕ), condition (ϕ_C), and system (ϕ_S) factors as shown below.

$$C = R_n \times \phi \times \phi_C \times \phi_S \quad (2)$$

In this equation, the product of the condition and system factors shall not be lower than 0.85 (i.e., $\phi_C \times \phi_S \geq 0.85$). Dead load effects are divided into two parts: structural components and attachments (DC) and wearing surface and utilities (DW). For reinforced concrete bridges, the dead load factors for structural components and attachments (γ_{DC}) and wearing surface and utilities (γ_{DW}) have a value of 1.25 and 1.5, respectively, for the Strength I limit state.

The LRFR Manual provides different live loads depending on the stage of the rating analysis. The first stage of the analysis is the *design load rating*, which specifies a live-load factor (γ_L) of 1.75 for inventory and 1.35 for operating. The second stage is the *legal load*

rating, which specifies a live-load factor based on the current ADTT (Average Daily Truck Traffic) on the bridge. A dynamic load factor (IM) of 33% is applied to the live-load effects (LL) caused by the vehicular loading. Further details related to the *design load rating* and *legal load rating* are given in the following sections.

Design Load Rating

In the *design load rating* stage, the bridge is evaluated under HL-93 loading at the Strength I limit state. The HL-93 loading consists of a design truck or tandem (see Figure 2), whichever produces the larger force effects, combined with the effects caused by the design lane load of 640 lb/ft. An additional vehicular live-load combination is specified to evaluate the negative moment between points of contraflexure and the reactions at the interior supports. The LRFD Article 3.6.1.3.1 (7) describes this combination to be “90% of the effect of two design trucks spaced a minimum of 50 ft between the lead axle of one truck and the rear axle of the other truck” as shown in Figure 3. Note that the middle-to-back axle spacing of both design trucks is 14 ft. and the truck effects are combined with those caused by 90% of the design lane load. This combination is really not a concern for RCS bridges because of the short span lengths.

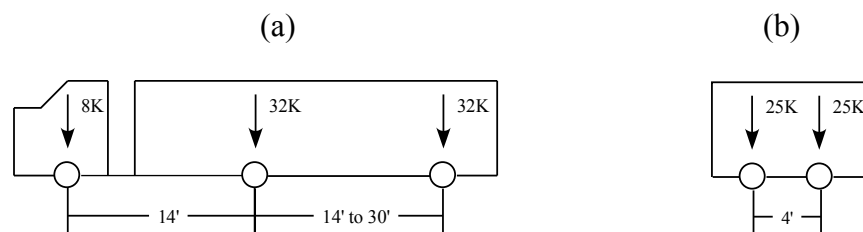


FIGURE 2. AASHTO design loads: (a) design truck and (b) design tandem.

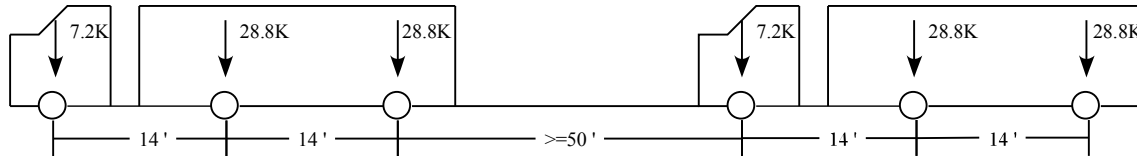


FIGURE 3. AASHTO design truck couple at 90%.

The LRFR Article 6.4.3 (4) specifies that the *design load rating* be performed at an inventory and operating level. Bridges that have an inventory rating factor less than one but a operating level greater than one are “safe for AASHTO legal loads and state legal loads having only minor variations from the AASHTO legal loads” (4). No additional evaluation is necessary unless the state legal loads differ substantially from AASHTO legal loads, which is not the case in New Mexico. Should the operating rating factor be less than one, a *legal load rating* must be performed which is discussed next.

Legal Load Rating

As defined in LRFR Article 6.4.4 (4), a *legal load rating* analysis is done to determine the single safe load capacity of a bridge at the Strength I limit state for a given legal load configuration. The three AASHTO legal loads that are considered include the Type 3, Type 3S2, and Type 3-3 (see Figure 4). These loads apply to all span lengths but with only one lane loaded. If the span lengths are long (i.e., greater than 200 ft), AASHTO also requires that two additional legal load configurations (not shown) be considered. Again, this extra legal loading is not a concern for short span bridges.

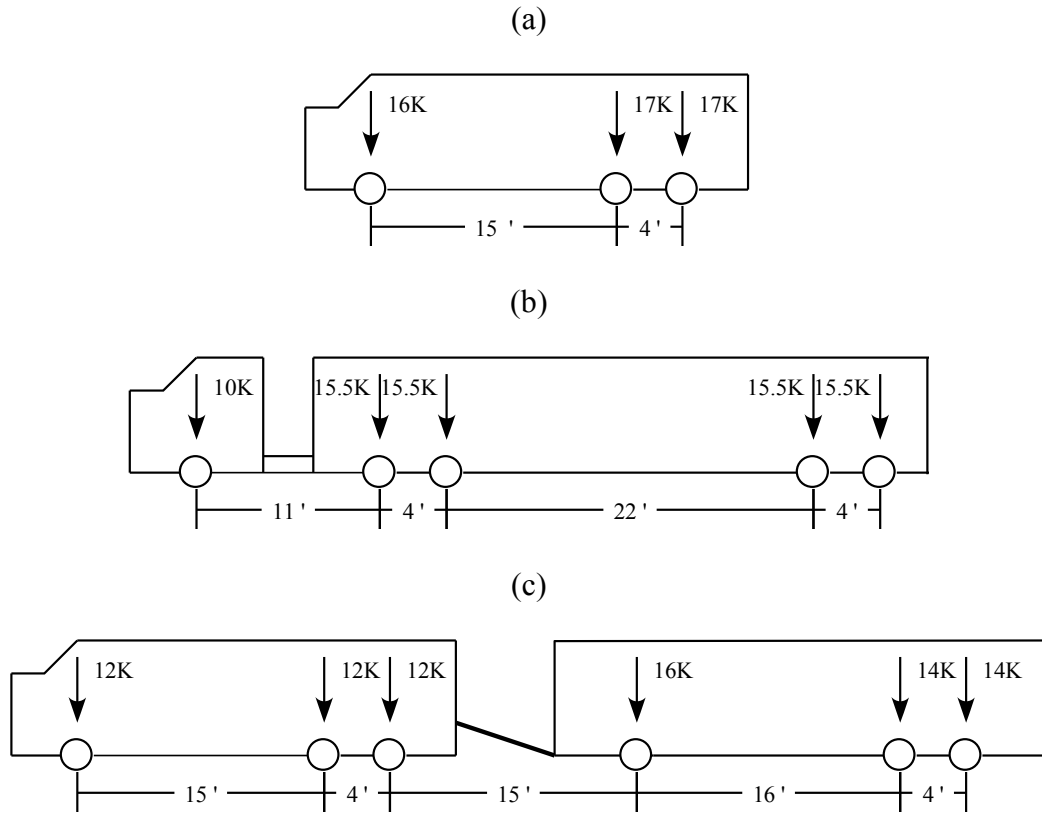


FIGURE 4. AASHTO legal loads: (a) Type 3, (b) Type 3S2, and (c) Type 3-3.

LOAD TESTING OF BRIDGES

The AASHTO approximate methods of analysis are primarily used to determine the live-load effects in the denominator of the LRFR equation (see Equation 1). These methods frequently overestimate the live-load effects, resulting in a low load rating for a RCS bridge (8). Alternatively, the LRFR Article 6.3.4 states that field testing may be used to “confirm the precise nature of load distribution to the main load carrying members of a bridge” (4). Field testing is an attractive option since it can be used to validate a new mathematical bridge model developed using refined methods of analysis such as the finite element method. Advanced models may then be used to re-evaluate the live-load response of the bridge to arrive at more realistic load rating factors (4).

Bridge capacity is often underestimated because the design-based assumptions used in the AASHTO load rating process sometimes do not reflect the real characteristics of the bridge. Some of the factors not commonly considered in design but that could affect the actual behavior of a bridge include: unintended composite action; unintended continuity and/or fixity; and participation of nonstructural members (9). Neglect of factors such as these may ultimately result in an overly conservative estimate of load capacity. For example, a diagnostic field test was performed in the state of Delaware on a non-composite slab-girder bridge built in 1939 (10). The bridge was classified as being in poor condition due to visible reinforcement deterioration and as a result, heavy truck traffic was restricted. Subsequently, analysis of the diagnostic test data determined that the bridge had a more favorable load distribution than that determined by AASHTO. As a result, the load restriction was removed from the bridge as well as several other bridges in the state after implementation of field testing in the rating process (10).

The parameter in the LRFR equation of primary interest in this RCS bridge study is the equivalent width used to determine the live-load effects. This width is used to distribute the longitudinal live-load moments across the cross-section of the slab (3). The LRFD Bridge Design Specifications provide empirical formulas to calculate the equivalent width. These AASHTO formulas “reduce the two-way bending problem into a beam (one-way) bending problem” and also do “not consider other load-carrying mechanisms, the effect of geometry, and boundary conditions” (6). The approach taken in the present study is to apply higher level evaluation techniques to re-compute the equivalent width.

Destructive vs. Non-destructive Load Testing

To obtain a more realistic estimate of bridge capacity, especially for older bridges, different experimental techniques have been employed. There are two broad categories of load tests, destructive and non-destructive, that are used to evaluate the safe load capacity of a bridge. Destructive testing is less common since the bridge usually needs to be decommissioned, awaiting replacement. A destructive test can determine the bridge's ultimate load capacity. Previous studies of RCS bridges built during the 1960's have found the measured load capacity to be as much as eight times the capacity calculated using AASHTO design-based procedures (9). The principal reason for the discrepancy between measured and AASHTO capacities was the higher actual strengths of the bridge materials (concrete and steel) compared to the minimum design values.

The approach more frequently employed to determine a bridge's load capacity is a non-destructive load test. This type of test provides a fast and practical option for measuring the live-load elastic response of a bridge under different load conditions and estimating its true load capacity. In a non-destructive test, the bridge's response under vehicular loading is measured with instruments such as strain gages and/or deflection transducers. Analysis of the test measurements can provide a more accurate realistic picture of the load distribution and boundary conditions of a bridge. This information can then be used to establish the size and configuration of vehicular live loads that are safe to cross the bridge (9).

Proof vs. Diagnostic Bridge Testing

There are two types of non-destructive load tests commonly used to evaluate the live-load response of an existing bridge: proof and diagnostic. The objective of a proof test is to evaluate the bridge response until a target proof load is reached, preferably without damaging

the structure. This type of test directly establishes the safe load capacity of the bridge; extrapolation to a load higher than that applied in the test is not necessary. This test is performed by applying increasing static loads below the elastic load limit using a special truck. However, only a few states, namely Alabama, Florida and Michigan have this capability in house.

The objective of a diagnostic test is to obtain information about the bridge response at a load well below the elastic limit. The loads can be applied to the bridge in two different ways: pseudo-static (in which the vehicular load traverses the bridge at crawl speed) and dynamic (in which the vehicular load crosses the bridge at normal speed to cause vibrations). As stated in LRFR Article 8.4.1.1, “diagnostic tests serve to verify and adjust the predictions of an analytical model...which are then used to calculate load-rating factors” (4). The major tasks involved in performing a diagnostic load test include instrumentation installation, traffic control, load truck operation, and data collection, all of which require dedicated personnel to ensure the test is a success. The time required to complete a test depends on the bridge characteristics such as geometry, location, traffic flow, and alternative routes.

Due to the continual advancement of measurement and data acquisition technology, the cost of performing a diagnostic load test has reduced considerably (10). A study by Iowa State University concluded that those involved in this type of testing find it to be cost effective (11). However, the initial investment required to establish diagnostic testing capabilities has kept some agencies from adopting the technique.

FINITE ELEMENT MODELING OF BRIDGES

A finite element model that is validated based on diagnostic load test data can provide a useful and accurate representation of the bridge response under vehicular live load. The

model can be originally developed based on the geometry, boundary conditions, and material properties given in the design plans (if available) and adjusted if necessary. Analyses under different load configurations can then be run to evaluate the transverse and longitudinal load distribution characteristics of the bridge (12). Furthermore, the advanced model can serve as an accurate record of the bridge behavior that can be further evaluated under other load configurations in the future (13).

There are different finite element programs available, each of which has distinct menus and tools for developing two- or three-dimensional models. A three-dimensional model is essential for RCS bridges to capture the two-way bending behavior (6). Nonstructural members such as curbs and barriers may also be included in a three-dimensional model. However, a two-dimensional model is always useful for checking the results of a three-dimensional model.

A few studies (3, 6, 8) have applied diagnostic load testing and/or refined methods of analysis to evaluate RCS bridges. The most common method of modeling a RCS bridge is using shell elements. The element characteristics specified in a shell model are simple and include modulus of elasticity, Poisson's ratio, and the slab thickness. The shell elements may be three or four node, but the latter is preferred. In the studies by Amer et al. (3), the affect of several parameters (including span length, bridge width, slab thickness, and edge beam size) on the equivalent width of RCS bridges was evaluated. This study confirmed that the slab thickness, which is not a factor in the AASHTO equivalent width equations, does not have a significant effect on the equivalent width. The edge beam is also not taken into account in the AASHTO equations, but was found to have a significant affect. The study by Mabsout et al. (6) also found that the edge beam contribution is important and also that the AASHTO LRFD

Bridge Design Specifications overestimate the slab moments for normal traffic on RCS bridges. In the study by Saraf (8), three continuous RCS bridges with different levels of deterioration were evaluated and the original AASHTO rating factors were improved. In conclusion, there is strong evidence that the equivalent width obtained using higher level techniques are greater than that calculated using the AASHTO equations which will positively influence the bridge capacity.

BRIDGE DESCRIPTION

BRIDGE LOCATION

The RCS bridge evaluated in this research project is shown in Figure 5. It is located in Las Cruces, New Mexico and was built in 1972 on Stern Dr. (also called the south frontage road) over Tortugas Arroyo. The NMDOT number for the frontage road bridge is 7270; it runs parallel to two similar bridges, numbered 7268 and 7269, on Interstate-10 (I-10) as shown in Figure 6.



FIGURE 5. Photograph of the Tortugas Arroyo slab bridge.

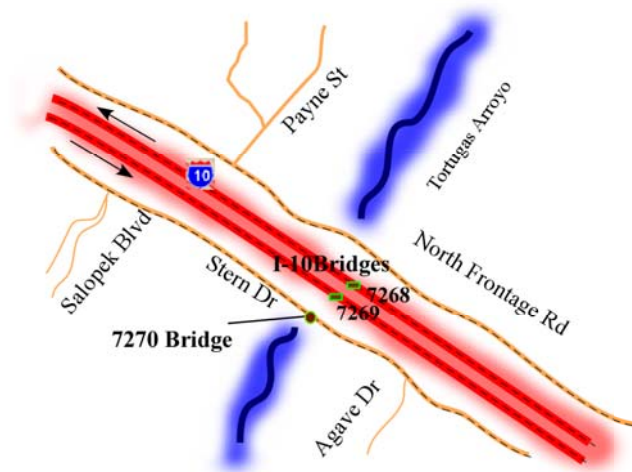


FIGURE 6. Location of the Tortugas Arroyo slab bridge.

The serviceability and safety evaluation of the I-10 bridges is very important since this interstate provides highway transportation for eight southern states. Due to traffic control issues, the decision was made to load test the frontage road bridge (Bridge 7270) located on Stern Dr. which has a much lower traffic volume. According to the 2005 field inspection, Bridge 7270 had an Average Daily Traffic (ADT) of 95 during 2002.

BRIDGE DETAIL

Bridges 7268, 7269, and 7270 were all designed and constructed with the same material properties, reinforcing layouts, slab thickness, and span lengths. The design live load for these bridges was an HS20-44 truck which was the requirement of the AASHTO Standard Specifications in 1969. There is one major difference between the interstate and frontage road bridges. The widths of the slab and the roadway for the I-10 bridges are 45 ft. and 42 ft., respectively, whereas Bridge 7270 has a slab width of 43 ft. and a roadway width of 40 ft. as shown in Figure 7. The reason for this difference in width is that the I-10 bridges serve one-way traffic traveling at 65 mph on two lanes and the south frontage road bridge serves two-way traffic traveling at 30 mph on one lane in each direction.

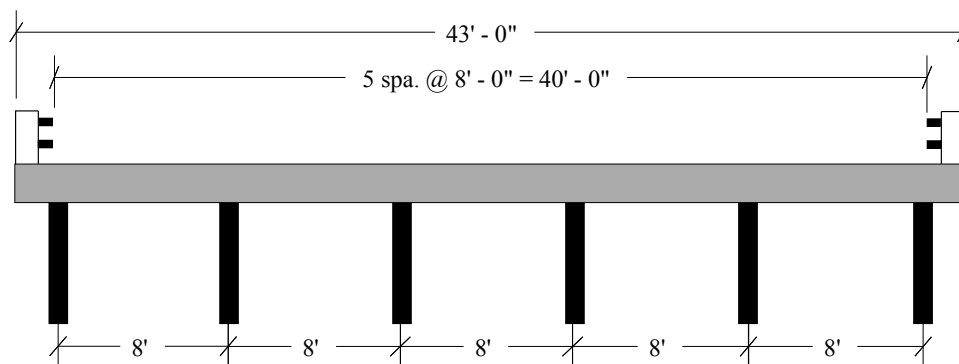


FIGURE 7. Cross-section of Bridge 7270 at pier location.

Bridge 7270 is a RCS, continuous over seven spans. The slab was cast-in-place in two sections with a total area of 7,181 sq. ft. Design details and a top view of the construction joint are shown in Figure 8. The two end spans of the bridge have a length of 20 ft. and the five interior spans have a length of 25 ft. (see Figure 9). Each pier has six 12 in. diameter, steel tube columns with a center-to-center spacing of 8 ft. Connection details between the slab and the supports (at the abutment and pier) are shown in Figure 10. All the interior spans were constructed with 0.25 in. camber to account for dead load deflection. The metal bridge railings are classified as A500 Grade B with a center-to-center post spacing of 10 ft.

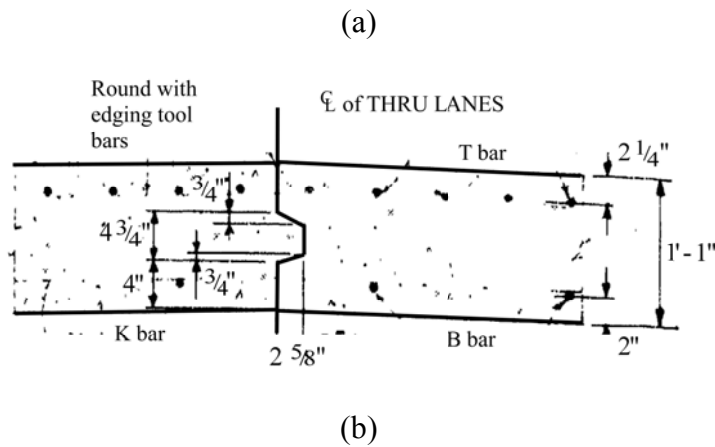


FIGURE 8. Construction joint of Bridge 7270:
(a) design details and (b) top view.

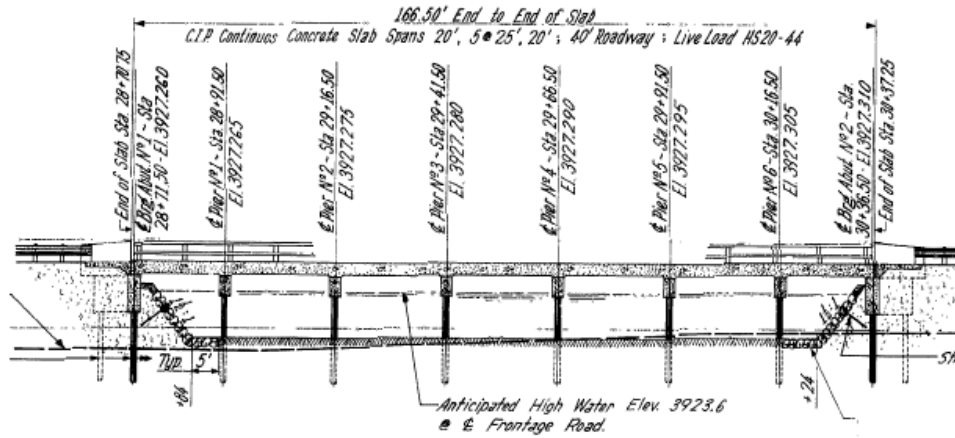


FIGURE 9. Elevation view of Bridge 7270.

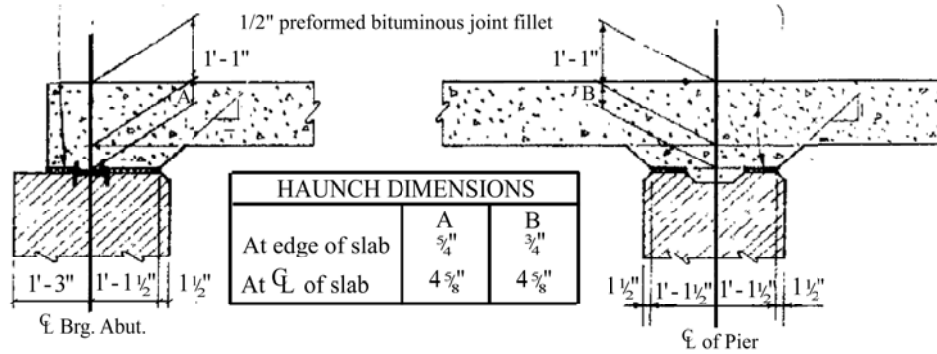


FIGURE 10. Connection between slab and supports of Bridge 7270.

The main bridge materials are concrete and reinforcing steel. The concrete is NMDOT Class A concrete which has a 28-day compressive strength of 3000 psi and the reinforcing bars are Grade 40 steel. The bridge has a slab thickness of 13 in. and is longitudinally reinforced with the centroid of the top steel mat located 2.25 in. below the top of the slab and the centroid of the bottom steel mat located 2 in. above the bottom of the slab. The top and bottom main reinforcing bars are oriented parallel to the traffic direction and consist of three different sizes (#7, #8, and #9 bars). The transverse reinforcement, oriented perpendicular to traffic, also consists of three different bar sizes (#4, #5, and #6 bars).

The bridge has a similar longitudinal bottom steel layout in the 20-ft. end spans and the 25-ft. interior spans as shown in Figure 11. The layout mainly consists of alternating #7, #8, and #9 bars, each with a center-to-center spacing of 18 in.

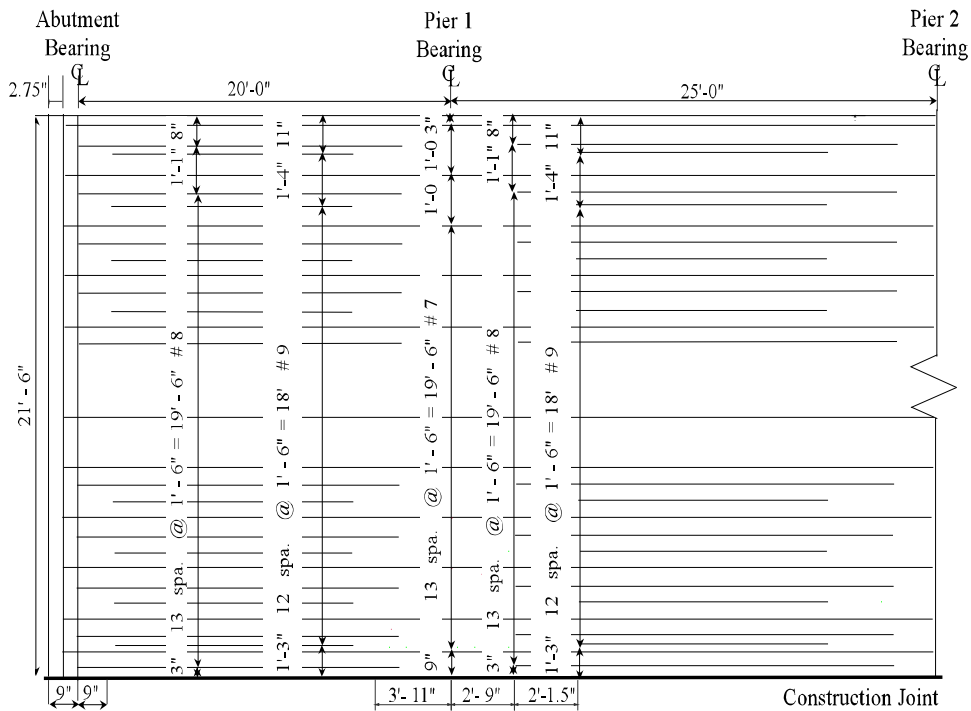


FIGURE 11. Bottom reinforcing layout of Bridge 7270.

On the other hand, there are two different longitudinal top steel layouts; the layouts for the first two spans are shown in Figure 12. The first pier steel layout consists of alternating #7, #8, and #9 bars, each with a center-to-center spacing of 18 in. The second pier steel layout consists of altering #7, #9, and #9 bars, with the same center-to-center spacing as the first pier. The bottom and the top reinforcing bars are tied by No. 9 gage wires that are used over the entire width of the slab.

predicted an ADT of 126 for 2022 and reported the bridge components to be in the following conditions (14):

- concrete slab – “Top side of deck has numerous transverse and longitudinal cracks with minor honeycombing and isolated areas of delamination. Deck edges have minor vertical cracks, small spalls, and honeycombing. Underside of deck has minor leaching with rust stains along the centerline construction joint, with a satisfactory condition”.
- steel columns – “They have moderate surface rust and minor section loss where exposed by scour with an overall fair condition”.
- concrete abutment – “Concrete walls have minor vertical and map cracks with leaching, water stains, rust stains, and honeycombing with an overall satisfactory condition”.

AASHTO LOAD RATING

In this chapter, an AASHTO load rating analysis of Bridge 7270 is conducted based on the original design plans and the observations from the most recent field inspection. The A7 example, *Reinforced Concrete Slab Bridge*, from the LRFR Manual was used as a guide for this evaluation. The MathCAD13 program (16) was used to document the rating calculations because of its efficiency and capability to perform repeated calculations with changing parameters. Bridge 7270 was modeled and analyzed using version 6 of the RISA-2D program (17). This program was used to determine the moment magnitudes at critical points along the bridge length for different load combinations.

RISA BRIDGE MODEL

The AASHTO load rating started by obtaining and organizing the design and inspection information for Bridge 7270. The physical characteristics of the bridge including the span length, deck width, roadway width, material strengths, and slab thickness were needed to perform the rating analysis. This general information was entered into the MathCAD13 program at the start of the rating calculations.

The slab was modeled as a one-dimensional beam with a rectangular cross-section (width = 12 in and thickness = 13 in) as shown in Figure 13. The concrete was assumed to be uncracked in the model with a modulus of elasticity and Poisson's ratio of 3155 ksi and 0.15, respectively; steel reinforcement was ignored. Three models with different element sizes were originally developed to determine the affect on the moment magnitudes along the bridge length. It was found that the length of the element did not significantly affect the moment values; the difference in moments with the bridge modeled with 165 elements versus 7 elements was less than 1.2%.

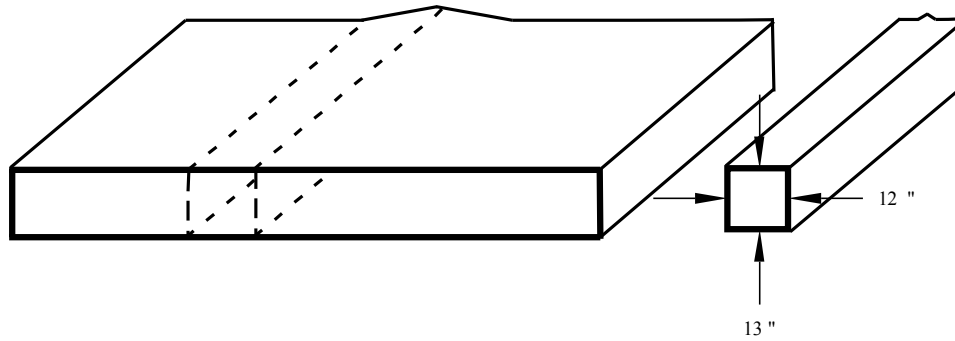


FIGURE 13. Slab cross-section for RISA model.

Thus, the final model employed was the one with 7 elements (see Figure 14) because of the many different load combinations that needed to be analyzed; the processing time for this model was also the least. Furthermore, the number of elements of this model conveniently matched the number of spans of the bridge.



FIGURE 14. Longitudinal view of RISA model.

DEAD LOAD ANALYSIS

The slab and the steel rails are the two dead load components of the structure with weights of 0.162 kip/ft and 1.39×10^{-3} kip/ft, respectively. The RISA model under the total dead load of 0.164 kip/ft is shown in Figure 15 and the resulting moment envelope for the first 100 ft. of the bridge is plotted in Figure 16. As shown in the figure, the maximum positive moment amounted to 4.55 kip-ft in the first span at a distance of 8 ft. from the abutment. In the second span, a maximum positive moment of 4.30 kip-ft occurred at a distance of 12.50 ft. from the first pier. The maximum positive moments in the third and fourth spans occurred at midspan of each span and equaled 4.22 kip-ft and 4.24 kip-ft, respectively.

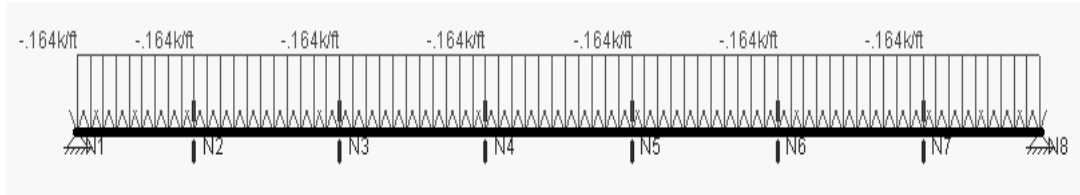


FIGURE 15. RISA model under dead load.

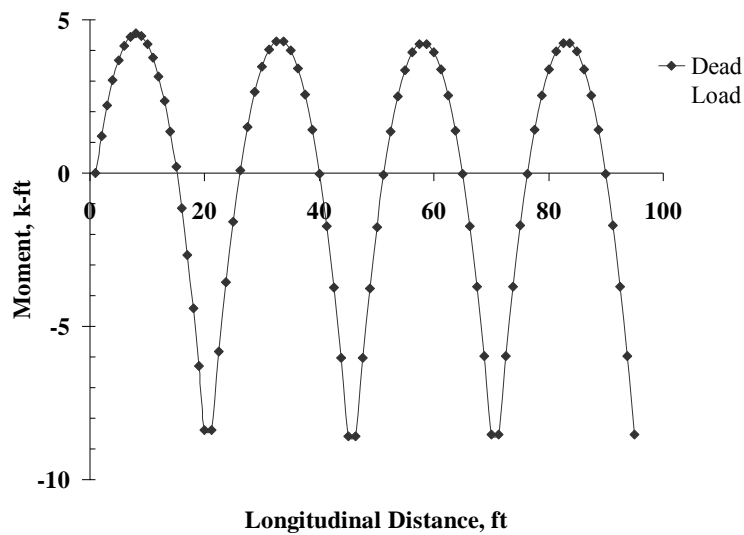


FIGURE 16. Moment envelope due to dead load.

At the second pier, located 45 ft. from the abutment, the maximum negative moment amounted to 8.59 kip-ft. The first and third piers, located 20 ft. and 70 ft. from the abutment, had maximum negative moments of 8.37 kip-ft and 8.53 kip-ft, respectively.

LIVE LOAD ANALYSIS

The live-load analysis considered two types of loading: vehicular and lane loading. The RISA model was first analyzed under lane loading equal to 0.64 kip/ft. Using influence lines, lane load patterns were determine that produced the maximum moments at different

locations along the bridge length. Two patterns were applied for positive moment; the first produced the maximum effects in the first and third spans and the second produced the maximum effects in the second and fourth spans as shown in Figure 17. The moment envelope resulting from the two lane load patterns is shown in Figure 18. As shown in the figure, the largest positive moment of 32.83 kip-ft occurred in the fourth span while the smallest positive moment of 27.63 kip-ft occurred in the first span.

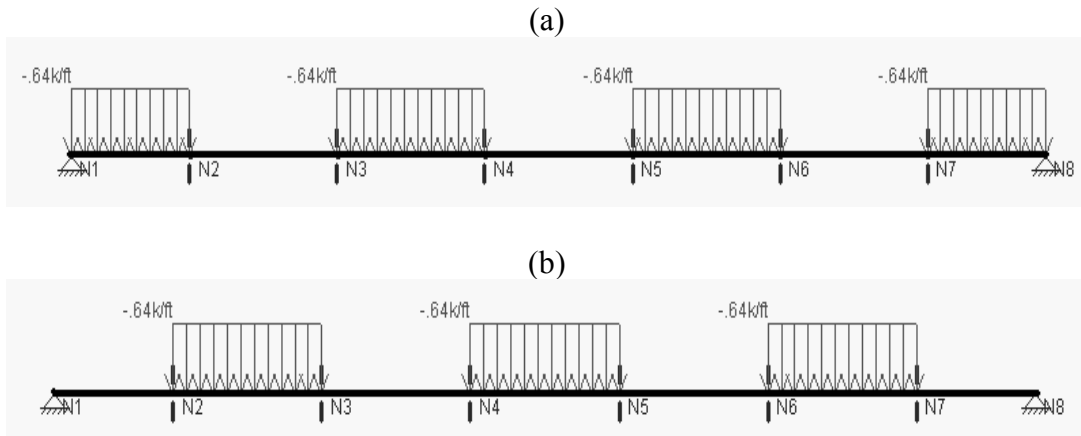


FIGURE 17. Lane load pattern for maximum positive moment: (a) 1st & 3rd spans and (b) 2nd & 4th spans.

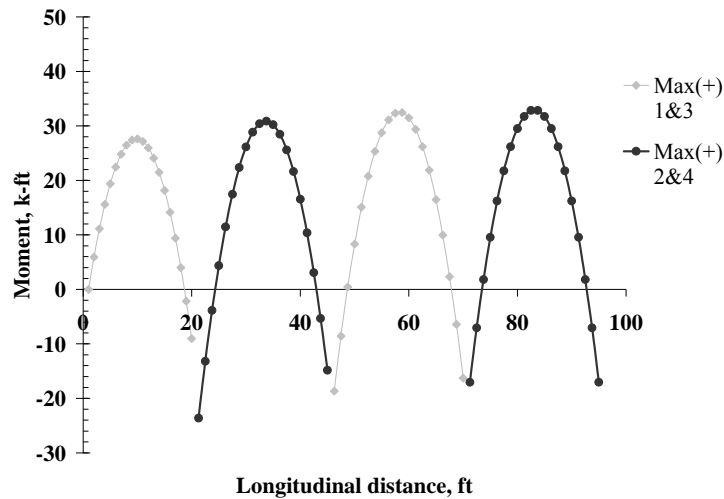


FIGURE 18. Positive moment envelope due to lane load.

Three different lane load patterns were applied to determine the maximum negative moments at the first three piers as shown in Figure 19; the results from the RISA analysis for these three patterns are plotted in Figure 20. The largest negative moment of 44.79 kip-ft occurred at the third pier and the smallest negative moment of 38.96 kip-ft occurred at the first pier.

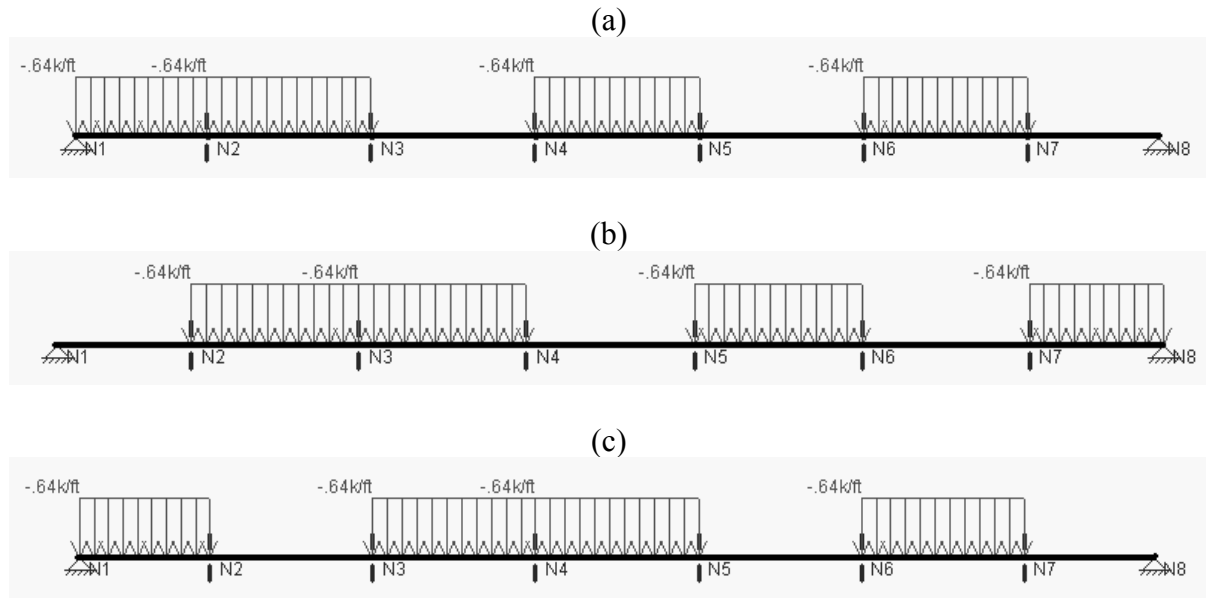


FIGURE 19. Lane load pattern for maximum negative moment: (a) 1st pier, (b) 2nd pier, and (c) 3rd pier.

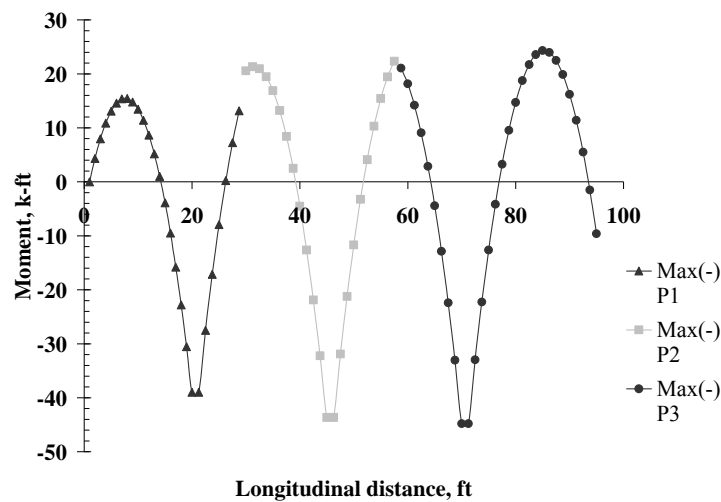


FIGURE 20. Negative moment envelope due to lane load.

Following the lane loading, the RISA model was then analyzed under the design truck (i.e., HS20) and design tandem loads as described in LRFD Articles 3.6.1.2.2 and 3.6.1.2.3, respectively. These two loads were positioned along the length of the bridge in increments of 0.5 ft. in both directions; Figure 21 shows the moment envelope for vehicular loading. The maximum moments occurred close to the midspans and piers. It is important to note that the design tandem controlled in the positive moment regions and the HS20 truck controlled in the negative moment regions. The RISA model was also analyzed under back-to-back HS20 truck loading as specified in LRFR Appendix B.6.1 for negative moment at the piers. However, this loading did not control due to the short span lengths of Bridge 7270. Furthermore, other critical longitudinal points (such as where the reinforcement changes) were also considered in the load rating analysis. The complete results of this analysis are given in Appendix A of Licon-Lozano (18).

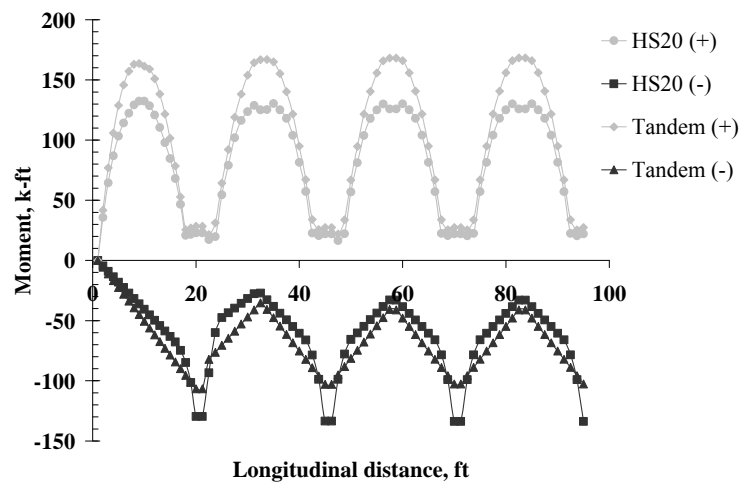


FIGURE 21. Moment envelopes due to HS20 truck and design tandem.

BRIDGE RATING USING LRFR METHOD

Equivalent Width

After the dead and live load analyses were completed, the next step was to calculate the equivalent width of longitudinal strips (interior and exterior) to obtain the live-load moment per unit width (i.e., 1 ft.) of the slab. Article 4.6.2.3 in the LRFD Specification (7) provides two equations to calculate the width of the equivalent interior strip; Equation 3 given below is used to determine the width for one lane loaded ($E_{i,1}$) and Equation 4 is used when more than one lane is loaded ($E_{i,2}$).

$$E_{i,1} = 10.0 + 5.0\sqrt{L_1 W_1} \quad (3)$$

$$E_{i,2} = 84.0 + 1.44\sqrt{L_1 W_1} \leq \frac{12.0W}{N_L} \quad (4)$$

where:

$E_{i,1}$ = equivalent width of interior strip for one lane loaded, in.

$E_{i,2}$ = equivalent width of interior strip for more than one lane loaded, in.

L_1 = modified span length (equal to the actual span but not greater than 60 ft.), ft.

W_1 = modified edge-to-edge width of bridge (equal to the actual width but not greater than 60 ft. for multilane loading and 30 ft. for single-lane loading), ft.

W = physical edge-to-edge width of the bridge, ft.

N_L = number of design lanes.

The equivalent width for the interior strip (E_i) is the smaller width resulting from Equations 3 and 4 (i.e., $E_i = \text{smaller of } E_{i,1} \text{ and } E_{i,2}$).

The width of the equivalent exterior strip (E_e) was calculated according to LRFD Article 4.6.2.1.4 (7). This article states that the exterior strip width may be taken as follows:

$$E_e = d_e + 12.0 + \frac{1}{4} E_i \leq \text{smaller of } \frac{1}{2} E_i \text{ or } 72 \text{ in.} \quad (5)$$

where:

d_e = distance between the edge of the slab to the inside face of the barrier, in.

Nominal Resistance

The main bridge information needed to calculate flexure resistance is the reinforcing amount, which was obtained from the original design plans. The quantity of steel per foot of slab width was taken as the effective reinforcement. Equation 6 was used to calculate the nominal flexural resistance which corresponds to LRFD Equation 5.7.3.2.2-1 (7).

$$M_n = A_s f_y \left(d_s - \frac{a}{2} \right) \quad (6)$$

where:

M_n = nominal moment capacity, kip-ft

A_s = area of tension reinforcement (varies), in²

f_y = specified yield strength of reinforcing bars (equal to 40 ksi)

d_s = distance from extreme compression fiber to the centroid of the tensile reinforcement (varies), in.

a = depth of the equivalent stress block, in.

In the calculation of nominal moment capacity, the maximum and minimum reinforcement limits were checked. The maximum limit is described in LRFR Article 6.5.6 which references LRFD Article 5.7.3.3.1 while Article 6.5.7 of LRFR specifies the minimum reinforcement limit which refers to LRFD Article 5.7.3.3.2. Bridge 7270 met both the maximum and minimum reinforcement requirements at all critical locations.

Design Load Rating

The first stage of the load rating analysis is the *design load rating* as described in LRFR Article 6.4.3. Ten critical points, including five locations for both positive and negative moments, were identified to evaluate the bridge. The critical points correspond to locations of highest moment under vehicular loads and where reinforcement was cutoff. The design rating information at the five critical points for positive bending including span number, position within the span, dead load moment, live-load moment (including impact), and effective reinforcement are given in Table 1. It is important to mention that the reported live-load moment represents the total moment and has not been divided by the equivalent width. Note also that the point located at 17.50 ft. from the abutment had the dead and live-load moments acting in the opposite sense. Similar to positive bending, the rating information at the five critical points for negative bending is given in Table 2. Note that the point located 7.75 ft from the third pier also had dead and live-load moments acting in opposite directions.

The rating analysis was based on the strength limit state for flexure; serviceability was not considered. In LRFR Article 6.5.9, it is mentioned that shear need not be checked in the design and legal load rating of in-service concrete bridges having no visible signs of shear distress. To obtain the factored bending resistance, the nominal capacity is multiplied by three factors. The first factor is the LRFD resistance factor (ϕ), specified in LRFD Article 5.5.4.2.1; for flexure of reinforced concrete members, this factor has a value of 0.9. Second, the condition factor (ϕ_c) is selected from Table 6-2 given in LRFR Article 6.4.2.3. Bridge 7270 was assigned a condition factor of 1.0 which corresponds to a satisfactory structure condition as reported during the 2005 field inspection. Note that the use of condition factors “may be considered optional based on an agency’s load rating practice” (4).

TABLE 1. Design rating information for positive bending.

Span	Position (ft)	M _{DL} (k-ft/ft)	M _{LL} (k-ft)	Reinforcement (in ² /ft)
1	9.26	4.47	245	1.59
1	15.5	0.48	136	0.93
1	17.5	-3.54	58.7	0.40
3	20.1	0.03	143	0.93
4	13.0	4.24	257	1.59

M_{DL} = dead load moment per foot

M_{LL} = total live-load moment under HL93 loading (including impact)

TABLE 2. Design rating information for negative bending.

Span	Position (ft)	M _{DL} (k-ft/ft)	M _{LL} (k-ft)	Reinforcement (in ² /ft)
1	16.8	-2.69	-139	0.93
1	20.0	-8.37	-211	1.59
3	25.0	-8.53	-223	1.73
4	3.63	-3.71	-140	1.07
4	7.75	1.41	-107	0.40

M_{DL} = dead load moment per foot

M_{LL} = total live-load moment under HL93 loading (including impact)

Moreover, there are many State bridge engineers who consider an arbitrary reduction in capacity based on a condition rating that represents the observed deterioration (that may or may not be critically located) is not in the best interest of the nation's highway system (Dr. Steve Maberry, NMDOT unpublished data). The third factor, or system factor (ϕ_s), reflects the level of redundancy of the superstructure and is specified as 1.0 in Table 6-3 of LRFR Article 6.4.2.4 for slab bridges.

In the *design load rating*, the evaluation is performed at an inventory and operating level according to LRFR Article 6.5.4.1. Different values for the live-load factor (γ_L) are used in Equation 1, as given in Table 6-1 of LRFR Article 6.4.2.2; the factor is 1.75 for inventory

and 1.35 for operating. The dead load factor for structural components and attachments (γ_{DC}) is the same for both inventory and operating and is equal to 1.25.

Legal Load Rating

The second phase of the load rating analysis is the *legal load rating* which is described in LRFR Article 6.4.4. The main difference between the design and legal load rating is the live loads employed. As described in LRFR Article 6.4.4.2.1, the live loads applied in the legal load rating are the Type 3, Type 3S2, and Type 3-3 vehicles. Moment envelopes for the three legal trucks are plotted in Figure 22.

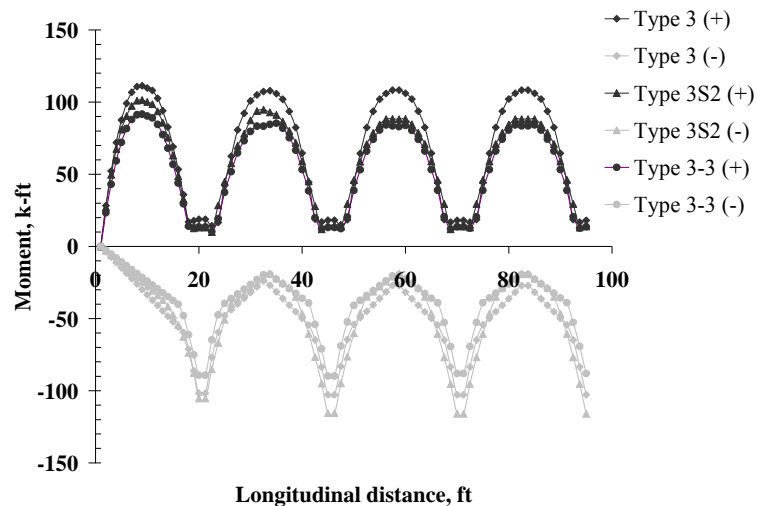


FIGURE 22. Moment envelopes due to legal trucks.

The moment magnitudes at the critical locations under the three legal trucks (including impact), for the positive and negative regions, are given in Tables 3 and 4, respectively. The controlling legal truck for positive moment was the Type 3 while the Type 3S2 controlled for negative moment except at one location. The live-load factor for legal loads is discussed in LRFR Article 6.4.4.2.3 and depends on the Average Daily Truck Traffic (ADTT) in one direction. The 2005 field inspection reported an ADTT less than 100 during 2002; consequently, the live-load factor was taken as 1.4 as specified in LRFR Table 6-5.

TABLE 3. Legal load moments for positive bending.

Span	Position (ft)	M_3 (k-ft)	M_{3S2} (k-ft)	M_{3-3} (k-ft)
1	9.26	148	135	122
1	15.5	81.5	74.3	67.1
1	17.5	35.1	32.0	28.9
3	20.1	85.9	78.3	70.7
4	13.0	144	117	111.1

M_3, M_{3S2}, M_{3-3} = total live-load moment under Type 3, Type 3S2, and Type 3-3 legal vehicle (including impact)

TABLE 4. Legal load moments for negative bending.

Span	Position (ft)	M_3 (k-ft)	M_{3S2} (k-ft)	M_{3-3} (k-ft)
1	16.8	-79.2	-83.3	-63.8
1	20.0	-135	-140	-119
1	25.0	-137	-154	-117
3	3.63	-86.3	-102	-70.1
4	7.75	-60.2	-46.3	-43.2

M_3, M_{3S2}, M_{3-3} = total live-load moment under Type 3, Type 3S2, and Type 3-3 legal vehicle (including impact)

Rating Factors

Rating factors at the critical locations were calculated for design and legal loading. The equivalent slab widths and rating factors for positive moment are given in Table 5; similar information is given in Table 6 for negative moment. As shown in Table 5, all the inventory rating factors for positive moment exceeded one. All but one negative moment location have inventory rating factors greater than one. The point located at 7.75 ft. from the third pier has an inventory rating factor less than one but the operating and legal rating factors exceed one as shown in Table 6.

TABLE 5. Rating factors for positive moment.

Span	Position (ft)	E (ft)	RF _{inv}	RF _{opr}	RF _{legal}
1	9.26	10.52	1.03	1.34	2.13
1	15.5	10.52	1.28	1.66	2.67
1	17.5	10.52	1.77	2.30	3.70
3	20.1	10.93	1.27	1.64	2.63
4	13.0	10.93	1.03	1.34	2.29

RF_{inv}, RF_{opr} = inventory and operating rating factors, respectively, under HL93 loading

RF_{legal} = rating factor under legal loading

NOTE: the reported equivalent width, E, corresponds to the interior strip (E_i) which controlled since it was smaller than the width of the exterior strip (E_e)

TABLE 6. Rating factors for negative moment.

Span	Position (ft)	E (ft)	RF _{inv}	RF _{opr}	RF _{legal}
1	16.8	10.73	1.04	1.35	1.97
1	20.0	10.52	1.07	1.39	2.24
1	25.0	10.93	1.11	1.43	1.99
3	3.63	10.93	1.22	1.59	2.10
4	7.75	10.93	0.84	1.08	1.13

RF_{inv}, RF_{opr} = inventory and operating rating factors, respectively, under HL93 loading

RF_{legal} = rating factor under legal loading

NOTE: the reported equivalent width, E, corresponds to the interior strip (E_i) which controlled since it was smaller than the width of the exterior strip (E_e)

Based on the rating factors for positive moment, Bridge 7270 has a safe load capacity for all AASHTO and state legal loads within the LRFD exclusion limits. One of the negative moment locations did not satisfy the inventory rating check but the operating rating factor exceeded one indicating the bridge has adequate capacity for AASHTO legal loads and state legal loads having only minor variations from the AASHTO loads. For further confirmation, a legal load rating was performed which yielded a factor of 1.13. Full details of the AASHTO load rating analysis of Bridge 7270 are given in Appendix B of Licon-Lozano (18).

DIAGNOSTIC LOAD TEST

Diagnostic load testing was an important part of this research project. The test equipment employed was the Structural Testing System II (STS II) developed by Bridge Diagnostics, Inc. (BDI). Due to traffic control issues, Bridge 7270 was tested over two days (August 25 and 26 of 2006). The NMDOT provided personnel for traffic control and also the vehicular trucks for testing the bridge. Strain measurements were made on the top and bottom surface of the concrete slab with the bridge under truck loading. This chapter describes the various aspects of the bridge testing including the BDI-STS II test equipment; instrumentation plan and installation; test truck configuration and application; load test execution; and the post-processing of the strain data.

TEST EQUIPMENT

BDI Strain Transducers

Strain transducers manufactured by BDI (also called BDI intelliducers) were used to measure the strain response of Bridge 7270. The physical size of each gage is 4.375" x 1.25" x 0.5" and the gage length is 3 in. The transducers are made of aluminum and each weighs 3 oz. Each gage is assigned a unique number as shown in Figure 23 that is automatically identified by the BDI-STS II power unit to access the gage's calibration factor. The power unit also controls the balancing and re-zeroing of the gages.



FIGURE 23. BDI intelliducer assembly (19).

Two holes spaced 3 in. apart are provided in the transducer for mounting the steel tabs. After preparing the surface of the concrete slab, the tabs are easily installed using quick-set adhesive. To account for the increase in strain caused by cracks in the concrete, the gage length was increased to 12" as shown in Figure 24. Extension gages were used in the tension areas of the slab (i.e., bottom side of slab at midspan locations and top side at pier locations).

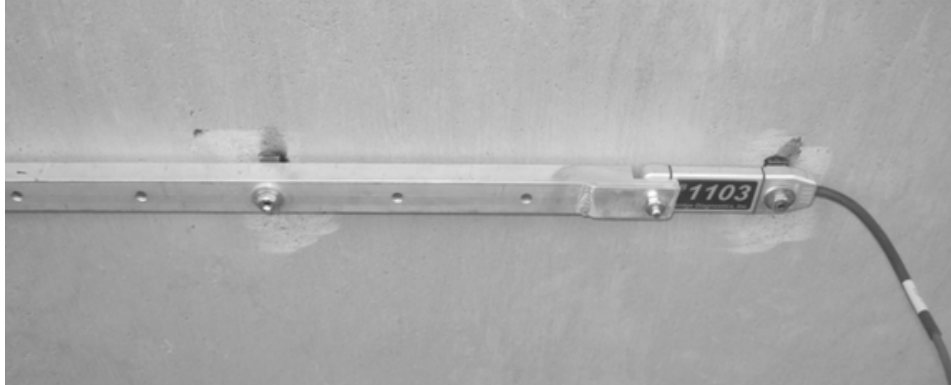


FIGURE 24. BDI intelliducer with extension (19).

There are several advantages in using BDI strain transducers including: easy installation (can be mounted in less than 5 minutes); cost-effectiveness (can be reused); excellent compatibility with most data acquisition systems; and high output. The BDI transducers have been field proven over the last two decades in several environmental conditions (19).

BDI-STTS II Modules and Power Unit

Each BDI-STTS II module connects four strain transducers to the power unit. Its function is to collect strain data from the transducers for transfer to the power unit. The modules each weigh 1.8 lbs. and measure 2.3" x 3.0" x 11.0" (see Figure 25). Furthermore, the modules can be connected directly to other units or through cables running in series and/or in parallel by means of a splitter.

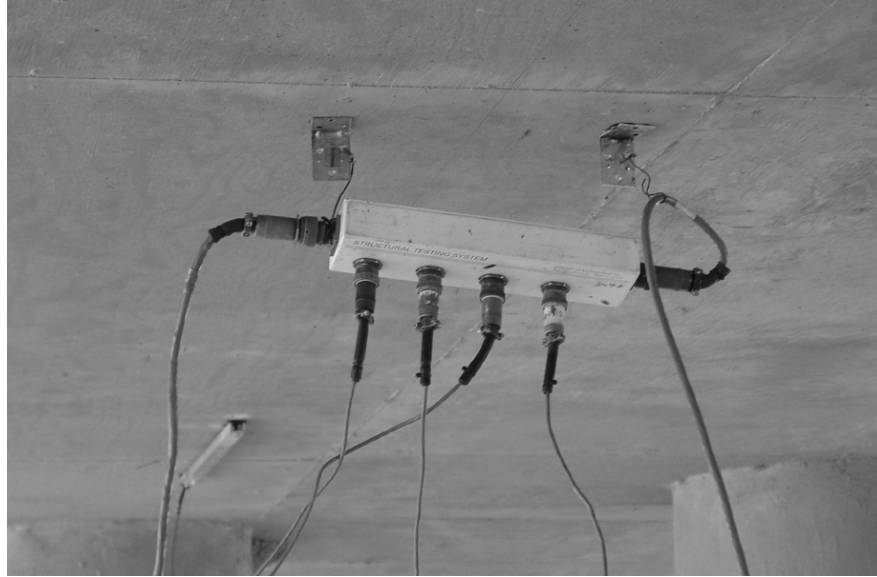


FIGURE 25. BDI-STTS II module (19).

After all the STS modules are connected, a single cable connects the modules to the power unit. The power unit provides the 5 volt excitation voltage required by each strain transducer. Power to the system may be provided by either an automobile battery or a generator. A laptop computer interacts directly with the power unit to collect the strain readings at a specific rate and to stop or start data collection. The system has a wide range of data collection options, one being the sampling rate which was set at 40 Hz (i.e., 40 samples per second) during testing of Bridge 7270.

BDI Autoclicker

The BDI autoclicker is used to track the longitudinal position of the test vehicle. As shown in Figure 26, the autoclicker assembly is mounted on the front fender of the truck using hooks and adjustable straps, and the face of the laser sensor is positioned in line with the reflective paddle. As the truck travels and the reflector passes in front of the sensor, it sends a radio signal to the laptop to identify the truck position during the test. The strain data can be subsequently given in terms of time or truck position.



FIGURE 26. BDI autoclicker assembly (19).

The radios are also used to maintain coordination between personnel. For example, the person in charge of guiding the truck driver during the test has to receive an order from the computer operator and vice versa.

TEST DETAILS

Instrumentation Plan and Installation

There were several goals considered in the development of the instrumentation plan for the positive and negative moment regions of Bridge 7270 that included: (1) evaluate the moment distribution along the slab width; (2) evaluate the neutral axis positions of the slab sections; and (3) validate a finite-element model of the bridge developed using SAP2000. Gage locations were marked on the bridge one day prior to testing to facilitate the actual tests. A total of thirty-two BDI strain transducers were installed each test day to measure the response of Bridge 7270.

The bridge was instrumented at the four sections shown in Figure 27: midspan of the first span (M1); 22 in. north from the first pier centerline (P1); midspan of the second span (M2); and 36 in. north from the second pier centerline (P2).

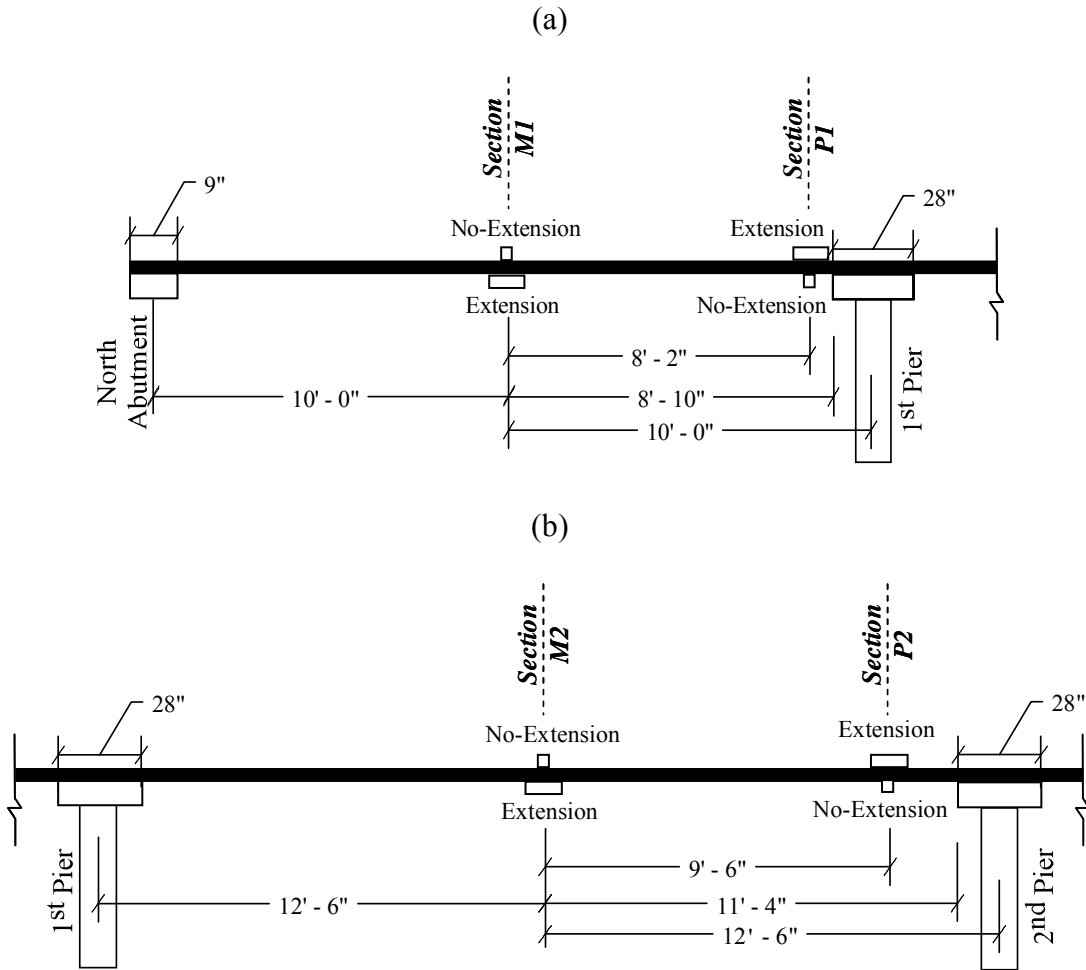


FIGURE 27. Instrumented sections of slab in (a) span 1 and (b) span 2.

Due to traffic control issues as mentioned before, half of the bridge was instrumented and tested on the first day and the other half the second day. Figure 28 shows the final gage layout on the top and bottom side of the slab at the midspan (M1 and M2) and pier (P1 and P2) sections. A view of the bottom side of span 1 with the gages installed on the east side of the slab on the second day of testing is shown in Figure 29.

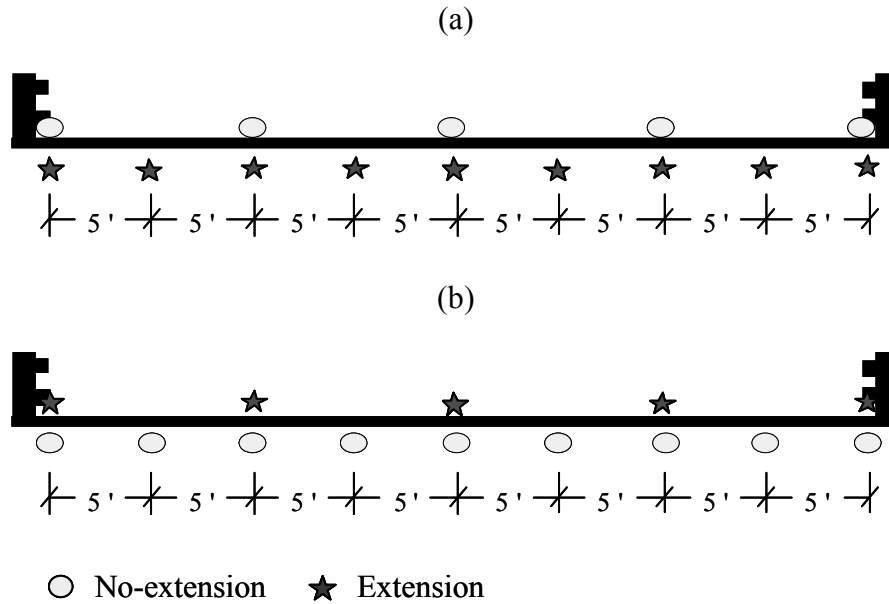


FIGURE 28. Gage layout at (a) midspan and (b) pier sections.



FIGURE 29. View of installed gages on bottom side of span 1.

Before the test dates, the batteries of the grinders and the three radios were charged overnight to provide service without delays. Tabs were cleaned up by soaking in acetone overnight and then attached to the transducers one day before the load test. Before installing the gages, the surfaces of the slab were cleaned and smoothed with a grinder. The top surface

of the slab was rough and needed rigorous grinding, much more compared to the bottom of the slab. After surface preparation was completed, the transducer tabs were mounted with the adhesive and accelerator. Extension gages were prepared and installed (see Figure 30) similar to the non-extension gages based on the instructions and recommendations provided in the BDI Manual (19). After installation of all the gages at the required locations was complete, the gages were connected to the STS modules and then to the power unit by means of cables. To avoid damage, the cables of the gages installed on the top side of the slab were protected with pipe insulation during the load test.

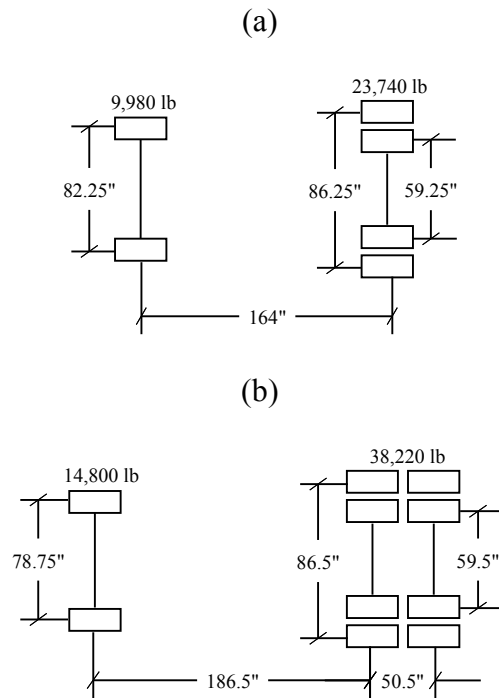


FIGURE 30. Installation of BDI intelliducer (with extension).

Test Truck Configuration and Application

Two dump trucks of 5 and 10 cubic-yard capacity (loaded with base material) served as the test vehicles. The front axle of the 5 cubic-yard (5YD) truck weighed 9,980 lbs. and the rear axle weighed 23,740 lbs. The center-to-center distance between the front and the rear axle was 164". Front and back axle weights of the 10 cubic-yard (10YD) truck were 14,800 lbs. and 38,220 lbs., respectively. The center-to-center distance between the rear axles was 50.5"

while the center-to-center distance between the front and the interior rear axle was 186.5". Foot prints of the 5YD and 10YD trucks are provided in Figure 31. The length of one revolution (i.e., circumference) of the front wheel was also measured before the tests which equaled 10.9 ft. and 10.6 ft. for the 5YD and 10YD trucks, respectively.



**FIGURE 31. Axle weights and spacings for
(a) 5YD and (b) 10YD test trucks.**

To evaluate the transverse behavior across the slab width, the 5YD and 10YD trucks were driven across the bridge along the five transverse paths shown in Figure 32. The paths were measured and marked with construction paint to provide reference lines to the driver. The left wheel of the truck served as the reference for path 1 (located 3.83 ft. from the east slab edge). The center of the truck was the reference for paths 2 through 4; paths 2 and 3 were located 12 ft. and 21.5 ft., respectively, from the east slab edge and path 4 was 12 ft. from the west slab edge. For path 5, the right wheel was located 3.83 ft. from the west slab edge. Each path started with the truck located a distance of 10 ft. from the north abutment.

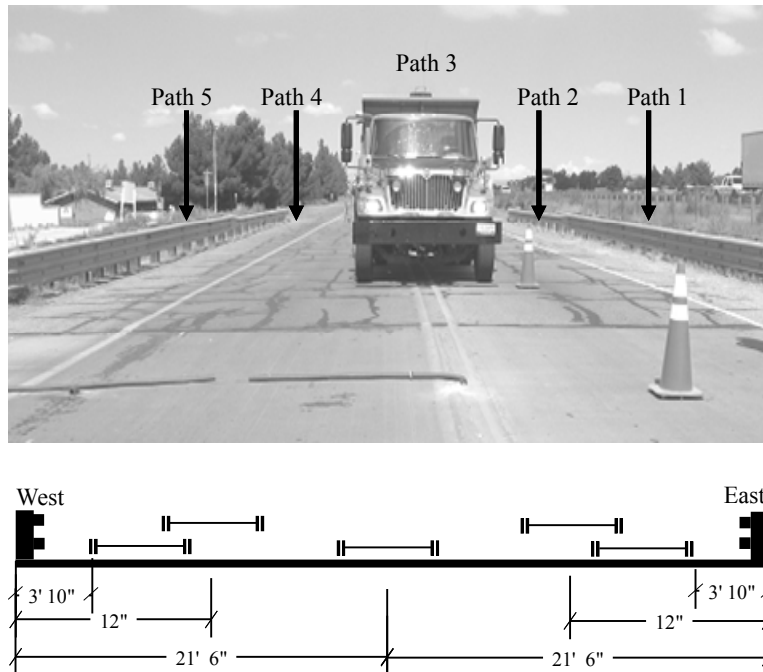


FIGURE 32. Transverse paths of test trucks.

Load Test Execution

There were a number of things that needed to be checked before starting the load test. After the test equipment was hooked up, the system was initialized to make sure that all gages and STS modules were correctly identified. Also, the strain transducers needed to “zero out” when balanced and the “clicks” from the autoclicker needed to be received properly.

On the test days, one lane of Bridge 7270 was closed to traffic and the other remained open. When no traffic was observed to be approaching the bridge, the BDI intelligiducers were balanced with the test truck positioned 10 ft. from the north abutment. The 5YD or 10YD test truck was then slowly driven across the bridge at approximately 5 mph (see Figure 33) to minimize dynamic effects. The driver’s responsibility was to maintain about the same truck speed for all the runs. All traffic was kept off the bridge during the truck passes; halted traffic was flagged through the bridge between runs to avoid a long traffic queue on the open lane.



FIGURE 33. Load test in progress.

Each run was stopped when the truck reached the south abutment and then the collected data was saved to the laptop while the truck was taking the next position. According to the BDI Manual (19), it is suggested that multiple runs be made for each truck path to check data consistency before moving to the next path. Thus, the test trucks were run two or three times per path. After the load tests were completed, the strain transducers were removed carefully from the bridge following the procedures given in the BDI Manual (19) to avoid damaging the equipment.

POST-PROCESSING OF STRAIN DATA

The first step in post-processing the strain data was to accurately determine the location of the truck front axle from the clicker times and the front wheel circumference. The next step was to apply corrections to the strain data obtained from extension gages. The BDI Manual (19) explains the necessary correction to account for strain amplification caused by longer gage lengths. The correction consists of multiplying the raw strain reading by 1.1 (to account for extension effects) and dividing by 4, the ratio of the extension length to the standard gage length (i.e., 12 in. / 3 in. = 4).

Based on the instrumentation plan and the gage locations on the slab, it was decided to plot two types of strain graphs. At transverse locations where top and bottom transducers were installed on the slab, the strain data for the gage pair were plotted together in the same graph. At locations with only one transducer, the strain data were plotted independently. Plot (a) of Figure 34 shows representative samples of gage pair readings at midspan section M1 and plot (b) shows a single gage reading. Similar plots are provided at pier section P1 in Figure 35. In these graphs, the x-axis represents the front axle position of the test truck and the y-axis represents the measured strains in micro units.

The total set of graphs for paths 1 through 5 of the 5YD and 10YD trucks are provided in Appendix B of Licon-Lozano (18). Several general observations were made from the strain graphs. First, in most of the strain plots corresponding to gage pairs, the top gage profile mirrored the bottom gage profile. Second, the peak strains occurred at about the same front axle position for each truck path. Third, the measured strains under the test truck loads plus the estimated dead load strains were higher than the concrete cracking strain at several locations. Fourth, the strain profiles were symmetrical between similar truck paths (i.e., paths 1 and 5 and paths 2 and 4). Fifth, there were some rare occurrences of erroneous strain profiles possibly due to bad gage readings. Sixth, some gage pair locations close to the piers experienced larger compressive strains than tensile strains, possibly due to arching action.

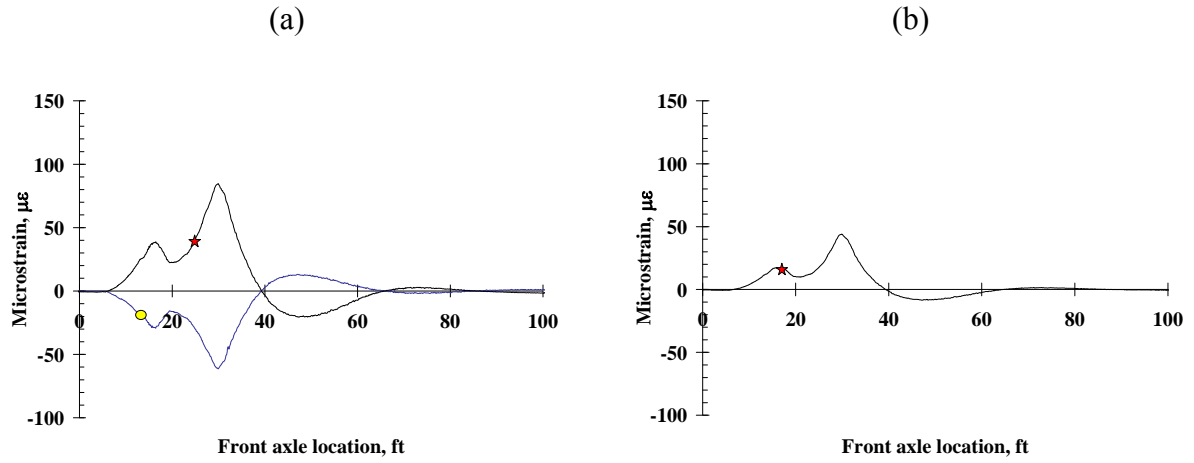


FIGURE 34. Representative strain readings at midspan section M1: (a) gage pair and (b) single gage.

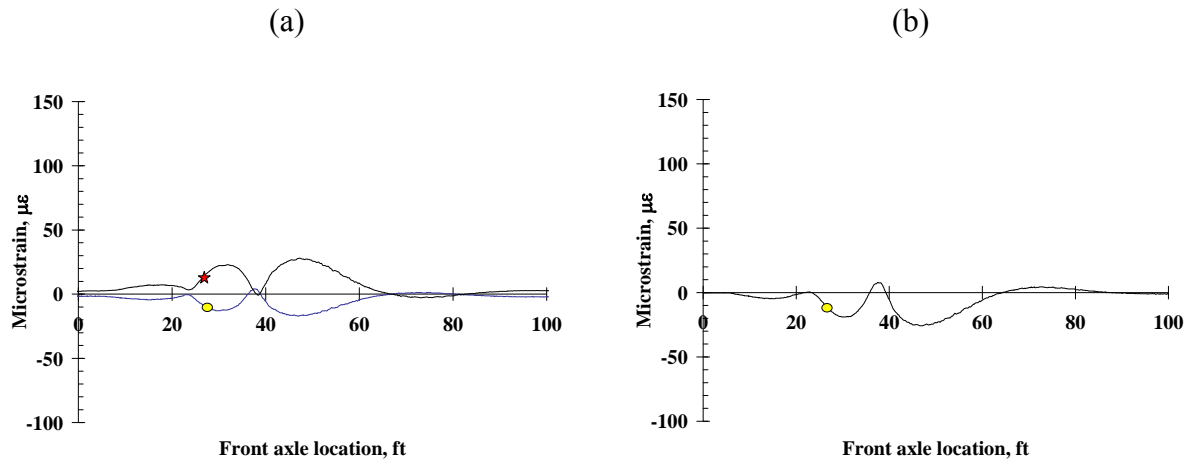


FIGURE 35. Representative strain readings at pier section P1: (a) gage pair and (b) single gage.

EVALUATION OF SLAB STIFFNESS

The raw data plots indicated that the measured tensile strains under truck loading plus the estimated dead load strains (equal to 47.8 $\mu\epsilon$ and 91.2 $\mu\epsilon$ at the positive and negative moment regions, respectively) exceeded the cracking strain of the concrete at several locations. The cracking strain (ϵ_{cr}) was taken as

$$\epsilon_{cr} = \frac{f_r}{E_c} = \frac{7.5\sqrt{f'_c}}{57,000\sqrt{f'_c}} = 131.58 \mu\epsilon \quad (7)$$

where f_r is the modulus of rupture and E_c is the modulus of elasticity (20). In this chapter, the experimental neutral axis positions across the slab width at the instrumented sections were computed from the measured strains and compared to the theoretical positions (based on uncracked and cracked behavior). This evaluation was performed for two main reasons. The first was to get an idea of the actual slab stiffness for later use in calculating the bending moments in the slab from the measured strains. The second was to evaluate the relative stiffness between the positive and negative moment regions and determine if the bridge was acting as a prismatic or non-prismatic structure. Findings from this evaluation provided very useful information for developing a finite element model of Bridge 7270 that represented the actual load distribution characteristics of the bridge.

THEORETICAL NEUTRAL AXIS POSITIONS

Along the length of the bridge, the theoretical neutral axis positions are not constant due to the variation in the effective reinforcement and the transition from positive to negative bending. The midspan sections, M1 and M2, have the same reinforcement layout with an effective top mat (A_T) of 0.40 in²/ft and bottom mat (A_B) of 1.59 in²/ft. The effective reinforcement layout per unit slab width at the midspan sections is shown in Figure 36.

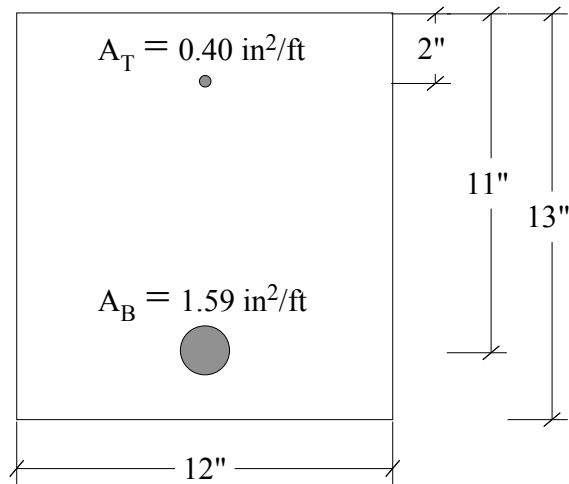


FIGURE 36. Effective reinforcement layout at midspan sections.

The two pier sections have different top reinforcing mats but the same bottom mats; A_T equals $1.59 \text{ in}^2/\text{ft}$ at P1 and $1.73 \text{ in}^2/\text{ft}$ at P2 and A_B equals $0.40 \text{ in}^2/\text{ft}$ at both sections. Details of the theoretical neutral axis calculations are provided in Appendix C of Licon-Lozano (19).

Uncracked Section Analysis

The neutral axis positions were calculated based on uncracked section behavior taking into account the tension and compression steel. For an uncracked section, the steel areas were transformed as shown in Figure 37.

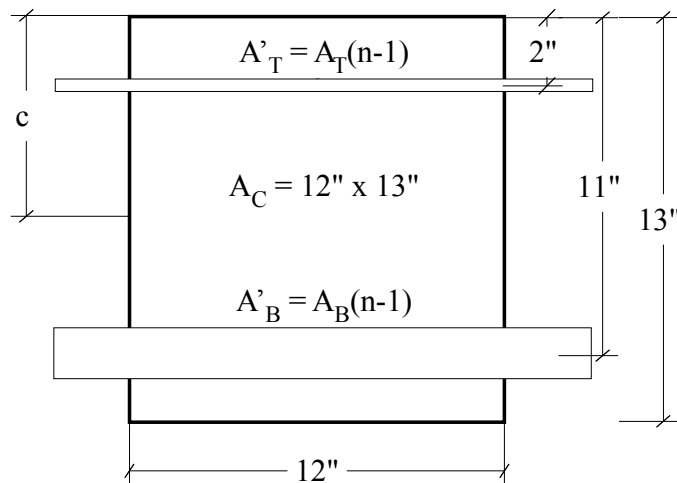


FIGURE 37. Transformed uncracked section at midspan locations.

The following centroid equation was used to calculate the positions of the uncracked neutral axes at the midspan sections with reference to the top of the slab:

$$c = \frac{A'_B (11'') + A_C (13''/2) + A'_T (2'')}{A'_B + A_C + A'_T} \quad (8)$$

The reinforcing steel areas were transformed to concrete using a modular ratio of 8.7, which is the ratio between the modulus of elasticity for steel and concrete (i.e., $n = E_s / E_c$). The uncracked neutral axis depths at both midspan sections was located a distance of 6.26 in. from the bottom of the slab. Based on a similar analysis, the neutral axes were located at 6.74 in. and 6.77 in., respectively, at the pier sections P1 and P2.

Cracked Section Analysis

The computations of the cracked neutral axis positions also took into account the tension and compression steel. For a cracked section, the reinforcing steel was transformed to concrete as shown in Figure 38.

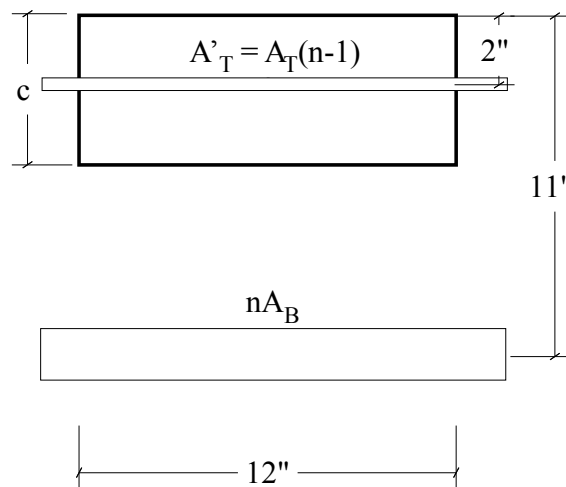


FIGURE 38. Transformed cracked section at midspan locations.

The neutral axis depths were then calculated by setting the first moment of inertia of the compression area equal to that of the tension area (ignoring the concrete in tension) as shown in the following equation:

$$nA_B(11'' - c) = \frac{(12'')^2 c^2}{2} + A'_T(c - 2'') \quad (9)$$

With respect to the bottom of the slab, the cracked neutral axis positions came out to 9.07 in. at the midspan sections. At the pier sections, the neutral axis depths were 3.93 in. at P1 and 4.06 in. at P2. Theoretical neutral axis depths along the bridge length (based on uncracked and cracked behavior) are plotted in Figure 39.

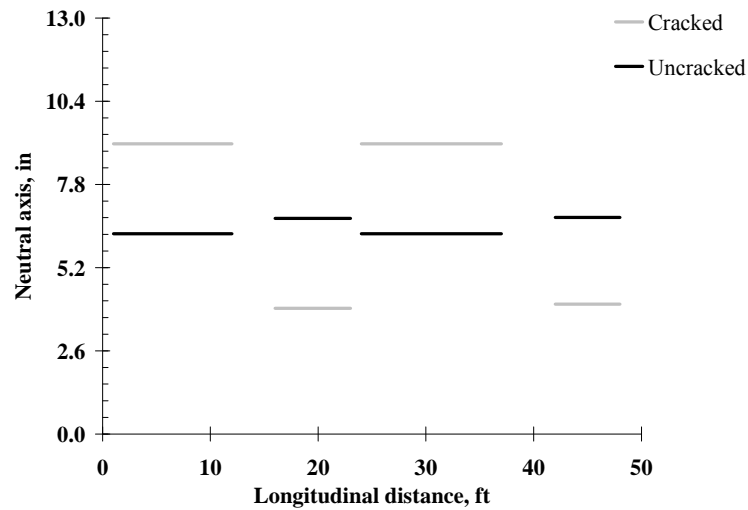


FIGURE 39. Theoretical neutral axis depths along bridge length.

EXPERIMENTAL NEUTRAL AXIS POSITIONS

As mentioned earlier, the main reason for using gage pairs was to estimate the experimental neutral axis positions (from the measured strains) across the slab width in the positive and negative moment regions. Top and bottom gages were installed every 10 ft. on the slab cross-section at the instrumented locations (see Figure 28). The following equation was used to estimate the experimental neutral axis depths

$$c = \frac{(13'') \mu\varepsilon_T}{\mu\varepsilon_B + \mu\varepsilon_T} \quad (10)$$

where $\mu\varepsilon_T$ and $\mu\varepsilon_B$ are the measured strains on the top and bottom side of the slab, respectively, as shown in Figure 40. This equation was derived based on the assumption that the strain distribution is linear over the slab depth.

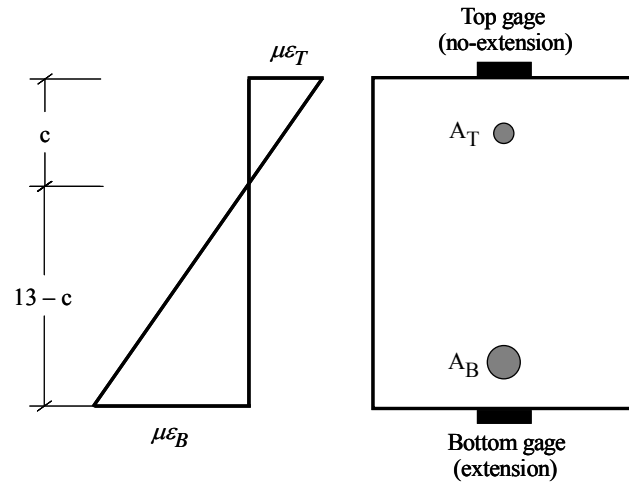


FIGURE 40. Assumed strain distribution between gage pair readings at midspan sections.

As mentioned earlier, the test trucks traveled along five paths; however, only the paths causing the highest strain readings for each gage pair were used to estimate the experimental neutral axis positions. The paths used depend on the transverse location of the gage pair (see Figures 28 and 32): paths 1 and 2 or 4 and 5 were used for the gage pairs located closest to the slab edges; paths 2, 3 and 4 were used for the gage pairs located 11.5 ft. from the slab edges; and all five paths were used for the gages pair located at the centerline. For each path, the neutral axis was evaluated over the range of strain readings between the two highest peaks (as illustrated in Figure 41) and then averaged; the two peaks occurred at different front axle positions for the four instrumented sections. The average served as the final estimate of the experimental neutral axis depth. Note that within the averaged range, the standard deviations of the neutral axis depths were less than 0.10 in. at all gage pairs.

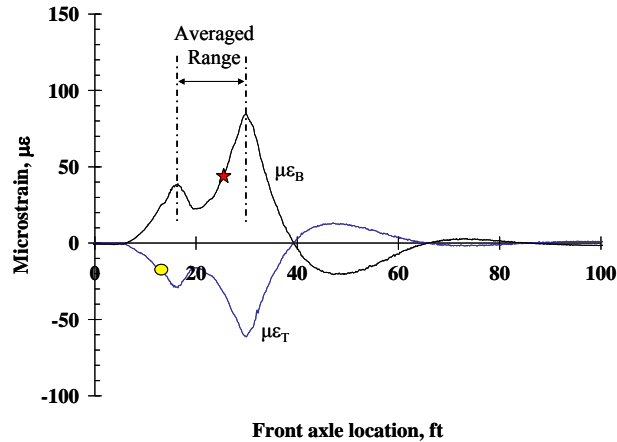


FIGURE 41. Averaged range of strain measurements for neutral axis evaluation at midspan section M1.

THEORETICAL VS. EXPERIMENTAL NEUTRAL AXIS POSITIONS

Neutral axis plots for the 5YD test truck at the midspan and pier sections of span 1 and span 2 are given in Figures 42 and 43, respectively. The plot for each section has 15 discrete points representing the experimental neutral axis depths across the slab width with reference to the bottom of the slab; different symbols are used for the experimental values for paths 1 through 5. Solid black and grey lines represent the theoretical neutral axis positions based on uncracked and cracked section behavior, respectively.

As shown in Figures 42 and 43, the experimental neutral axis positions vary over the slab width. At midspan section M1 (see Figure 42(a)), 86% of the experimental values fit between the theoretical limits. Furthermore, the average of the theoretical depths (equal to 7.6 in.) is similar to the average of the fifteen experimental values (equal to 7.0 in.). Pier section P1 (see Figure 42(b)) showed a slightly larger disparity between the experimental and theoretical neutral axis depths; 67% of the experimental values fit within the theoretical limits compared to 86% at midspan section M1. At this pier location, the theoretical average equaled 5.34 in. while the experimental average was 6.04 in.

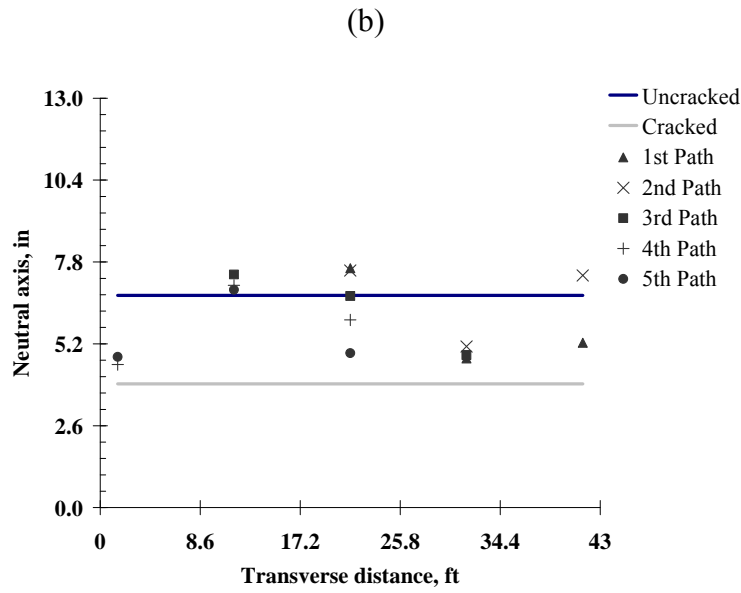
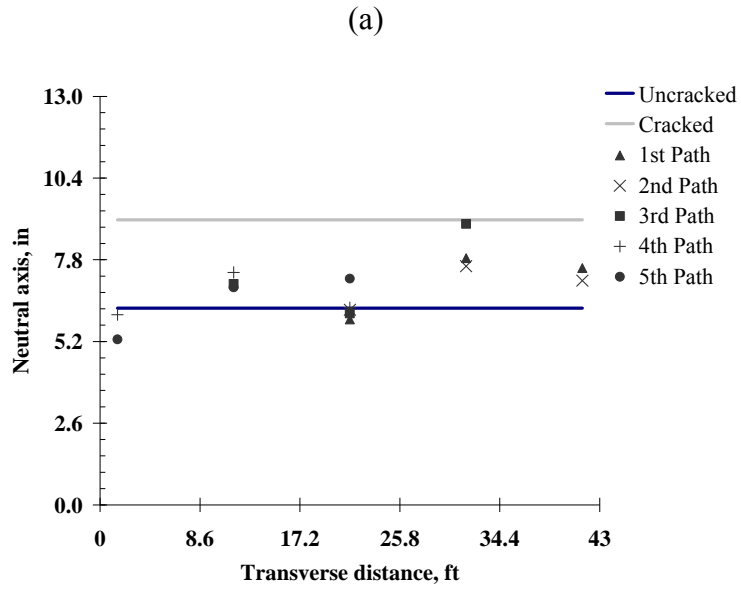


FIGURE 42. Neutral axis positions for 5YD truck at (a) midspan section M1 and (b) pier section P1.

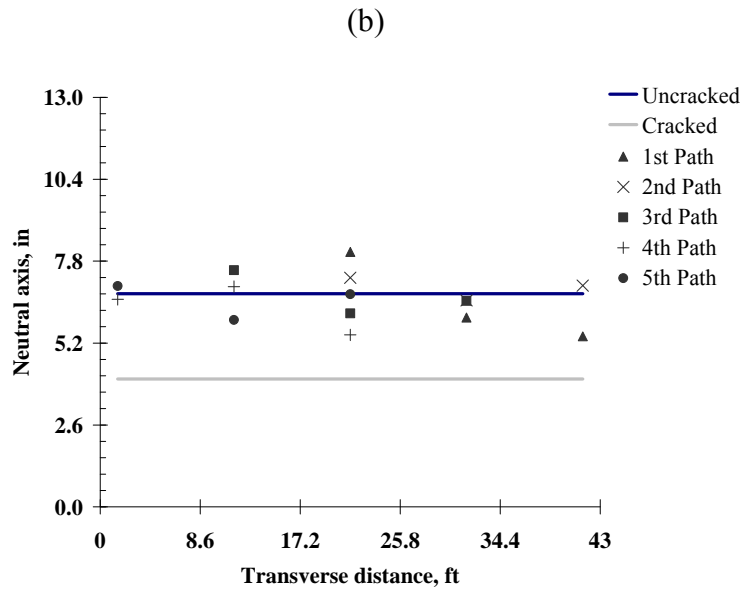
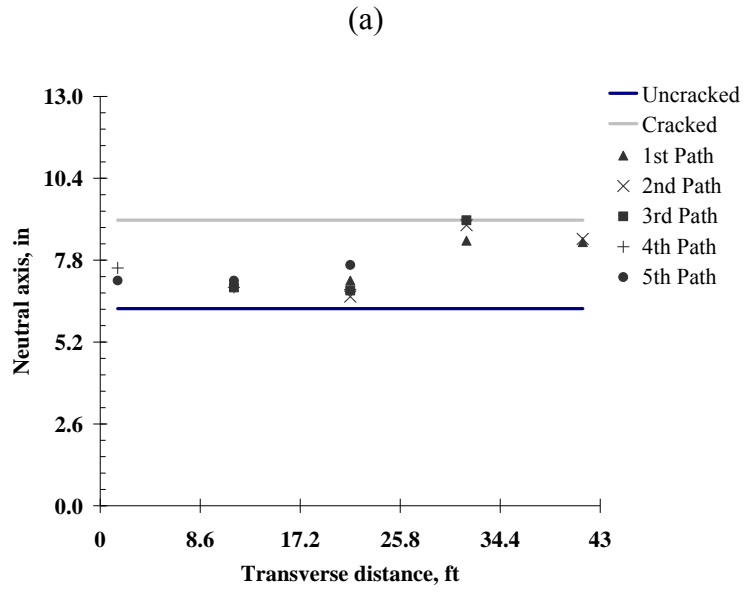


FIGURE 43. Neutral axis positions for 5YD truck at (a) midspan section M2 and (b) pier section P2.

Midspan section M2 (see Figure 43(a)) showed similar results as M1; at M2, all fifteen experimental values fit between the theoretical limits and the experimental average was 7.61 in. which is about equal to the theoretical average of 7.67 in. Pier section P2 (see Figure 43(b)) also showed similar results as P1; at P2, the experimental average equaled 6.62 in. which is 1.2 in. higher than the theoretical average.

In summary, the fifteen experimental neutral axis depths across the slab width averaged out to values within 8% of the theoretical average at M1 and 1% at M2. The experimental and theoretical averages were within 12% and 9%, respectively, at P1 and P2. Neutral axis plots for the 10YD test truck (similar to those for the 5YD truck) are given in Figures 44 and 45, respectively. No major differences (i.e., less than 0.10 in. on average) were observed in the experimental neutral axis depths between the 5YD and 10YD test trucks.

FINAL REMARKS

Based on the comparison between the experimental and theoretical depths presented in this chapter, the neutral axis appears to be halfway between an uncracked and cracked section in the positive moment regions. At the piers or negative moment regions, the experimental neutral axis positions were also found to fit within the theoretical limits but more towards an uncracked section. As shown in plot (b) of Figures 42 through 45, there were several experimental points that fell above the uncracked neutral axis position. Higher compressive strains compared to the tensile strains were measured at the pier sections possibly due to arching action and/or horizontal thrust, however, this behavior was not verified. If indeed this is taking place, the true experimental neutral axis is further down closer to the theoretical average between uncracked and cracked behavior (similar to the midspan sections).

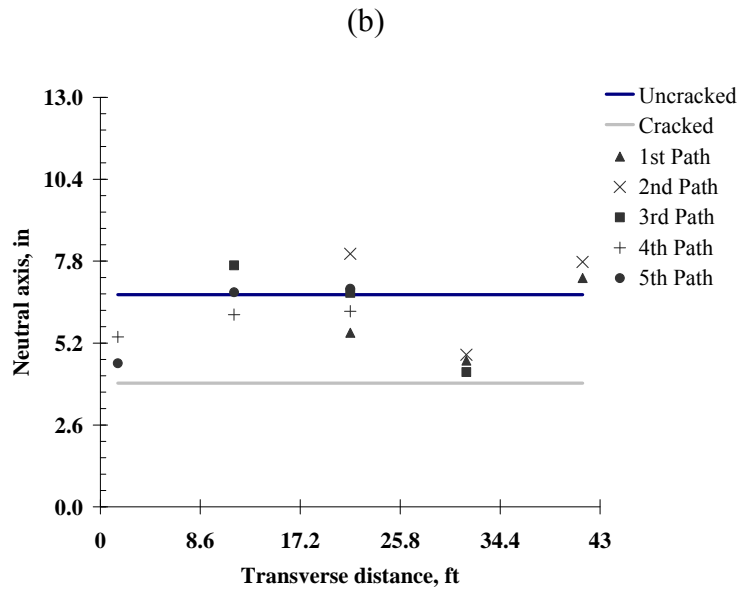
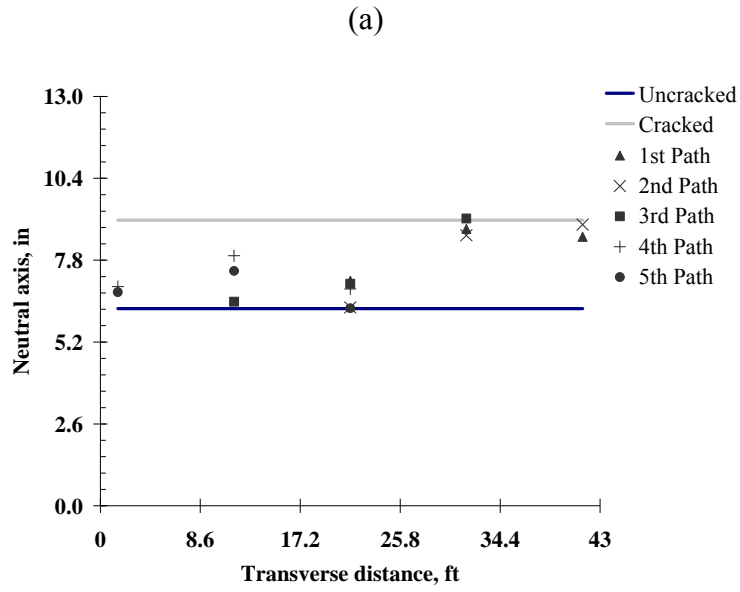


FIGURE 44. Neutral axis positions for 10YD truck at (a) midspan section M1 and (b) pier section P1.

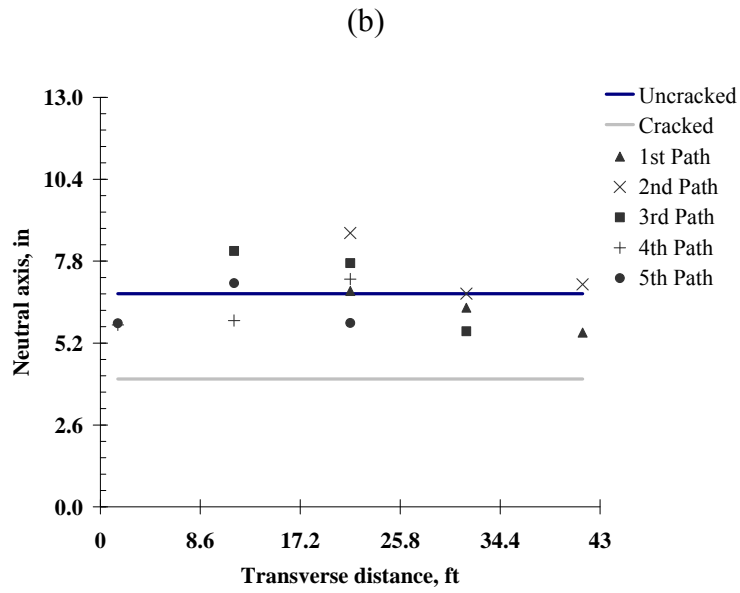
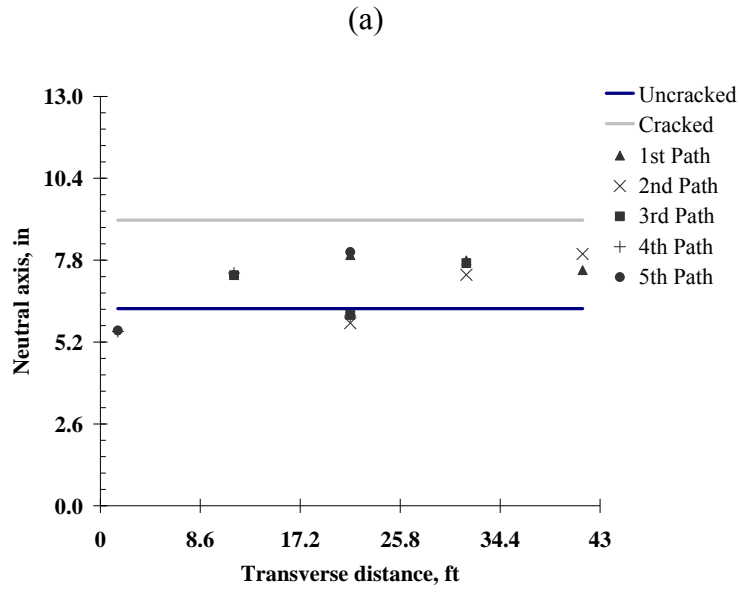


FIGURE 45. Neutral axis positions for 10YD truck at (a) midspan section M2 and (b) pier section P2.

Consequently, this would suggest that the positive and negative moment regions have about the same bending stiffness and thus, the bridge behavior is prismatic rather than non-prismatic. If there is a significant difference in stiffness between the midspan and pier sections, some load redistribution will occur to the stiffer areas (i.e., the piers) but not of significant magnitude. It was ultimately decided that linear-elastic, homogeneous material properties (i.e., prismatic assumptions) would be used to develop the finite element model of Bridge 7270. Furthermore, the neutral axis evaluation supported the use of an intermediate section modulus for computing the experimental bending moments of the slab.

FINITE ELEMENT MODEL

There are many finite element programs that can be used to create a model and determine the analytical response of a structure. The software used to model and analyze Bridge 7270 was Version 10 of the Structural Analysis Program 2000 (SAP2000) developed by Computers and Structures, Inc. (5). Based on the findings from the neutral axis evaluation provided in the previous chapter, the bridge was modeled as a prismatic, concrete slab with linear-elastic and homogeneous material properties. A detailed description of the model and the loading procedure are given in this chapter.

MODEL DESCRIPTION

Material Properties and Element Definition

For Bridge 7270, only the concrete slab superstructure was modeled and the reinforcing steel was ignored. Material properties specified for the slab included the density (0.150 kcf), modulus of elasticity (3,320 ksi), and Poisson's ratio (0.20). These properties were extracted from the structural drawings.

Quadrilateral shell elements were used to model the slab, which have been shown to accurately represent the three-dimensional behavior of concrete slab bridges in previous studies (3, 6, 21). This element type has a total of four nodes with six degrees of freedom (three translational and three rotational) at each node. In SAP2000, the shell thickness was defined as thin-plate which neglects shear deformation. The shells were also given a constant membrane and bending thickness of 13 in., equal to the design slab thickness.

Mesh Configuration and Boundary Conditions

The element dimensions were chosen based on the bridge geometry and the locations of the instrumentation. The shell-element mesh was refined in the first three spans to facilitate the

placement of vehicle axle loads and to obtain accurate bending moments across the slab width at the instrumented sections in the first two spans. Square shells with 12 in. x 12 in. dimensions were used to model the first three spans (70 ft.) of the bridge; the remaining four spans (95 ft.) were modeled with 12 in. x 30 in. rectangular shells as shown in Figure 46. This modeling scheme resulted in a total of 4,796 nodes and 7,644 shell elements.

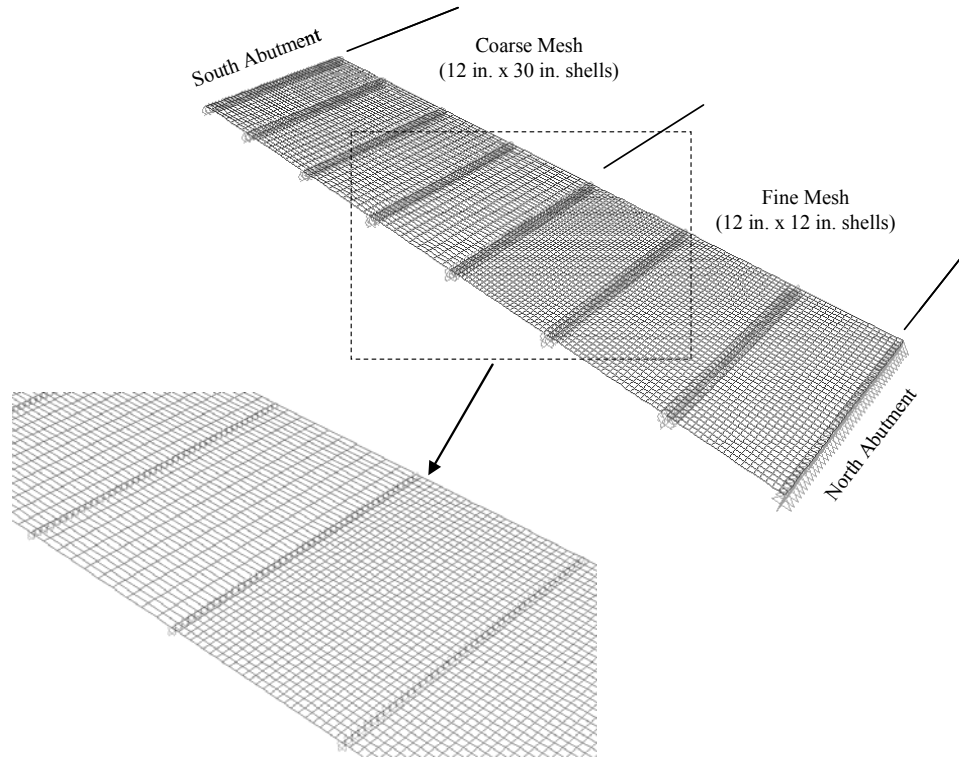


FIGURE 46. Finite element model of Bridge 7270.

The north abutment was modeled as a pinned support (with translational restraint in the longitudinal, transverse, and vertical directions). The six piers and south abutment were modeled as roller supports (with translational restraint in the transverse and vertical directions). This modeling approach assumes the substructure elements provide rigid vertical support and ignores the bending stiffness of the piers. In addition, since the shell elements are situated at the mid-height of the slab, the effects of the offset relative to the support face was neglected.

To check the accuracy of the SAP2000 three-dimensional model, a dead load analysis was carried out and compared to the results from RISA. The total force across the slab width of the SAP2000 model was obtained by summing the forces of the 43 shell elements at the cross-section. The separate analyses showed that the SAP2000 and RISA results agreed to within 1% for both moment and shear.

APPLICATION OF LIVE LOAD

The wheel loads of the 5YD and 10YD test trucks were applied as nodal loads in the finite element model. In most cases, the wheels did not coincide with the nodes of the shell elements but rather fell within the element (but not exactly at the center). For simplicity, the wheel load was equally divided among the four nodes of the shell element. Using this approach, the rear-axle weight of the 5YD truck (equal to 23,740 lbs.) was distributed to 12 nodes and the front-axle weight of 9,980 lbs. was distributed to 8 nodes as shown in Figure 47(a). For the 10 YD truck, the rear-axle weight of 38,220 lbs. was distributed to 24 nodes and the front-axle weight of 14,800 lbs. was distributed to 8 nodes as shown in Figure 47(b).

Results from the SAP2000 and RISA analyses under loading from the test trucks (for paths 1 to 5) were compared to further verify the accuracy of the SAP2000 model. Similar to the dead load analysis, the slab moments and shears from SAP2000 were within 1% of RISA.

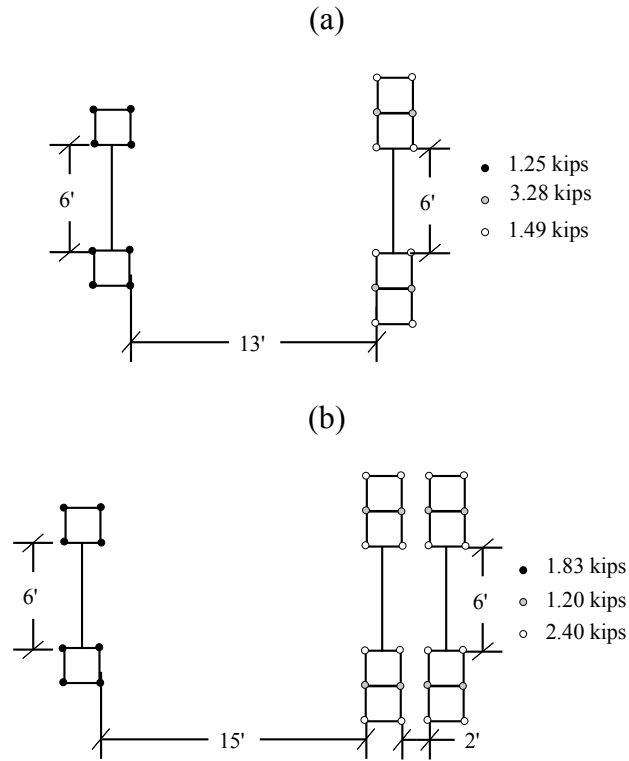


FIGURE 47. Nodal loads applied to finite element model representing (a) 5YD truck and (b) 10YD truck.

EVALUATION OF SLAB MOMENTS

SLAB MOMENTS FROM FIELD DATA

To assess the SAP2000 models under live load (i.e., 5YD and 10YD trucks), experimental moments in the slab were derived from the strain measurements and compared with the slab moments obtained from finite element analysis. Experimental slab moments were determined from the maximum tensile strains (ϵ_{\max}) recorded for each truck path at the four instrumented sections. The following equations were used to calculate the moments based on uncracked (gross) and cracked section behavior:

$$M_{gr} = ES_{gr}\epsilon_{\max} \quad (11)$$

$$M_{cr} = ES_{cr}\epsilon_{\max} \quad (12)$$

where:

M_{gr} = experimental moment based on uncracked (gross) section, kip-in

M_{cr} = experimental moment based on cracked section, kip-in

E = modulus of elasticity, 3320 ksi

S_{gr} = uncracked (gross) section modulus on tension side, in³

S_{cr} = cracked section modulus on tension side, in³

At locations having gage pairs (i.e., top and bottom gages), the experimental slab moments at the instrumented bridge sections may be estimated based on the measured compressive or tensile strains. It was decided that the tensile strains would be used since these strains are measured over a longer gage length. This approach was also taken to circumvent using the excessive compression strains measured at the piers possibly caused by arching action and/or the horizontal thrust. Thus, the measured tensile strains on the bottom of the deck were used to calculate the positive moments at the midspan sections (i.e., M1 and M2). To calculate the

negative moments at the pier sections (i.e., P1 and P2), the tensile strains measured on the top of the deck were used.

SLAB MOMENTS FROM FINITE ELEMENT ANALYSIS

The 5YD and 10YD truck loads were applied to the SAP2000 model along the same five transverse paths followed in the diagnostic test. For each path, the truck was positioned longitudinally to maximize the bending moment at the four instrumented sections resulting in a total of twenty load cases per truck. The magnitudes and locations of the nodal loads were entered into the SAP2000 program using the interactive database editing option that was also used to generate the joint coordinates. Figure 48 shows the SAP2000 model loaded with the 5YD test truck to maximize the bending moment at the first midspan section (i.e., M1) for the third truck path.

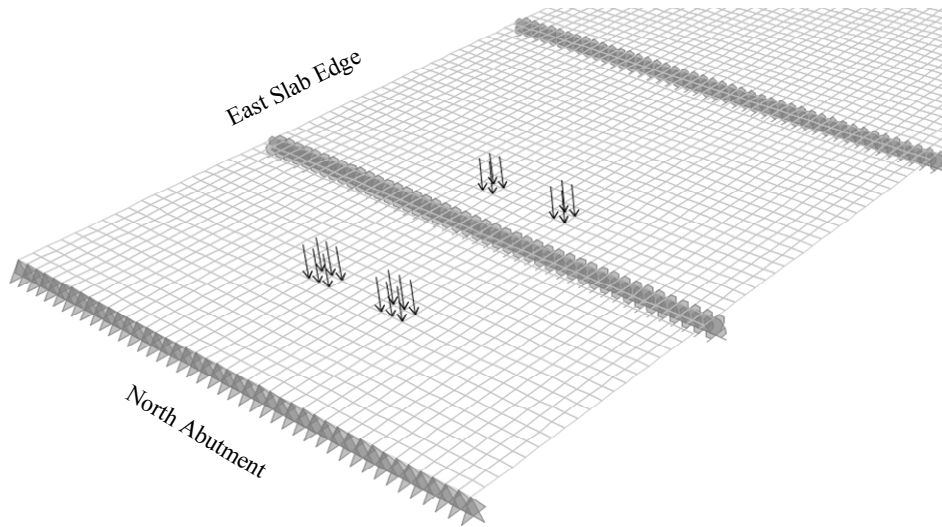


FIGURE 48. Finite element model loaded with 5YD test truck.

After the truck load cases were created and analyzed, the SAP2000 results were exported to the Excel spreadsheet program for further processing.

EXPERIMENTAL VS. ANALYTICAL MOMENTS

For purpose of comparison, the experimental moments (derived from measured strains) and analytical moments (determined from finite element analysis) in the slab were plotted jointly. Figures 49 through 53 show the slab bending moments under the 5YD truck load for the five transverse positions (from the first to the fifth path, respectively) at the four instrumented sections. Plot (a) of each figure represents the positive moments at section M1 and the negative moments at section P1 of the first span; plot (b) corresponds to sections M2 and P2 of the second span. The horizontal axis represents the transverse location along the bridge width (from the west to east edge) and the vertical axis represents the magnitude of bending moment in the slab. Experimental moments are labeled M_{gr} and M_{cr} which were calculated based on gross and cracked section behavior, respectively. The dashed lines labeled M_{av} represent the average of the M_{gr} and M_{cr} moments. These moments can also be interpreted as

$$M_{av} = ES_{av} \varepsilon_{\max} \quad (13)$$

where:

$$S_{av} = \text{average section modulus on tension side, in}^3$$

Analytical moments are labeled SAP. Again, positive moment values represent the slab response at midspan of the span and negative values represent the response close to the pier.

Table 7 provides the total longitudinal moments at the instrumented sections determined analytically from SAP2000 and experimentally from the M_{av} magnitudes for the 5YD truck. The total analytical moments were computed by summing the discrete moments of the forty-three shell elements across the slab width. The total experimental moments were computed by summing the M_{av} moments across the width assuming a linear distribution between transverse gage locations.

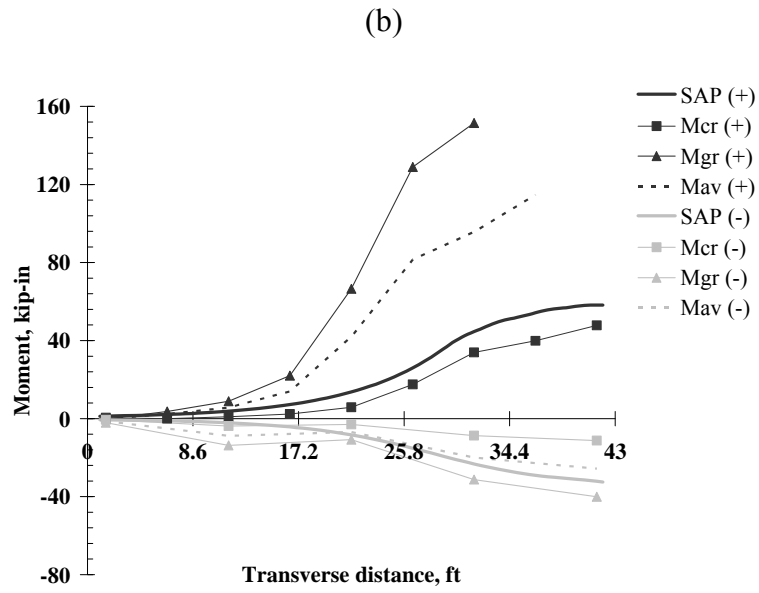
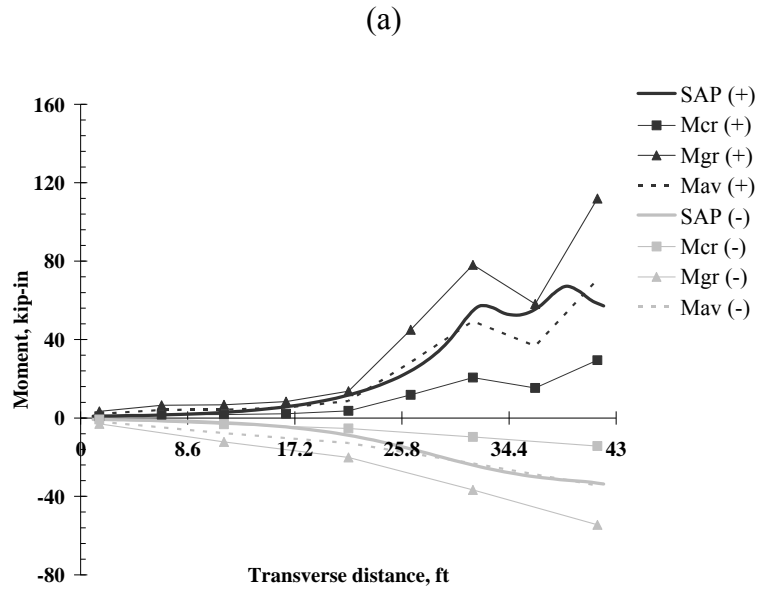


FIGURE 49. Slab moments for first path of 5YD truck: (a) first span and (b) second span.

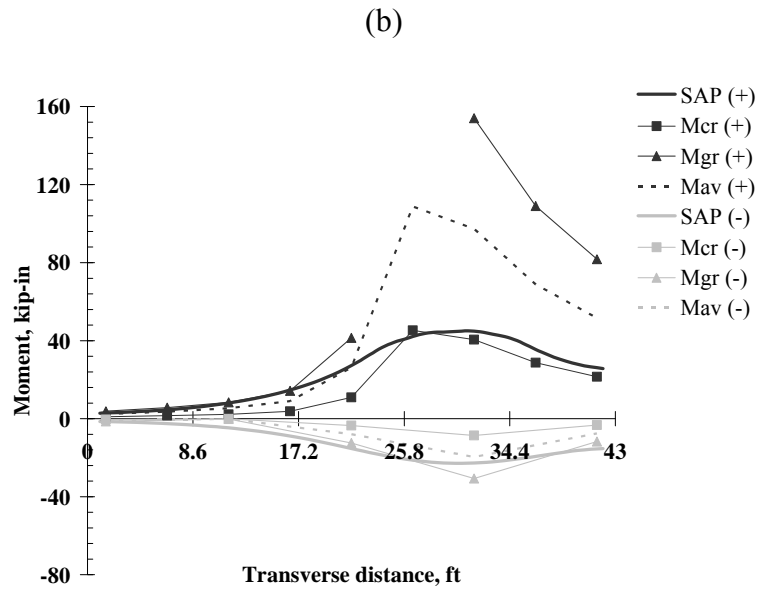
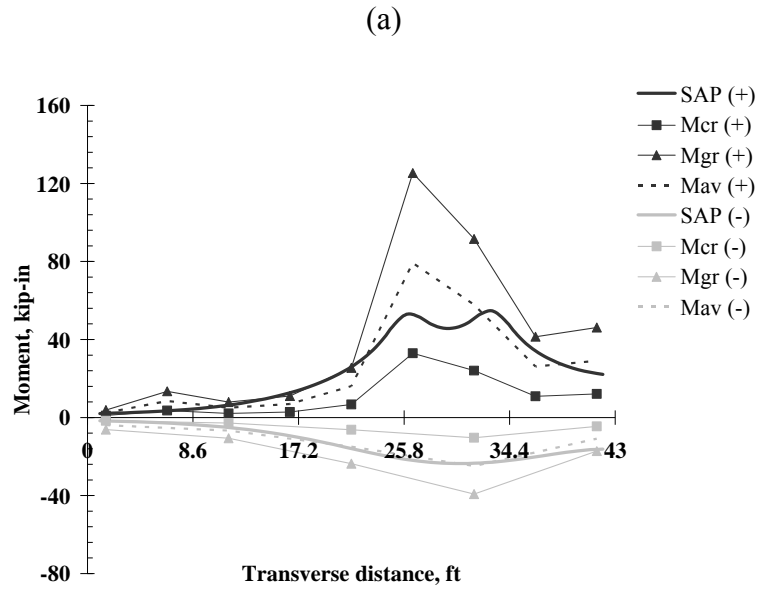


FIGURE 50. Slab moments for second path of 5YD truck: (a) first span and (b) second span.

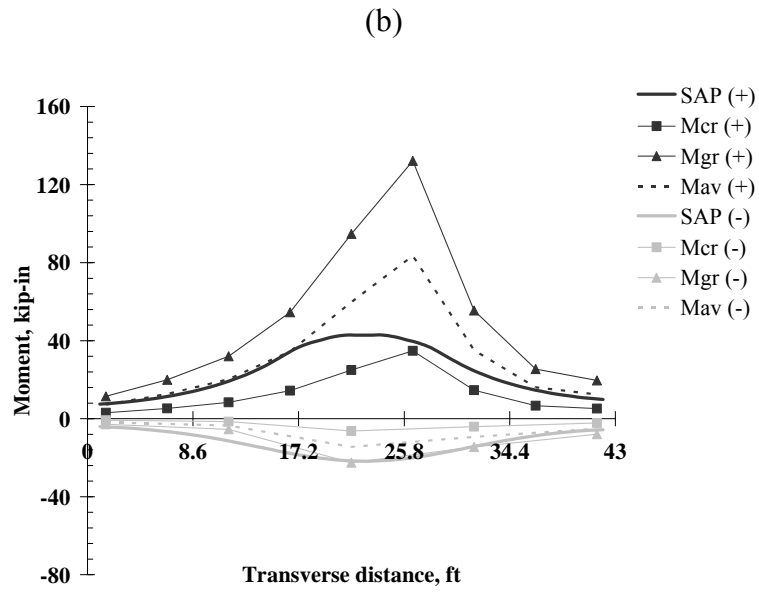
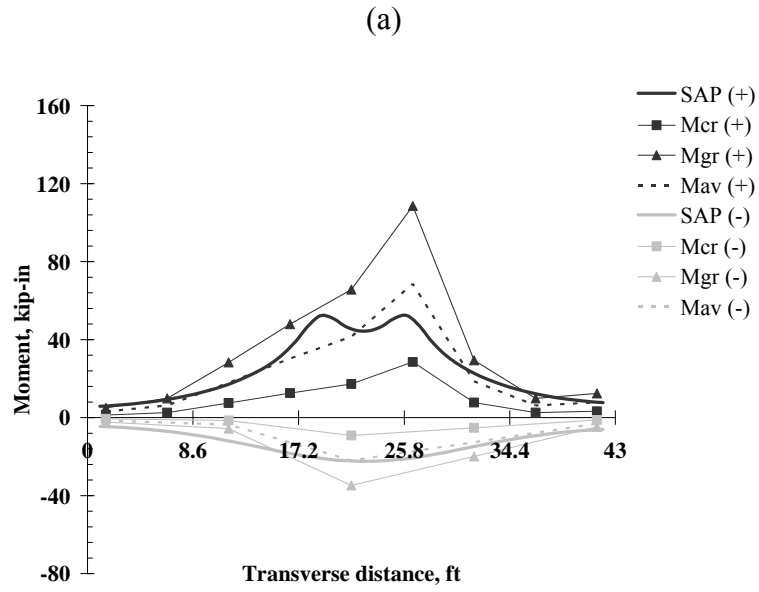


FIGURE 51. Slab moments for third path of 5YD truck: (a) first span and (b) second span.

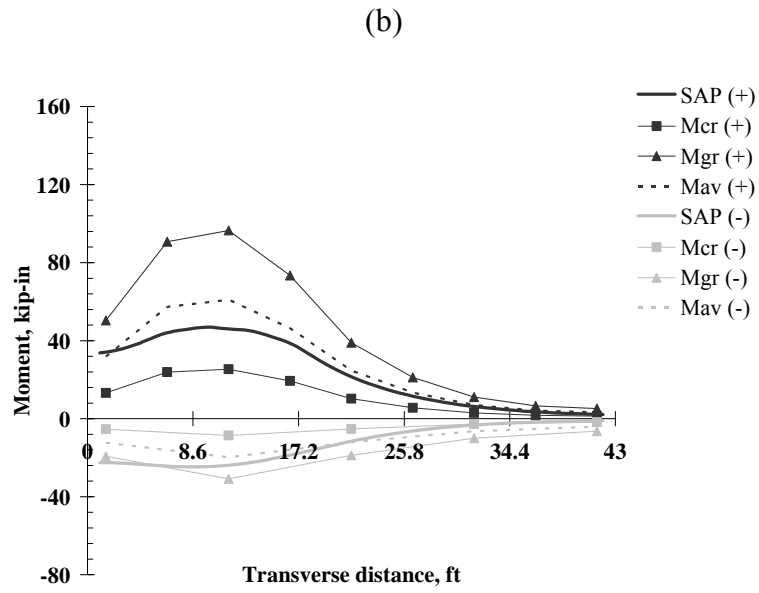
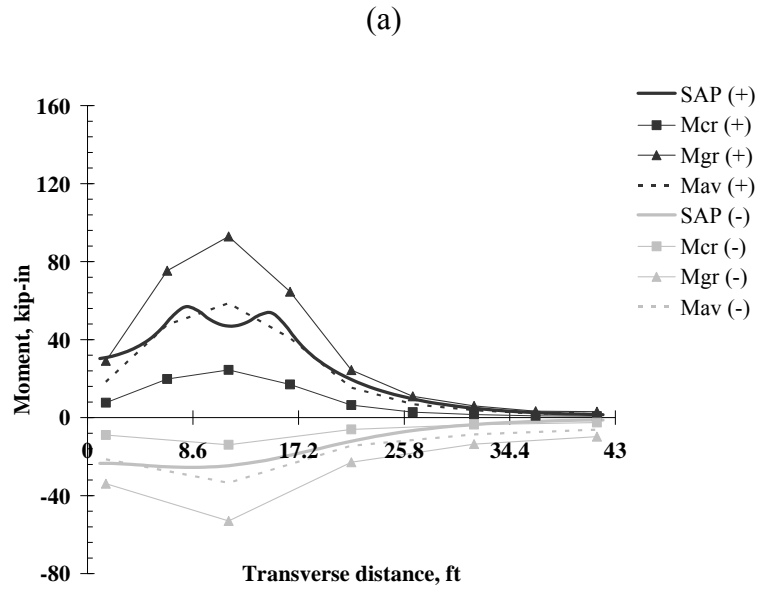
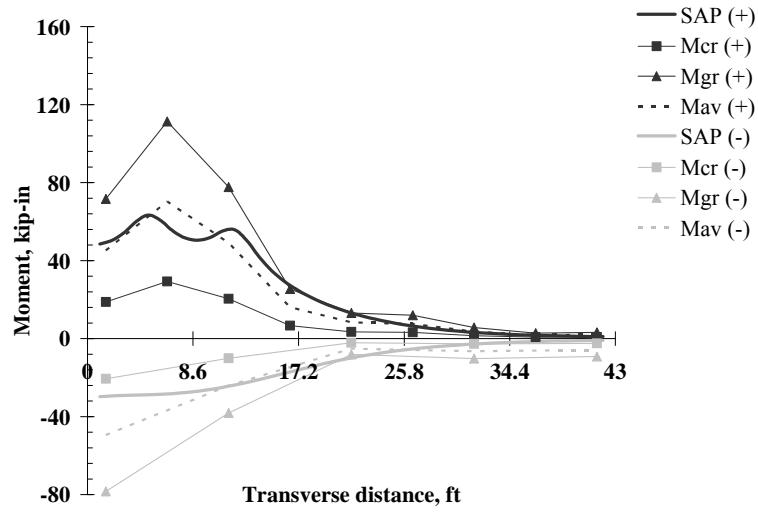


FIGURE 52. Slab moments for fourth path of 5YD truck: (a) first span and (b) second span.

(a)



(b)

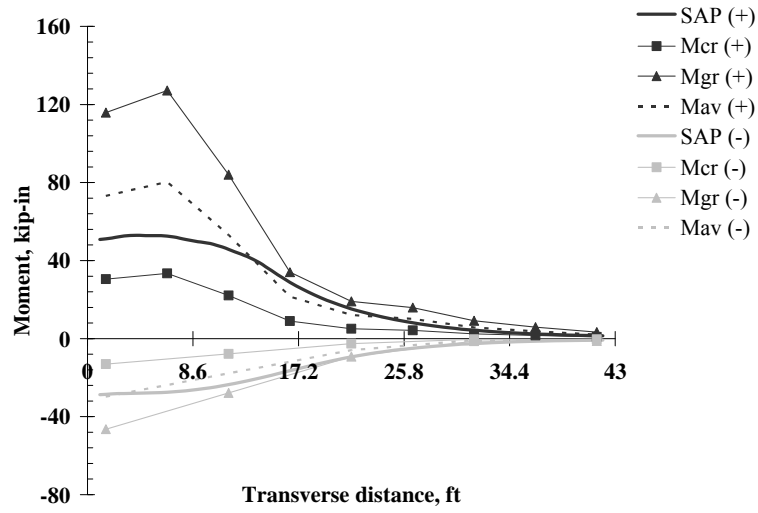


FIGURE 53. Slab moments for fifth path of 5YD truck: (a) first span and (b) second span.

TABLE 7. Total analytical vs. experimental moments for 5YD truck.

Section	Moment Definition	Total Longitudinal Moment (kip-ft)				
		First Path	Second Path	Third Path	Fourth Path	Fifth Path
M1	SAP	85.2	85.4	85.4	85.4	85.3
	Mav	79.3 (0.91*)	94.0 (1.10)	82.6 (0.97)	81.6 (0.96)	82.6 (0.97)
P1	SAP	-47.5	-47.1	-47.1	-47.2	-47.4
	Mav	-55.7 (1.17)	-47.7 (1.01)	-35.0 (0.74)	-62.9 (1.33)	-58.2 (1.23)
M2	SAP	83.1	83.6	83.6	83.5	83.2
	Mav	138 (1.66)	152 (1.82)	116 (1.39)	102 (1.23)	103 (1.24)
P2	SAP	-45.6	-45.3	-45.3	-45.4	-45.5
	Mav	-44.5 (0.97)	-28.4 (0.63)	-26.9 (0.59)	-41.4 (0.91)	-36.2 (0.80)

* Ratio of experimental and analytical moments, M_{av} / SAP

Plot (a) of Figure 49 shows a strong agreement between the SAP and M_{av} moments (magnitudes and distribution) in the first span; in addition, Table 7 reports a M_{av} / SAP ratio of 0.93 at section M1 and 1.17 at section P1. In the second span, the SAP moments at section M2 are closer to the M_{cr} moments while at section P2 there is closer agreement with the M_{av} moments (see plot (b) of Figure 49). Note that the M_{gr} moments corresponding to the first two gages installed on the east edge of the slab were not plotted since they were exceedingly high, possibly due to the proximity of the gages to a crack. From Table 7, the total M_{av} moment is 66% greater at section M2 and 3% lower at section P2 than the total SAP moment.

Figure 50 for the second truck path shows a similar comparison between the experimental and analytical moments as the first path. That is, the SAP moments were within 10% of the M_{av} moments at sections M1 and P1 (see Table 7). In the second span, the SAP moments agreed best with the M_{cr} moments at section M2 and with the M_{gr} moments at section P2. The high M_{gr} moments at section M2 estimated near the mid-width of the slab may possibly be due to poor transfer of the transverse bending moment across the bridge construction joint.

Recall that the joint was observed to have “minor leaching with rust stains” during the 2005 routine inspection which could indicate deterioration of the projecting mild reinforcement.

Plot (a) of Figure 51 for the third truck path again shows a good comparison between the SAP and M_{av} moments in the first span; the difference in total longitudinal moment was only 3% at section M1 and 26% at section P1 (see Table 7). Plot (b) of Figure 51 showed a slight change in behavior at section M2. Recall that the SAP moments came close to the M_{cr} moments for the first and second truck paths. For these two paths, the truck was situated on the east side of the slab. For the third path, however, the truck straddled the construction joint and the SAP moments correlated a little better with the M_{av} moments. This behavior may be an indication of a larger degree of cracking on the east side of the joint at both midspan sections especially M2. Section P2 showed similar behavior for the third path as the first two paths (i.e., the SAP and M_{gr} moments agreed well).

Plots (a) and (b) of Figure 52 for the fourth truck path show a close fit between the SAP and M_{av} moments at the four instrumented sections, particularly at M1 and P2 where the total moment ratios were 0.96 and 0.91, respectively. The other two sections (i.e., P1 and M2) showed a larger difference of about 30% between the total SAP and M_{av} moments. Figure 53 for the fifth truck path revealed a similar moment comparison as the fourth path. The difference between the SAP and M_{av} moments was only 3% at section M1 and less than 24% at the remaining three sections (i.e., P1, M2, and P2). Note that the truck was situated on the west side of the construction joint for the fourth and fifth paths.

Similar to the 5YD truck, the analytical and experimental moments for the 10YD truck for the first through fifth truck paths are plotted in Figures 54 through 58, respectively. In addition, Table 8 reports the total longitudinal moments under the 10YD truck load.

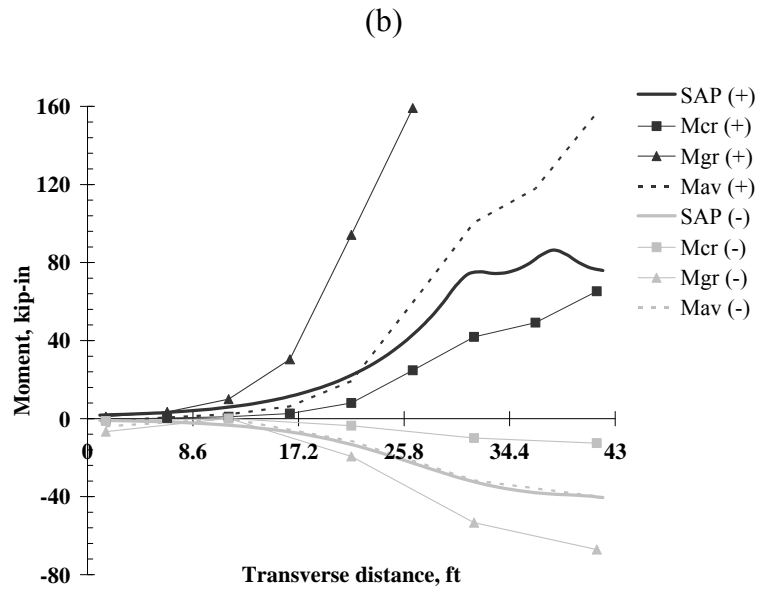
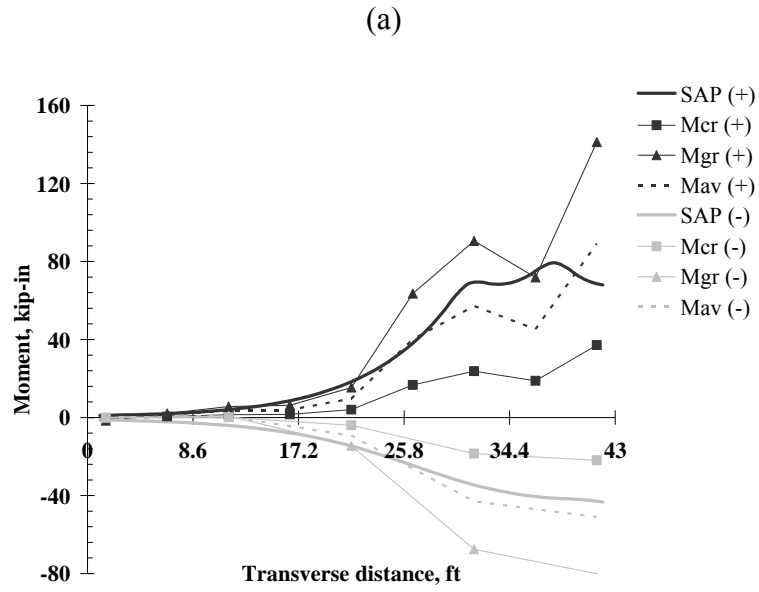


FIGURE 54. Slab moments for first path of 10YD truck: (a) first span and (b) second span.

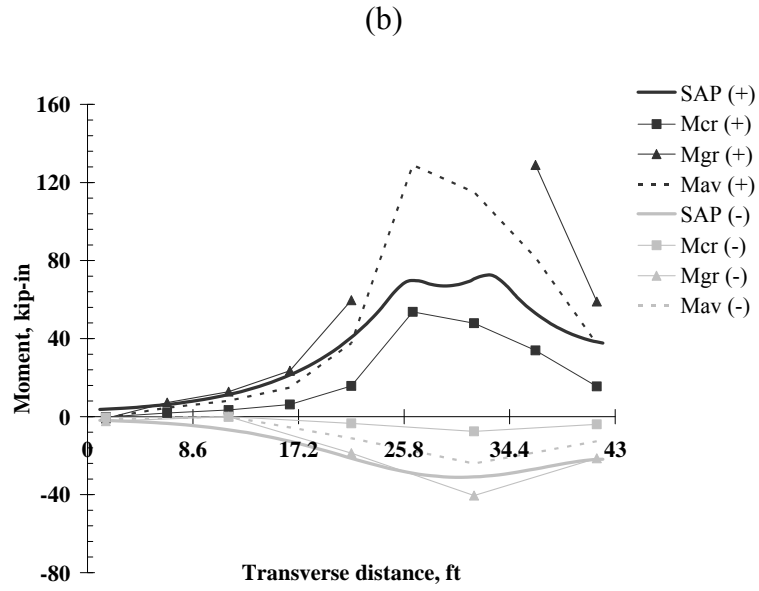
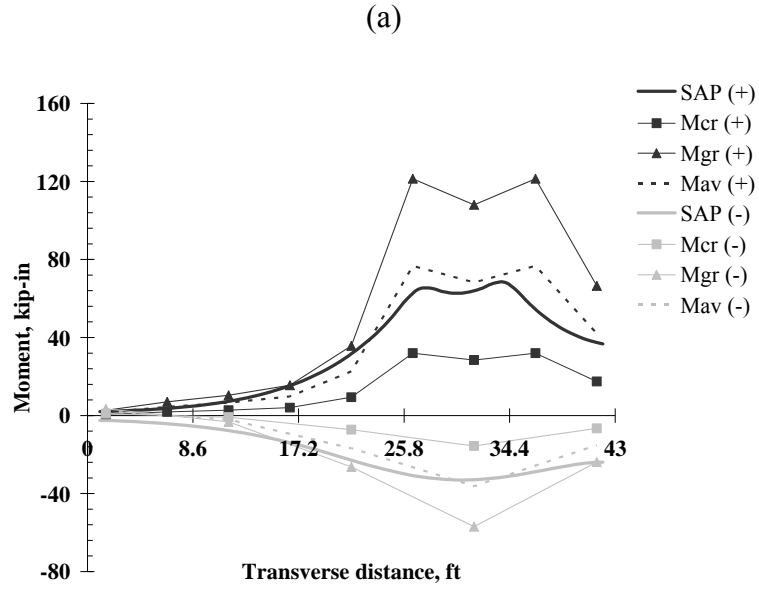


FIGURE 55. Slab moments for second path of 10YD truck: (a) first span and (b) second span.

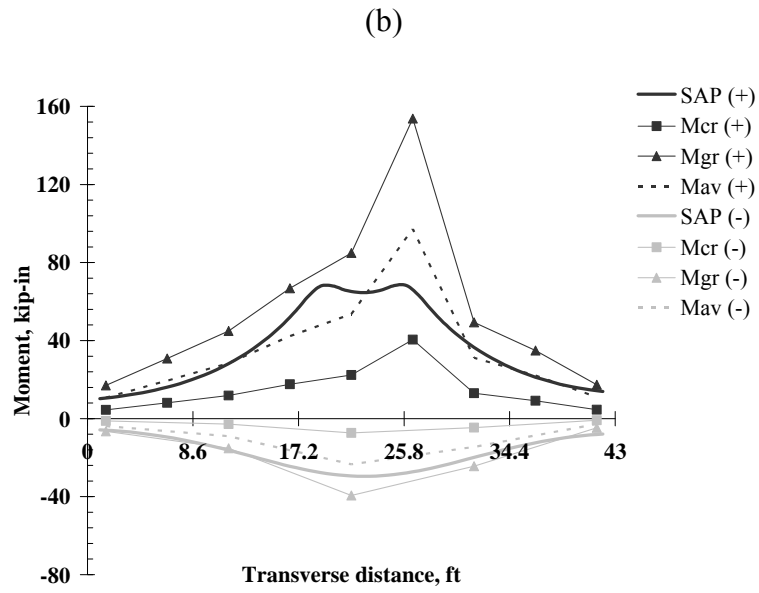
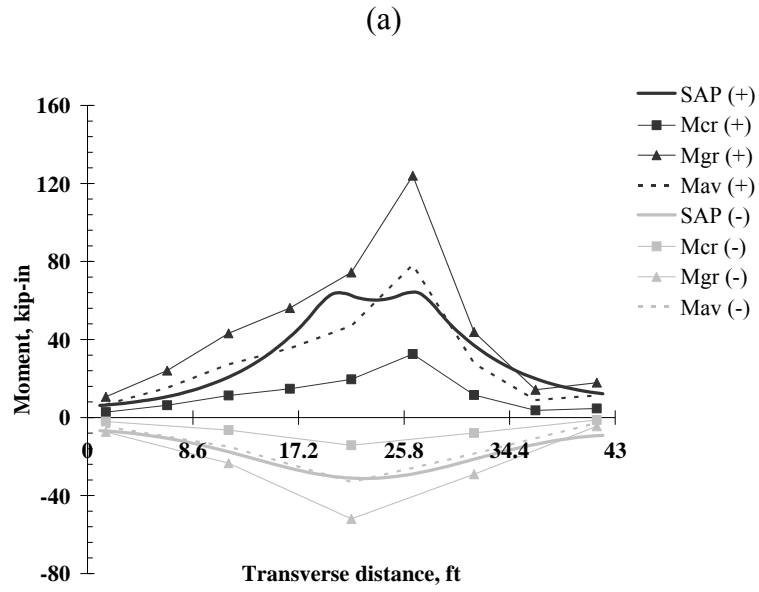


FIGURE 56. Slab moments for third path of 10YD truck: (a) first span and (b) second span.

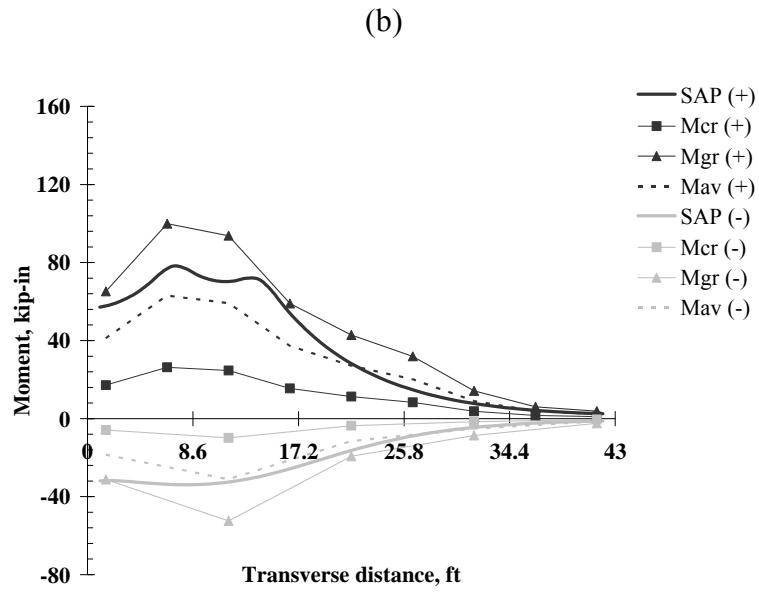
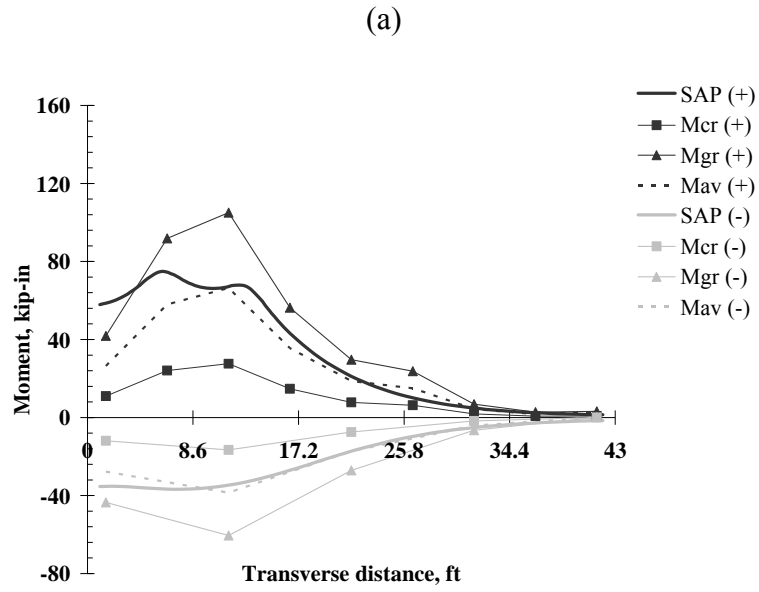


FIGURE 57. Slab moments for fourth path of 10YD truck: (a) first span and (b) second span.

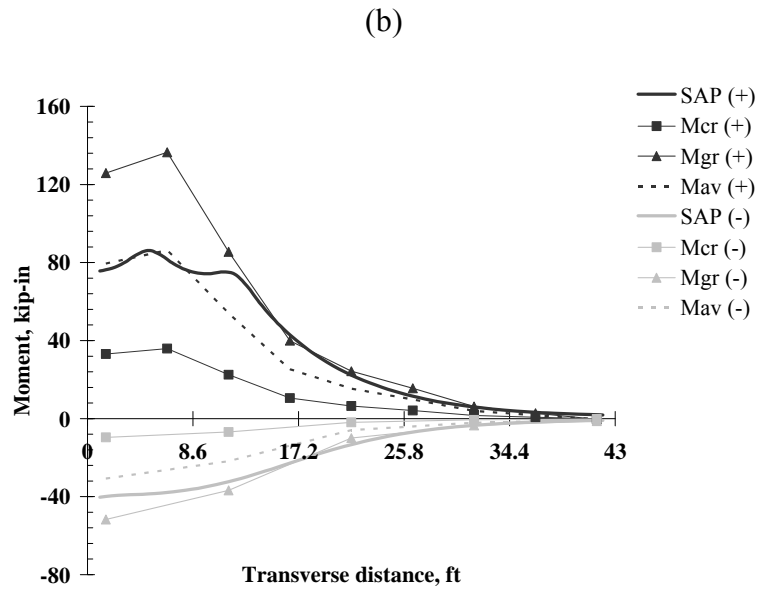
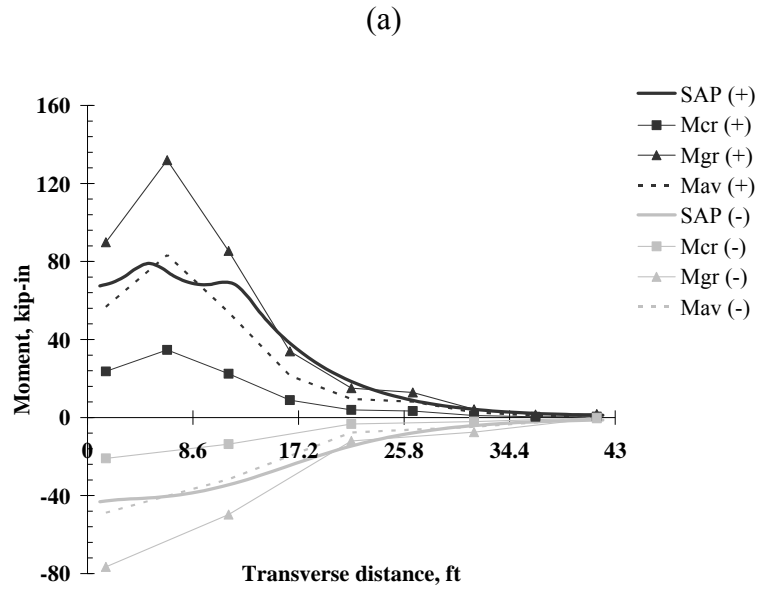


FIGURE 58. Slab moments for fifth path of 10YD truck: (a) first span and (b) second span.

TABLE 8. Total analytical vs. experimental moments for 10YD truck.

Section	Moment Definition	Total Longitudinal Moment (kip-ft)				
		First Path	Second Path	Third Path	Fourth Path	Fifth Path
M1	SAP	113	113	113	113	113
	Mav	94.0 (0.83*)	127 (1.13)	106 (0.94)	94.7 (0.84)	96.0 (0.85)
P1	SAP	-68.0	-67.6	-67.4	-66.3	-66.2
	Mav	-70.2 (1.03)	-54.6 (0.81)	-61.1 (0.91)	-65.8 (0.99)	-62.5 (0.94)
M2	SAP	127	127	127	127	127
	Mav	177 (1.40)	178 (1.40)	131 (1.03)	108 (0.85)	109 (0.86)
P2	SAP	-63.0	-62.7	-62.7	-62.8	-63.0
	Mav	-58.9 (0.94)	-37.5 (0.60)	-43.8 (0.70)	-51.6 (0.82)	-41.4 (0.66)

* Ratio of experimental and analytical moments, M_{av} / SAP

A qualitative comparison of the graph sets of the slab moments for the 5YD and 10YD trucks revealed no significant differences in behavior between the two load configurations. One minor difference was that the SAP and M_{av} moments agreed more closely at all four sections under the 10YD truck. As mentioned earlier, the 5YD truck weighed 33,720 lbs and the 10YD truck weighed 53,020 lbs (an increase of 19,300 lbs or about 60%). On average, the M_{av} / SAP ratio for the five truck paths of the 5YD truck came out to 0.98, 1.10, 1.47, and 0.78 at sections M1, P1, M2, and P2; for the 10YD truck, the ratios were 0.92, 0.94, 1.11, and 0.74. These ratios indicate that the SAP moments are within 10% and agree best with the M_{av} moments at the first span sections. In the second span, the SAP moments correlate best with the M_{cr} moments at the midspan section and with the M_{gr} moments at the pier section.

FINAL REMARKS

It is not a trivial matter to develop a finite element model that accurately represents the behavior of a reinforced concrete slab bridge because of the nonlinear behavior and load redistribution caused by cracking. From the comparison between the experimental and analytical moments presented in this chapter, it was found that the SAP model (with linear

elastic and isotropic properties) agreed reasonably well with the measured behavior of Bridge 7270. Finite element moments in the slab determined for the 5YD and 10YD trucks along the five transverse paths fit between the experimental M_{cr} and M_{gr} moments which represent the limits of cracked and gross section behavior, respectively. At the midspan and pier sections of the first span (i.e., M1 and P1), the SAP moments approximated the M_{av} moments while in the second span, the SAP moments agreed best with the M_{cr} moments at M2 and the M_{gr} moments at P2. Recall that the M_{av} moments are the average of the M_{cr} and M_{gr} moments.

It is important to mention that for this particular bridge (i.e., Bridge 7270), the measured response agreed reasonably well with the baseline finite element model. Moreover, the diagnostic test results did not reveal any sort of unintended behavior that would improve the performance of the bridge. For instance, the participation of stiff edge members (e.g., concrete jersey barriers) has been shown to favorably influence the load distribution of bridge structures. If observed, this type of behavior may be included to calibrate the bridge model to match the test measurements. However, this was not a factor for Bridge 7270 since the metal railing had virtually no impact on the bridge response. Another issue that can affect the performance of reinforced concrete slab bridges is unintended continuity. For simple span bridges, the joints between the separate spans may close up resulting in some degree of continuity across the joints. Again, the finite element model can be adjusted to capture this behavior. Nonetheless, Bridge 7270 was built as a continuous structure and not as a series of simple spans. A last point is that the actual material properties may be different than those given in the design plans. For Bridge 7270, the strength of the concrete may be larger than the design value. Yet, a change in the concrete stiffness of a linear-elastic, prismatic model (such as the one used to model Bridge 7270) will have no effect on the slab moments.

HIGHER LEVEL LOAD RATING

In the preceding chapter, it was shown that the experimental moments (derived using the measured tensile strains and average section modulus) agreed reasonably well with the analytical moments (obtained from a baseline finite element model). Consequently, the finite element model was used to evaluate the equivalent strip widths of Bridge 7270 in the positive and negative moment regions of the first and second spans. In this chapter, the equivalent widths determined using the AASHTO equations (an approximate method of structural analysis as defined in Article 6.3.2 of the LRFR Manual) are compared with those obtained from finite element analysis (a refined method of analysis as defined in Article 6.3.3 of the LRFR Manual). In addition, the effect of equivalent widths from refined analysis on the load rating factors is discussed.

It is important to mention that the response of the finite element model used in this research is linear although the observed behavior of Bridge 7270 was non-linear in the diagnostic load test. However, the lower bound theorem of simple plastic analysis states that a load computed based on a statically admissible moment diagram (i.e., one that is in equilibrium with the applied load and does not exceed the moment capacity at any location) is equal to or less than the true ultimate collapse load. Hence, a linear finite element analysis will give a conservative load rating at the strength limit state as long as the structure is ductile and capable of redistributing load. In the AASHTO load rating of Bridge 7270, the maximum reinforcement limit was satisfied indicating that the slab is underreinforced and thus, has adequate ductility.

SLAB RESPONSE UNDER ONE LOADED LANE

To evaluate the equivalent strip width using the finite element method, it was first necessary to determine the vehicular loads that caused the largest longitudinal bending moments in the positive and negative regions. From the AASHTO load rating analysis presented earlier in the report, the critical vehicles are the design tandem for positive moment and the HS20-14 design truck for negative moment. The tandem and HS20-14 loads were placed on the finite element model to evaluate the equivalent strip width at two locations (midspan and pier) of the first and second spans. Legal loads were not considered in the higher level evaluation of the equivalent width, only design loads.

To maximize the positive moment at midspan of the first span, the design tandem was placed longitudinally as shown in Figure 59. The critical transverse position was then found by moving the tandem transversely in 2.0 ft. increments towards the centerline of the bridge width starting at 4.0 ft. from the edge of the slab as shown in Figure 60.

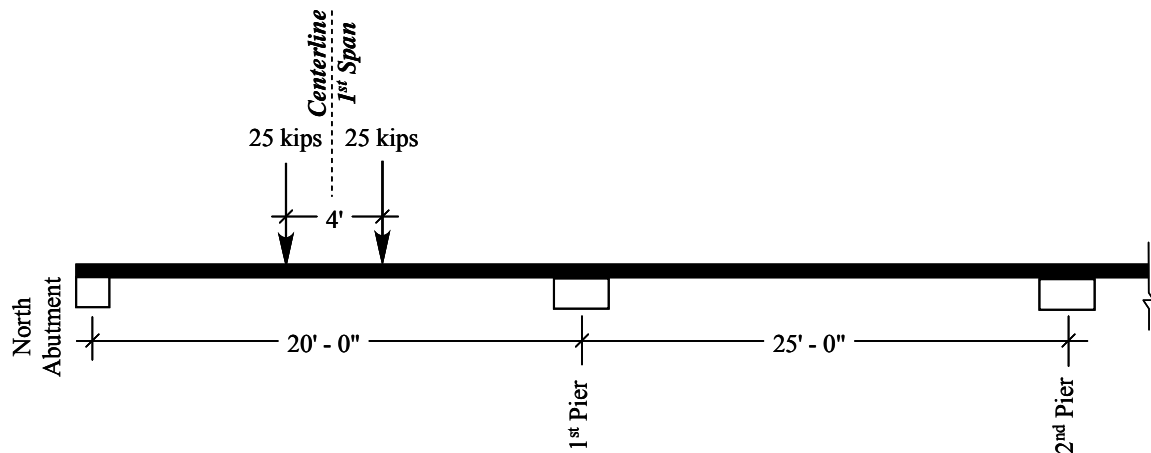


FIGURE 59. Critical longitudinal position of design tandem for positive moment at first midspan.

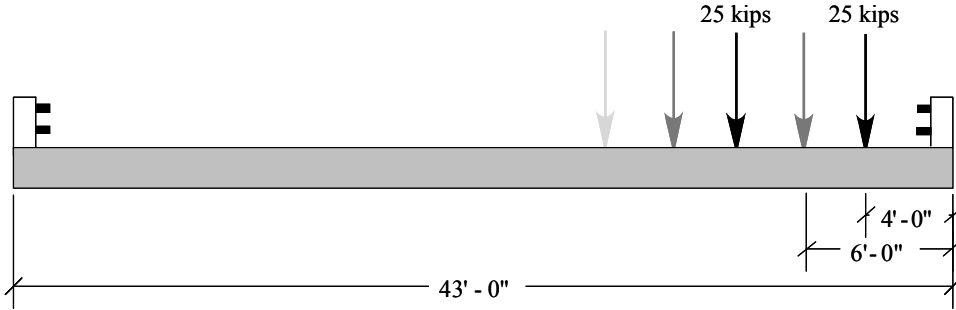


FIGURE 60. Transverse positions of design tandem for positive moment.

According to Article 6.2.3.2 of the LRFR Manual, the wheel line spacing of the design vehicles is 6.0 ft. In addition, the same article states that the center of a wheel line should be no closer than 2.0 ft. from the edge of a traffic lane or face of the curb. Note that the width of the steel rail is 1.5 ft. (see Figure 7) which places the closest wheel line at 3.5 ft. from the slab edge instead of 4.0 ft. However, a comparison of the slab moments for these two positions showed no significant differences. Consequently, the 4.0 ft. starting position was used since it simplified the loading of the finite element model.

The slab moments at the first midspan for nine different transverse positions of the design tandem is shown in Figure 61.

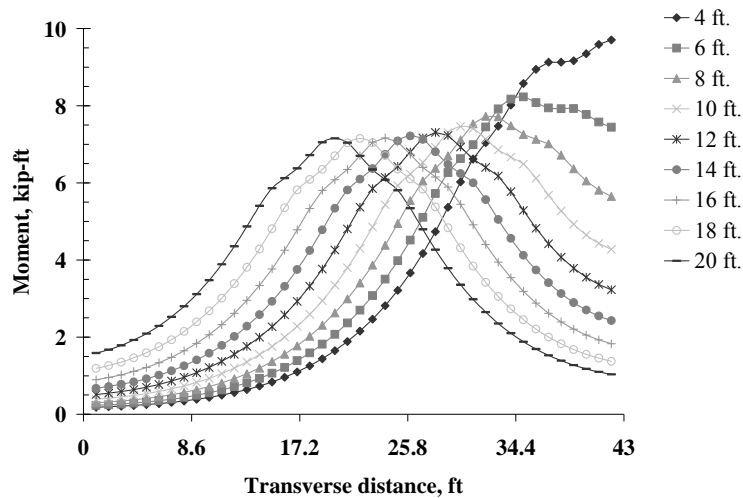


FIGURE 61. Slab moments due to design tandem at first midspan.

As shown in the figure, the peak moment of 9.71 kip-ft/ft occurred at the edge of the slab with the tandem positioned closest to the rail (i.e., 4.0 ft.). At the next transverse position of the tandem (i.e., 6.0 ft.), the peak slab moment decreased by about 18% and was located 8.0 ft. from the slab edge. A similar procedure was followed to determine the maximum slab moment at the second midspan.

The equivalent width evaluation at the negative moment regions (piers) was similar to the evaluation at the positive moment regions. As discussed earlier, the one major difference was the vehicular load applied (i.e., the HS20-14 design truck was critical instead of the design tandem). At the first pier, the HS20-14 was positioned longitudinally as shown in Figure 62.

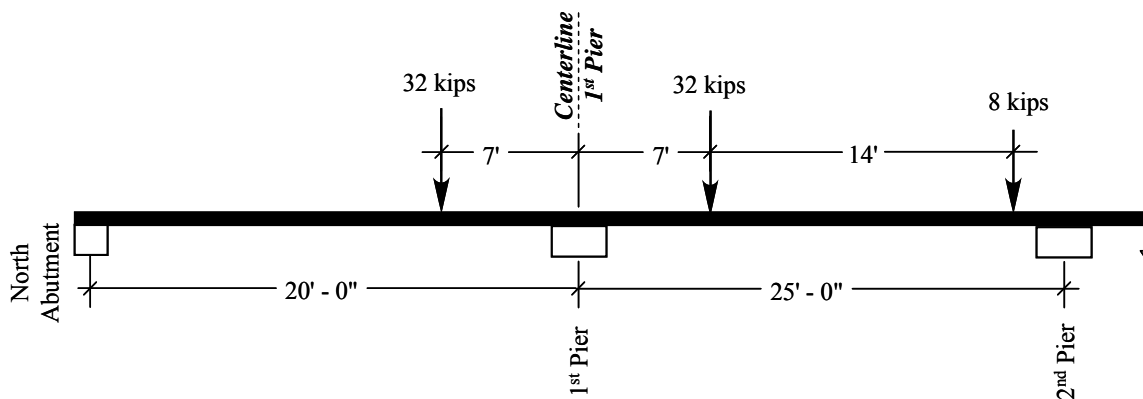


FIGURE 62. Critical longitudinal position of design truck for negative moment at first pier.

The slab moments for the nine transverse positions of the design truck are shown in Figure 63. This figure shows a peak moment of 8.92 kip-ft/ft at a transverse distance of 3.0 ft. from the slab edge with the truck positioned adjacent to the rail. The peak moment for the next position was about 14% lower and located 8.0 ft. from the slab edge. Similar behavior was observed at the second pier. Thus, the critical transverse position of the design vehicles (for one lane loaded) was the one closest to the rail for both positive and negative moment.

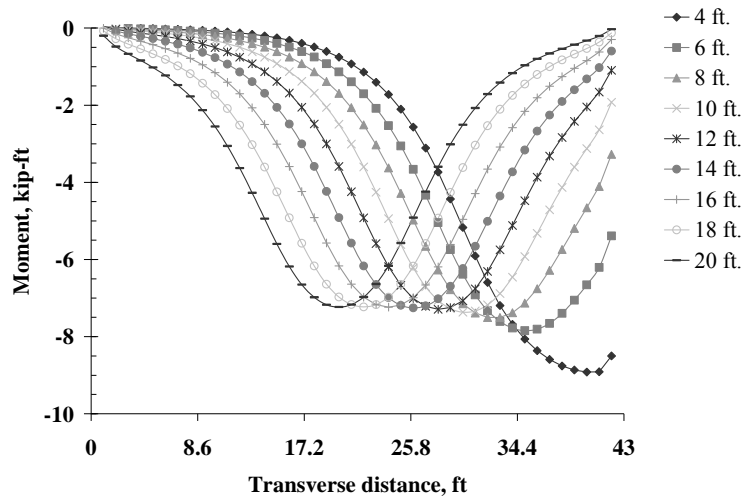


FIGURE 63. Slab moments due to HS20-14 design truck at first pier.

SLAB RESPONSE UNDER MULTIPLE LOADED LANES

Recall that the multiple loaded lanes controlled the equivalent width of an interior strip in the AASHTO load rating analysis. Consequently, the finite element model was analyzed with one, two, and three lanes loaded as shown in Figure 64. The lanes were situated towards the rail due to the findings for one lane loaded presented in the previous section. Based on Article 3.6.1.1 of the LRFD Bridge Design Specifications (7), the standard lane width is 12.0 ft. In addition, the distance between the wheel lines of adjacent trucks is limited to 4.0 ft. as stated in LRFR Article 6.2.3.2 (4). Care was taken to adhere to these provisions when placing the design vehicles on the finite element model. The three loading configurations given in Figure 64 were applied to the finite element model at the two midspan and two pier locations. The total longitudinal moment at each location was determined by summing the moments of the forty-three shell elements (each 1.0 ft. wide) across the slab width. To verify the finite element results, the total SAP moments results were compared to those obtained from RISA 2-D and the moments differed by less than 1.0 percent.

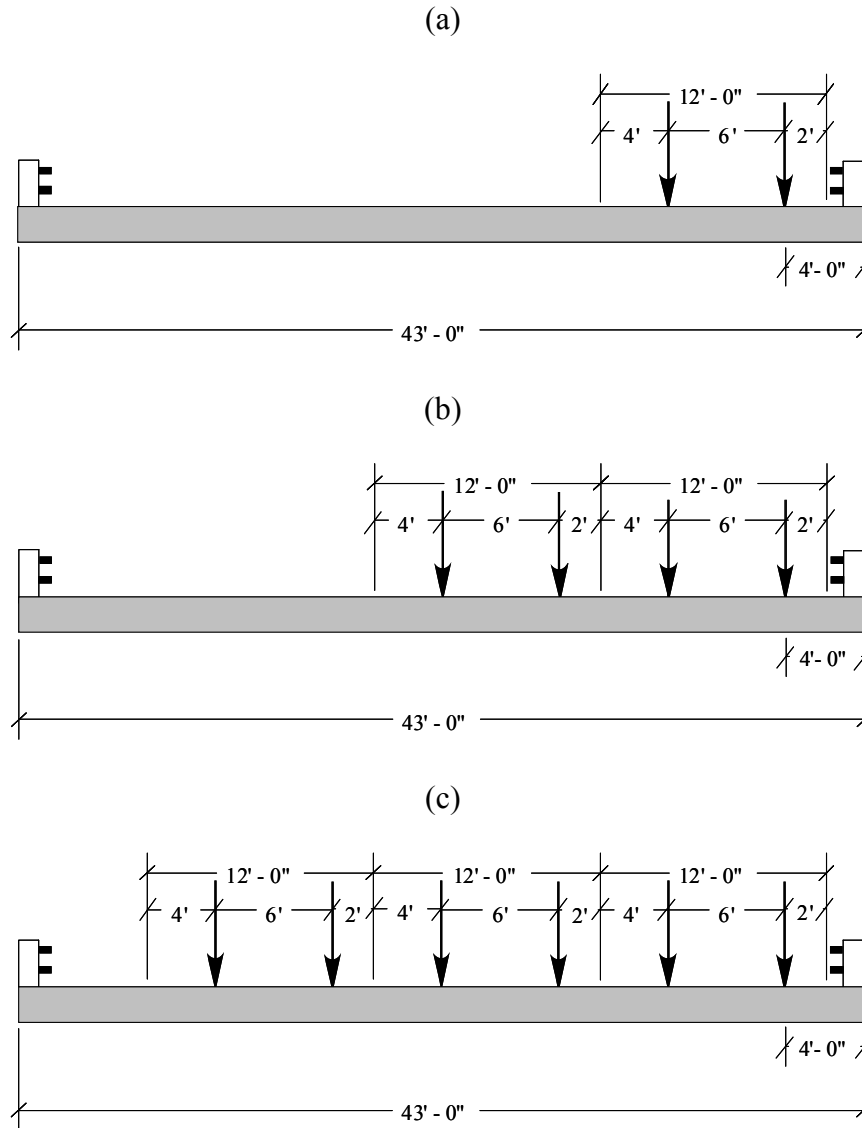


FIGURE 64. Vehicular live load configurations for (a) one, (b) two, and (c) three loaded lanes.

Plots (a) and (b) of Figure 65 show the slab moments in the first and second span, respectively, for the three combinations of loaded lanes. The moment magnitudes plotted in the figures were determined by multiplying the finite element moments by the multiple presence factors (m) described in LRFD Article 3.6.1.1.2. In brief, m depends on the number of loaded lanes and equals 1.20 for one lane, 1.00 for two lanes, and 0.85 for three lanes.

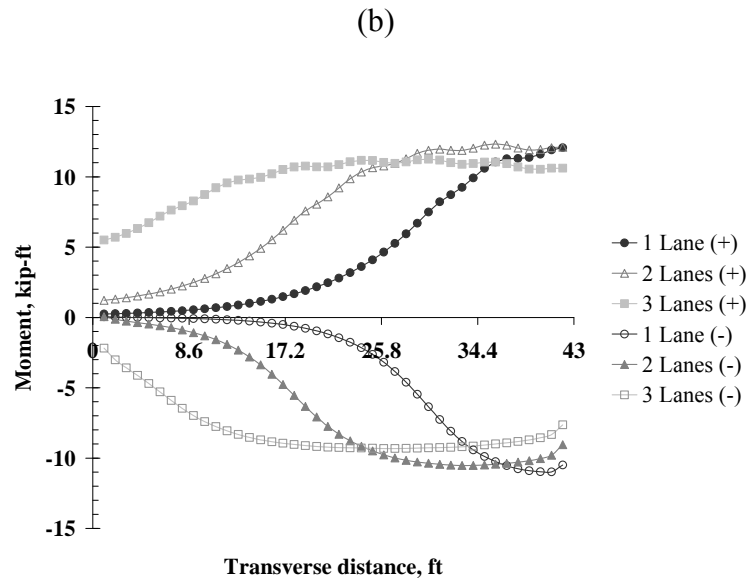
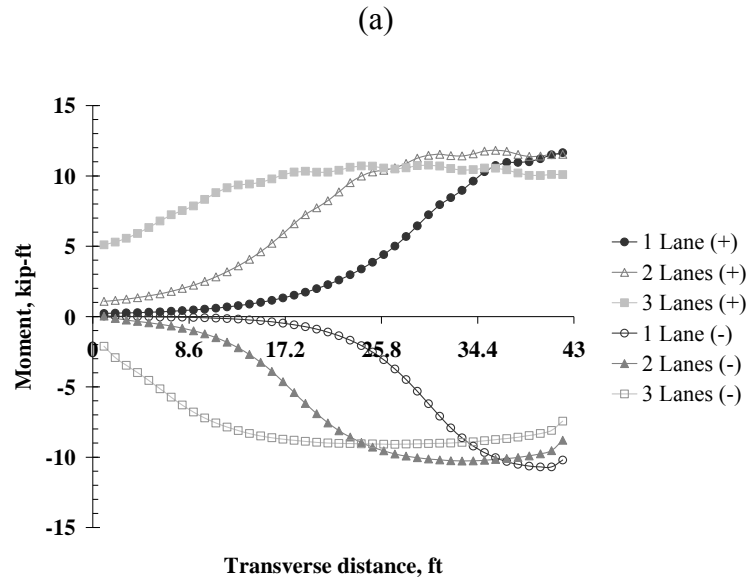


FIGURE 65. Slab moments from finite element analysis for (a) first span and (b) second span.

The single presence factor (i.e., $m = 1.20$) greater than unity signifies the following: “when a single vehicle is on the bridge, it can be heavier than each one of a pair of vehicles and still have the same probability of occurrence” (7). Hence, a single lane loaded with 120% of the full design live load has equal likelihood as two lanes (100% fully loaded) or three lanes

(85% fully loaded) and all three combinations should be checked to determine the one that is most critical.

In the first span (see Figure 65(a)), the peak slab moments were produced by two loaded lanes for positive moment and one loaded lane for negative moment. The maximum positive moment equaled 11.8 kip-ft/ft and occurred at a transverse distance of 36.0 ft. while the maximum negative moment was 10.7 kip-ft/ft at 40.0 ft. Similar behavior was observed in the second span (see Figure 65(b)) but with a slight increase in the moment magnitudes; the maximum positive and negative moments were 12.3 kip-ft/ft and 11.0 kip-ft/ft, respectively.

RATING FACTORS FROM REFINED ANALYSIS

The equivalent strip widths were determined from the finite element results by dividing the total longitudinal moment (for one lane loaded) by the maximum slab moment per foot (including the multiple presence factors). Table 9 shows the equivalent widths for one, two, and three loaded lanes determined from refined analysis at the two midspan and two pier locations.

TABLE 9. Equivalent strip widths from refined analysis.

Number of Loaded Lanes	Equivalent Width (ft.)			
	First Midspan	First Pier	Second Midspan	Second Pier
One	13.45	12.14 *	13.57	12.14 **
Two	13.27 *	12.60	13.35 **	12.62
Three	14.58	14.23	14.63	14.24

* Equal to 10.52 ft. (first midspan) and 10.73 ft. (first pier) using approximate analysis.

** Equal to 10.93 ft. (second midspan and second pier) using approximate analysis.

As shown in the table, two lanes loaded controlled the equivalent widths at the midspan locations while one lane loaded controlled at the pier locations. The least critical case was

three loaded lanes at all four locations. The equivalent widths from refined analysis at the midspan and pier locations were 13.27 ft. and 12.14 ft., respectively, in the first span and 13.35 ft. and 12.14 ft. in the second span.

A comparison of the equivalent strip widths obtained by approximate and refined methods of analysis is also provided in Table 9. Recall that the controlling case for the equivalent width of an interior strip used in the AASHTO load rating was “more than one lane loaded” for positive and negative moment. On the other hand, the critical equivalent widths from refined analysis were based on different load cases; two loaded lanes controlled at the midspan locations (i.e., positive moment) and one loaded lane controlled at the pier locations (i.e., negative moment). By comparison, the widths obtained from refined analysis were greater than those determined from the AASHTO approximate method of analysis at the four locations. The refined widths are 26.1% and 13.1% larger at the first midspan and first pier, respectively. At the midspan and pier locations in the second span, the refined widths are 22.1% and 11.1% greater. This comparison indicates that the approximate method gives conservative values for the equivalent strip width, particularly for positive moment.

The inventory and operating rating factors for positive moment using the approximate and refined methods of analysis are shown in Table 10; similar information is given in Table 11 for negative moment. In both tables, the rating values listed for the approximate method were extracted from Tables 5 and 6. The factors given for the refined method were obtained by replacing the equivalent widths from approximate analysis by those determined by finite element analysis. As a result, the rating factors increased by the same percent increase in the equivalent widths.

TABLE 10. Rating factors from approximate and refined analysis for positive moment.

Span	Position (ft)	RF _{inv}		RF _{opr}	
		Approx.	Refined	Approx.	Refined
1	9.26	1.03	1.30	1.34	1.69
1	15.5	1.28	1.61	1.66	2.09
1	17.5	1.77	2.23	2.30	2.93
3	20.1	1.27	1.55	1.64	2.00
4	13.0	1.03	1.26	1.34	1.64

TABLE 11. Rating factors from approximate and refined analysis for negative moment.

Span	Position (ft)	RF _{inv}		RF _{opr}	
		Approx.	Refined	Approx.	Refined
1	16.8	1.04	1.18	1.35	1.53
1	20.0	1.07	1.21	1.39	1.57
3	25.0	1.11	1.23	1.43	1.62
4	3.63	1.22	1.36	1.59	1.77
4	7.75	0.84	0.93	1.08	1.20

As shown in Table 10, the rating factors for positive moment increased by 26.1% in the first span (i.e., an exterior span) and by 22.1% in the third and fourth spans (i.e., interior spans). For the third and fourth spans, the equivalent widths obtained from the refined analysis of the second span were employed. From Table 9, the refined widths differed by less than 1% in the first and second span which implies that the behavior of the other interior spans will be similar to the second span. For negative moment, the rating factors increased by 13.1% in the exterior span and 11.1% in the interior spans (see Table 11).

SUMMARY AND CONCLUSIONS

SUMMARY

A seven-span continuous, reinforced concrete slab bridge (NMDOT #7270), built in 1972 and located in Las Cruces, NM was evaluated in this research project. The AASHTO load rating factor for this type of bridge mainly depends on the live-load moment per foot of slab width. To improve the load rating, a higher level evaluation of Bridge 7270 was conducted (using diagnostic load testing and finite element analysis) to determine a more accurate equivalent strip width. An increase in the equivalent width decreases the live-load moment thereby increasing the load rating factor. Brief summaries of the various parts of the project are provided in the following paragraphs.

An AASHTO load rating analysis of Bridge 7270 was first performed based on the LRFR method. In this initial analysis, the live-load effects were determined using the code-prescribed equations for equivalent strip width (an approximate method of analysis) given in LRFR Article 6.3.2. In addition, the existing traffic volume and superstructure condition provided in the 2005 inspection report were explicitly considered in the LRFR analysis; the degree of structural redundancy of the bridge was also taken into account. Rating factors at the design load level (inventory and operating) and the legal load level were calculated for the positive and negative moment regions of the bridge.

In the next phase of the study, a diagnostic load test of the bridge was performed. The bridge was loaded with two different dump trucks (having 5 and 10 cubic-yard capacities) and strain measurements were taken at four separate sections (the positive and negative moment regions of the first and second spans). At each section, strain transducers were installed across the bridge width on the top and bottom side to estimate the slab stiffness (i.e.,

neutral axis positions) and moment distribution characteristics. In conjunction with the load test, the bridge was modeled and analyzed by the finite element method (a refined method of analysis as defined in LRFR Article 6.3.3). Under dump-truck loading, the analytical moments (determined from finite element analysis) and experimental moments (derived from measured strains) in the slab were compared to validate the finite element model.

The final phase of the research focused on re-evaluating the equivalent strip widths of the bridge in the positive and negative moment regions using the finite element method and performing a higher level load rating. Equivalent widths and rating factors determined by refined analysis were ultimately compared with those obtained by approximate analysis.

CONCLUSIONS

The following conclusions were drawn from the AASHTO load rating of Bridge 7270 (using the approximate method of analysis):

- The largest vehicular live-load effects were produced by the design tandem in the positive moment regions and the HS20 design truck in the negative moment regions. The controlling legal truck for positive moment was the Type 3 while the Type 3S2 controlled for negative moment (except at one location).
- Using the approximate method of analysis (i.e., the AASHTO equations for equivalent strip width), the lowest rating factors for positive moment were $RF_{inv} = 1.03$ and $RF_{opr} = 1.34$. These ratings occurred close to midspan of the first (exterior) and fourth (interior) spans. For negative moment, the smallest ratings occurred at a rebar cutoff location and equaled $RF_{inv} = 0.84$, $RF_{opr} = 1.08$, and $RF_{legal} = 1.13$.

- Based on the rating factors obtained from approximate analysis, Bridge 7270 has a safe load capacity for AASHTO legal loads and state legal loads having only minor variations from the AASHTO loads.

The following conclusions were drawn from the diagnostic load testing and slab stiffness evaluation of Bridge 7270:

- The measured tensile strains under the test truck loads plus the estimated dead load strains exceeded the concrete cracking strain at several locations in the positive and negative moment regions. These results confirmed that the concrete was cracked and thus, implied that the slab was not a gross section.
- In the positive moment regions, the experimental neutral axis locations varied across the slab width but overall lied about halfway between the theoretical limits based on uncracked and cracked section behavior. In the negative moment regions, the experimental neutral axis positions also varied and fit within the theoretical bounds but more towards an uncracked section.
- The experimental neutral axis depths did not vary significantly under the 5-yard and 10-yard dump trucks, indicating that the slab had about the same stiffness under both loads. On the whole, the neutral axis evaluation supported the use of an intermediate section modulus for computing the experimental bending moments of the slab.

The following conclusions were drawn from the refined analysis of Bridge 7270 (using the finite element method):

- Bridge 7270 was modeled as a prismatic, concrete slab with linear-elastic and homogeneous material properties. Finite element moments in the slab determined under the 5-yard and 10-yard dump trucks fit between the experimental M_{cr} and M_{gr}

moments (derived from measured tensile strains) which represent the limits of cracked and gross section behavior.

- At the midspan and pier sections of the first span, the finite element moments approximated the M_{av} (i.e., the average of M_{cr} and M_{gr}) moments. In the second span, the finite element moments agreed best with the M_{cr} moments at midspan and the M_{gr} moments at the pier. Overall, the experimental moments (determined using the average section modulus) agreed reasonably well with the analytical moments from a baseline finite element model which considered only the concrete slab superstructure.
- The diagnostic test results did not reveal any sort of inadvertent behavior (e.g., edge member participation, unintended continuity) that could further improve the behavior of this particular bridge beyond that captured by the baseline model. Yet there may be cases where the load distribution may be more favorable than that determined by a baseline model. For example, slab bridges having Jersey barriers joined continuously along the edge (rather than discretely connected metal rails) may benefit from the stiffness contribution of the edge members; however, such type of behavior should be verified through load testing before it is included in the refined analysis.

The following conclusions were drawn from the higher level load rating of Bridge 7270 (using refined analysis):

- In the positive and negative moment regions, the critical transverse position of the design vehicles (for one lane loaded) was the one with the nearest wheel line located a distance of 2 ft. from the edge of the rail. For multiple loaded lanes (i.e., two and three lanes), the critical configuration happened with the lanes positioned right next to the rail and no horizontal separation between the lanes.

- Under design loading and including the multiple presence factors, the largest slab moments from finite element analysis were produced by two loaded lanes for positive moment and one loaded lane for negative moment. The smallest moments were produced by three loaded lanes.
- The critical equivalent widths from refined analysis were based on different load cases; two loaded lanes controlled in the positive moment regions and one loaded lane controlled in the negative moment regions. On the other hand, the controlling case from approximate analysis was “more than one lane loaded” for both positive and negative moment.
- The equivalent widths obtained by refined analysis were greater than those determined using the AASHTO approximate method of analysis. The refined widths were 26.1% and 13.1% larger at the first midspan and first pier, respectively. At the midspan and pier locations of the second span, the refined widths were 22.1% and 11.1% greater. This comparison indicated that the approximate widths were conservative, particularly for positive moment.
- The increase in the equivalent strip widths obtained from refined analysis signifies a decrease in live-load effects, which in turn proportionally increases the rating factors. That is, the rating factors increased by the same percent increase in the equivalent widths. As a result of the higher level evaluation, the lowest inventory and operating rating factors improved from 0.84 to 0.93 and 1.08 to 1.20 (an increase of 11%), respectively. The factors increased by just 11% (rather than over 20%) since the rating was controlled by negative moment and not positive moment.

REFERENCES

1. Ryan, T. W., R. A. Hartle, J. E. Mann, and L. J. Danovich. *Bridge Inspector's Reference Manual*. Publication FHWA NHI 03-001. FHWA, U. S. Department of Transportation, 2006.
2. National Bridge Inventory (NBI) Homepage. FHWA, U. S. Department of Transportation, Washington. <http://www.fhwa.dot.gov/bridge/nbi.htm>. Accessed November 1, 2007.
3. Amer, A., M. Arockiasamy, and M. Shahawy. Load Distribution of Existing Solid Slab Bridges Based on Field Tests. *Journal of Bridge Engineering*, Vol. 4, No. 3, 1999, pp. 189-193.
4. *Manual for Condition Evaluation and Load and Resistance Factor Rating (LRFR) of Highway Bridges*, 1st ed. AASHTO, Washington, D.C., 2003.
5. *SAP2000 User's Manual*. Version 10.0.9. Computers & Structures, Inc., Berkeley, Calif., 2006.
6. Mabsout, M., K. Tarhini, R. Jabakhanji, and E. Awwad. Wheel Load Distribution in Simply Supported Concrete Slab Bridges. *Journal of Bridge Engineering*, Vol. 9, No. 2, 2004, pp. 147-155.
7. *LRFD Bridge Design Specifications*, 3rd ed. AASHTO, Washington, D.C., 2004.
8. Saraf, V. K. Evaluation of Existing RC Slab Bridges. *Journal of Performance of Constructed Facilities*, Vol. 12, No. 1, 1998, pp. 20-24.
9. Azizinamini, A., Y. Shekar, G. Barnhill, and T. E. Boothby. Old Concrete Slab Bridges: Can They Carry Modern Traffic Loads?. *Concrete International*, Vol. 16, No. 2, 1994, pp. 64-69.

10. Chajes, M.J., H. W. Shenton III, and D. O'Shea. Use of Field Testing in Delaware's Bridge Management Program. *Proceedings of the 8th International Bridge Management Conference*, TRB, National Research Council, Denver, Col., 1999.
11. Wipf, T. J., B. M. Phares, F. W. Klaiber, D. L. Wood, E. Mellingen, and A. Samuelson. *Development of Bridge Load Testing Process for Load Evaluation*. Report No. TR-445. Center for Transportation Research and Education, Iowa State University, 2003.
12. Commander, B. and J. Schulz. A Field Verified Load Rating Method for Reinforced Concrete Slab Bridges. *Proceedings of Structures Congress XV (Building to Last)*, ASCE, Structural Engineering Institute, Portland, Oreg., 1997.
13. Bell, E. S., B. Brenner, M. Sanayei, and D. Lattanzi. Defining Baseline Model for Bridge Analysis and Design. *Proceedings of the 85th Annual Meeting of the Transportation Research Board*, TRB, National Research Council, Washington, D. C., 2006.
14. *Bridge Inspection Report: Bridge No. 7270*. New Mexico Department of Transportation, Santa Fe, New Mex., 2005.
15. *Recording and Coding Guide for the Structure Inventory and Appraisal of the Nation's Bridges*. FHWA-PD-96-001. FHWA, U. S. Department of Transportation, 1995.
16. *Mathcad User's Guide*. Version 13. Mathsoft Engineering and Education, Inc., Cambridge, Mass., 2005.
17. *RISA-2D General Reference*. Version 6. RISA Technologies, Foothill Ranch, Calif., 2004.
18. Licon-Lozano, A. *Non-Destructive Strength Evaluation of a Continuous, Reinforced Concrete Slab Bridge*. MS thesis. New Mexico State University, Las Cruces, New Mex., 2007.

19. *Structural Testing System II Operation Manual*. Bridge Diagnostics, Inc., Boulder, Col., 2005.
20. *Building Code and Commentary: ACI 318-05*. American Concrete Institute, Farmington Hills, Mich., 2005.



New Mexico Department of Transportation
RESEARCH BUREAU
7500B Pan American Freeway NE
PO Box 94690
Albuquerque, NM 87199-4690
Tel: (505) 841-9145